GEOLOGICAL SURVEY OF CANADA

OPEN FILE 2049

GEOLOGICAL, FLUID INCLUSION, AND STABLE ISOTOPIC STUDIES OF THE ST. ROBERT W-Ag-Bi VEIN DEPOSIT, EASTERN TOWNSHIPS, QUÉBEC[1]

Sergio Cattalani[2] and A.E. Williams-Jones[3]

[1] Contribution to the Federal Asbestos Initiatives, Geoscience Research Program 1984-1987. DSS Contract 03SQ.23233-4-0447.

[2] The Mineral Exploration Research Institute, P.O. Box 6079, Station "A", Montreal, Quebec, H3C 3A7.

[3] Department of Geological Sciences, McGill University, 3450 University Street, Montreal, Quebec, H3A 2A7.

ABSTRACT

Tungsten-silver-bismuth mineralization at St.Robert, Eastern Townships, Quebec, occurs in high-level hydrothermal quartz veins. The major veins are steeply dipping and include a silver-bearing set in the southern part of the property and tungsten and bismuth-bearing sets in the central and northern parts respectively. Narrower, subhorizontal veins enrich the centre and north zones in tungsten. Concordant granodioritic, and discordant lamprophyric dyke swarms are concentrated within a 2.5 km x 400 m thermal metamorphic aureole, indicating a larger intrusive stock at depth. The aureole is overprinted by fault-controlled alteration of proximal argillic and distal phyllic facies.

Microthermometric data on fluid inclusions in quartz, scheelite and sphalerite indicate the presence of early, low salinity fluids containing variable proportions of H_2O and a carbonic phase, and later, low salinity, post-ore aqueous fluids. Eutectic temperature estimates point to the presence of Ca^{2+} in solution. Raman microprobe analysis of the carbonic phase confirms the presence of CO_2, CH_4 and N_2 where $CH_4 + N_2$ concentrations show a positive correlation with tungsten contents of the veins. Entrapment temperatures for the early fluid and oxygen isotope geothermometry based on quartz and sheelite analyses suggest average temperatures within the range 220° to 270°C, whereas sulphur isotope geothermometry points to average temperatures in the range 320° to 370°C. Later aqueous fluids were trapped at temperatures ranging from 140° to 210°C.

Oxygen and sulphur isotopic data and phase equilibrium calculations suggest that the metals were transported with sulphur of marine origin in a meteoric water-dominated hydrothermal system with a solution ph between 3.0 and 5.0. Mineral deposition is believed to have occurred as a result of CO_2-dominant, volatile phase effervescence and pH and fO_2 fluctuations during episodic wall-rock fracturing and resealing, where the observed mineral zonation was likely controlled by the local stratigraphy.

TABLE OF CONTENTS

1- INTRODUCTION

The J.A.G. Mines, St. Robert deposit, located about 2 km east of the town of St. Robert de Bellarmin, in the Eastern Townships of Quebec (Fig. 1), consists of several sets of W, Bi, Ag, Pb, Zn-bearing hydrothermal quartz veins which are hosted by a variety of clastic sedimentary rocks of Ordovician age (Harron, 1976). The St. Robert W-Bi-Ag deposit provides a good opportunity to investigate the processes involved in concentrating tungsten to economic levels, as it shares numerous features with other deposits of its class: association with a felsic intrusive; early W and Bi mineralization; late base metal mineralization; mineralization within high-level, sheeted quartz veins; evidence of low pressure, tensional environment, etc. (c.f. Eadington, 1983; Higgins, 1985; Kelly and Rye, 1979; Landis and Rye, 1974; Ramboz, 1980).

A large scale (1:5000) mapping and sampling project was carried out during the summers of 1984 and 1985, with the object of delineating and characterizing the various zones of economic and geologic interest. Over 13,170 metres of drill core were also logged. Three zones of economic interest were delineated, hosting four major mineralized quartz vein sets (Fig. 4). In addition, a well defined zone of intense phyllic and local argillic alteration, which is largely fault-controlled, was mapped. Mineralization was found to vary macroscopically from one vein set to another and permitted recognition of a southern, silver-rich zone, a central tungsten-rich zone, and a northern bismuth-rich zone.

An extensive fluid inclusion and stable isotope study of the deposit was undertaken to place physico-chemical constraints on the conditions of vein formation. The results of this study were used in conjunction with the mapped field relationships and pertinent petrological data to develop a genetic model for the St. Robert deposit.

1.1 Exploration History

Silver- and tungsten-bearing veins have been known to occur in the area since the late 19th century. In fact, the St. Robert showing has the distinction of being the first reported occurence of free scheelite in Canada (Little, 1959; Mulligan, 1983). It was not, however, until the 1950's that serious exploration of these veins was undertaken.

The first extensive exploration of the deposit was conducted by the St. Robert Metals Corporation (1951-1958). This program delineated a zone of scheelite-bearing veins outcropping at surface and precious metal mineralization at depth. Drill intersections of the latter included 14.14 oz/t Au over 1 foot, 11.8 oz/t Au and 6.58 oz/t Ag over 0.9 feet, and 25.00 oz/t Au and 5.8 oz/t Ag over 0.3 feet. Two adits, the Lacombe adit and the Lee tunnel were driven to exploit the mineralized zones. The

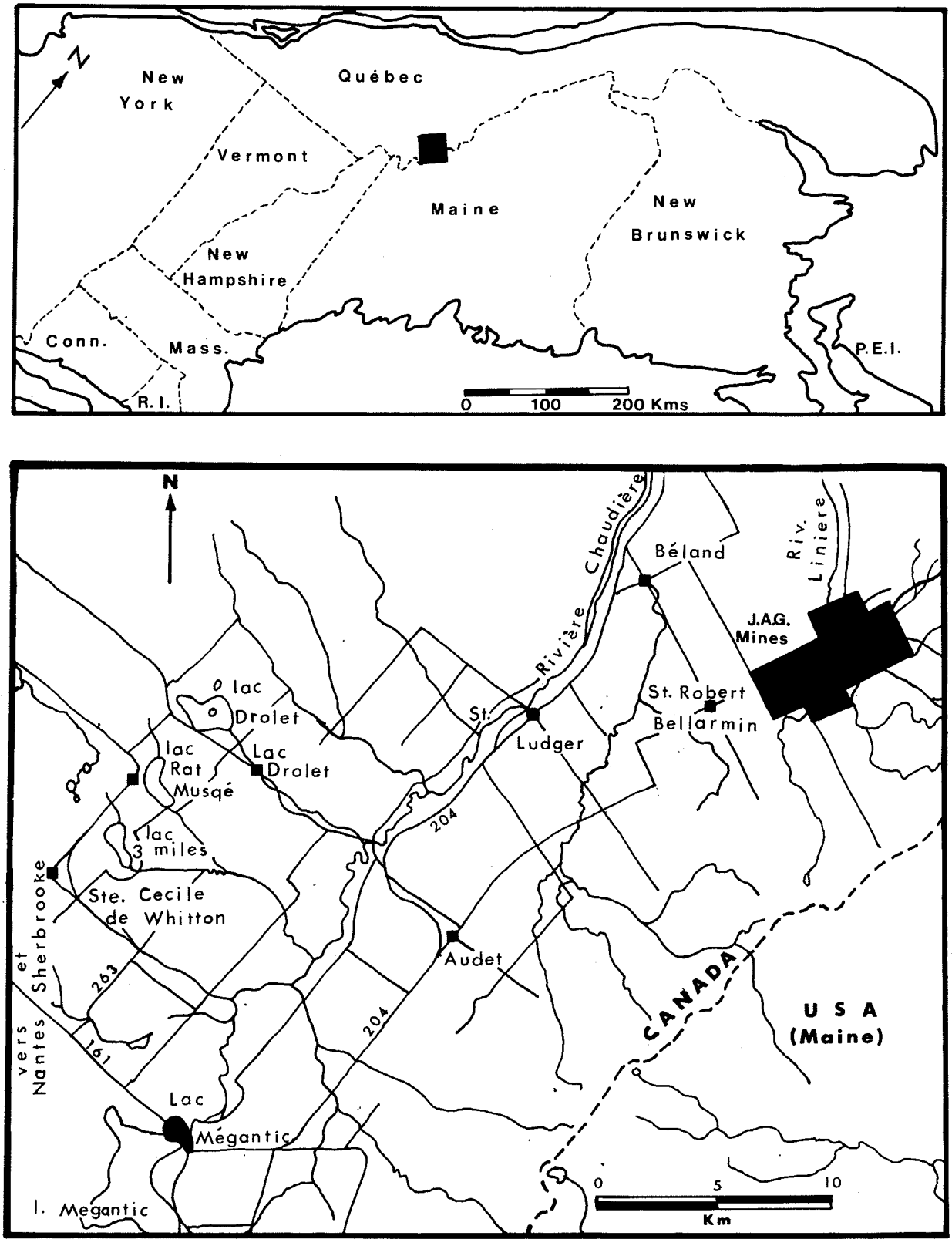

Figure 1 Geographic location map for the St. Robert property.

property was brought briefly into production, primarily as a tungsten mine, in 1958. Unfortunately, the Lee tunnel, which was to exploit the precious metal zones, had to be abandoned before it reached its target.

Subsequent exploration of the property by Nouvelle Mining (1970-1974), and J.A.G. Mines (1977-present), has focused on its precious metal potential. Neither company has however been able to reproduce the drilling results of the St. Robert Metals Corporation. The best recent intersections by J.A.G. Mines have been 37.8 oz/t Ag and 8.8% Zn over 1.2 feet, and 27.81 oz/t Ag and 3.16% Pb over 2.1 feet.

1.2 Geological Setting

The Saint Robert de Bellarmin property is largely underlain by sedimentary rocks of the Frontenac Formation, a miogeoclinal sequence of possible Early Ordovician age (Harron, 1976). These rocks were deformed during the Middle Devonian Acadian orogeny and are exposed in the Boundary Mountain anticlinorium, a structure of the same age (St. Julien and Beland, 1982). The property is located immediately to the south of the fault-bounded contact between the Boundary Mountain anticlinorium, and the more northerly Gasp{2-Connecticut Valley synclinorium. A swarm of Acadian and possibly younger dykes cut the Frontenac Formation within the property limits.

1.21 Sedimentary Rocks

The sedimentary rocks consist of a sequence of clastic turbiditic sediments largely comprising alternating light to medium gray quartzites, medium to dark gray slates, and light to medium brownish calcareous greywackes, as well as thin interbeds of black graphitic shales.

The quartzites, slates, and graywackes form well consolidated, cleanly fractured beds which range from less than one metre to several metres in thickness. By contrast, the shale interbeds rarely exceed 20 to 30 centimetres in thickness and generally appear to be contorted and folded. The shales commonly contain numerous millimetre to centimetre size, white opaque quartz veinlets which parallel the foliation. The various rock types described above are found throughout the property without any obvious pattern to their distribution. They are overlain by unconsolidated Pleistocene glacial till, and recent alluvium, that together locally reach thicknesses in excess of 70 m.

1.22 Igneous Rocks

The intrusive rocks consist of numerous subparallel felsic dykes striking east-northeast, and much less common, thinner and later, cross-cutting mafic dykes. The felsic igneous rocks can

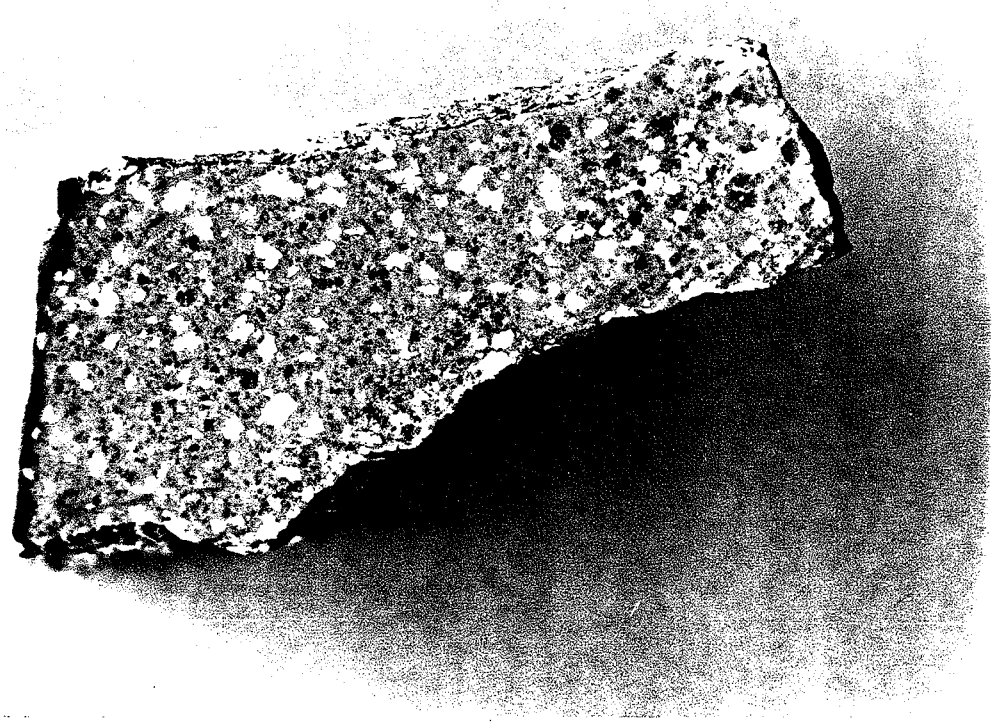

Plate 1 Sample of first intrusive rock type (granodiorite porphyry).

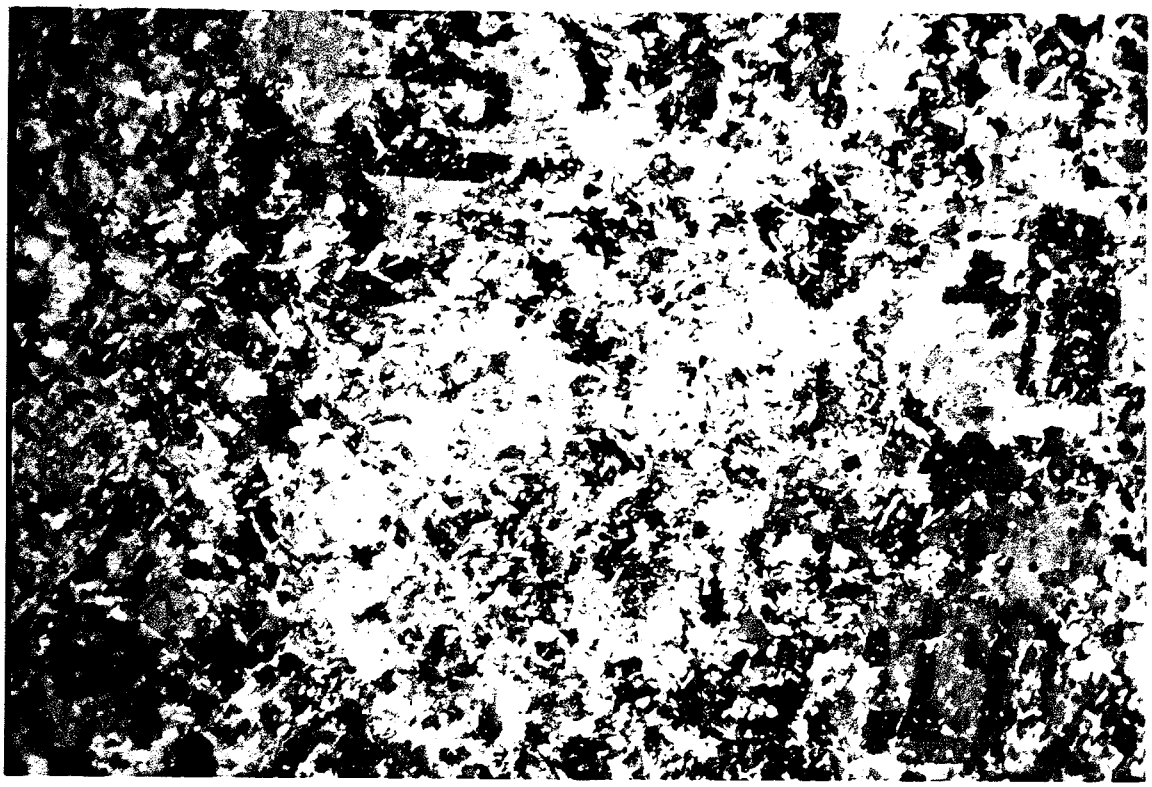

Plate 2 Thin section of granodiorite porphyry showing pervasive alteration of feldspars by sericite and calcite. Width of field of view is 0.8 mm.

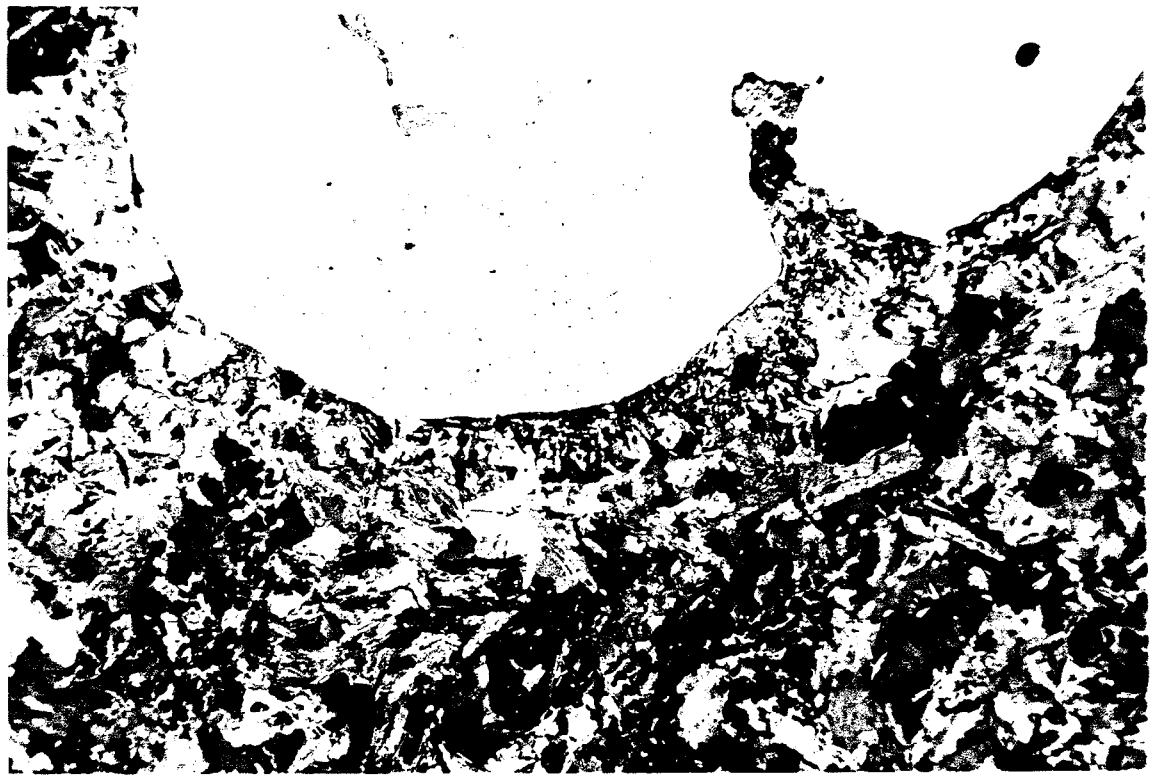

Plate 3 Thin section of granodiorite porphyry showing granophyric quartz overgrowth on a rounded quartz phenocryst. Width of field of view is 3.3 mm.

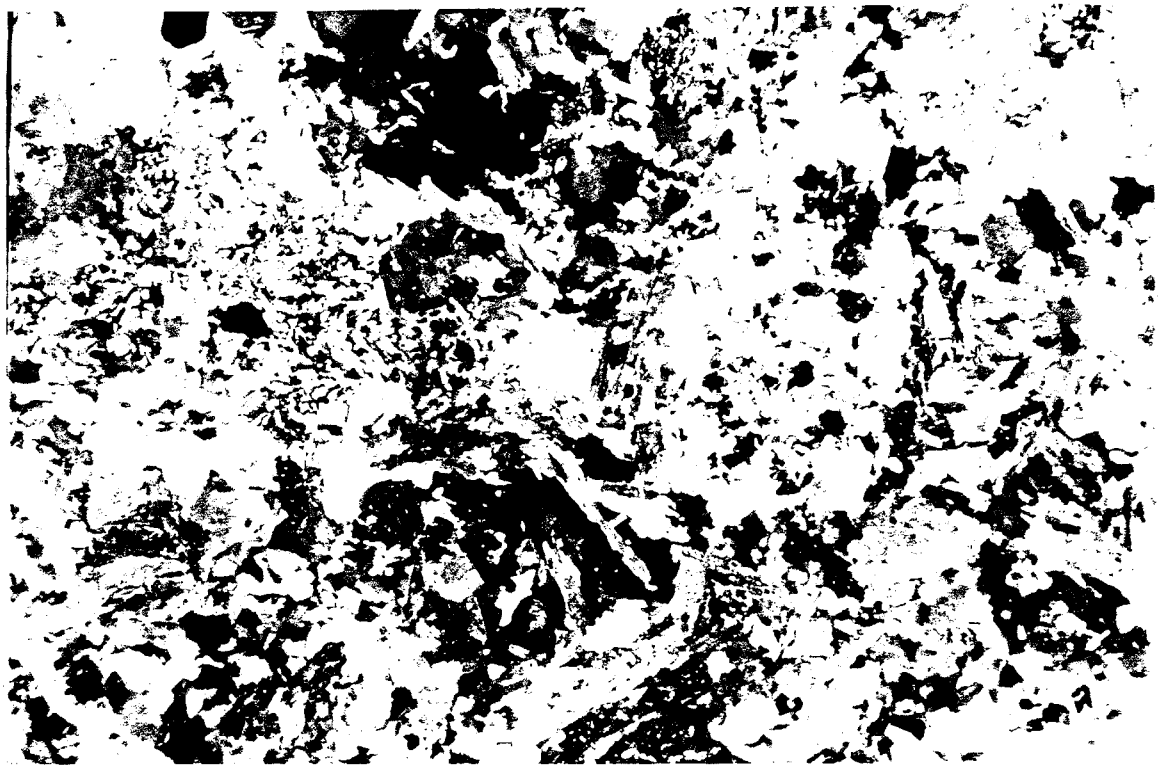

Plate 4 Thin section of granodiorite porphyry showing granophyric textured quartz and abundant sericite and calcite in the matrix. Width of field of view is 2.1 mm.

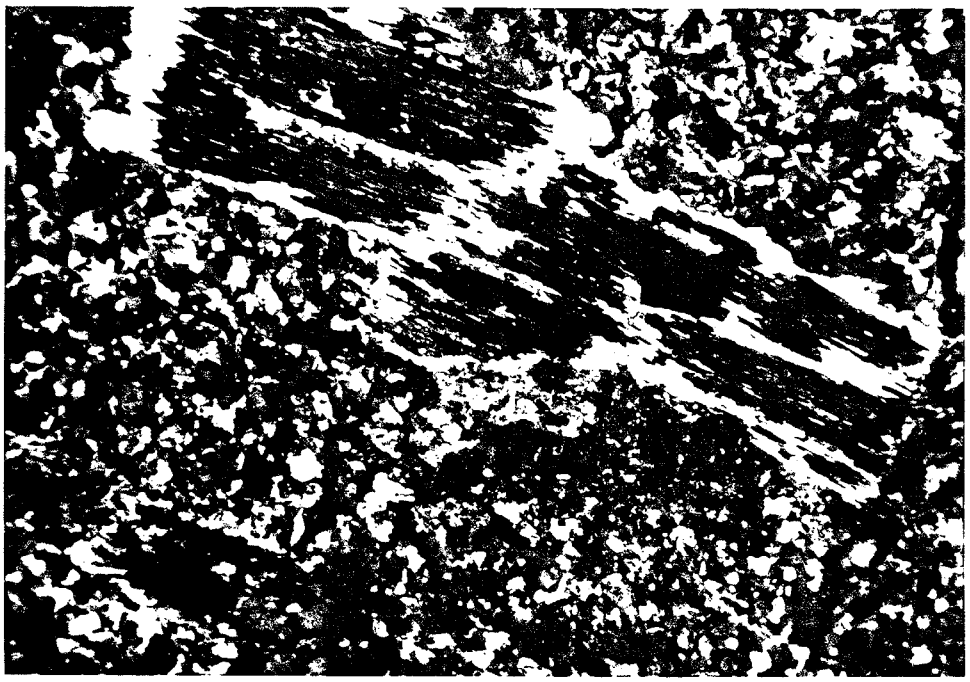

Plate 5 Thin section of granodiorite porphyry showing a biotite phenocryst pervasively altered to chlorite, calcite, sericite, rutile and leucoxene. Width of field of view is 2.6 mm.

Plate 6 Core sample of second intrusive rock type (intrusive dacite).

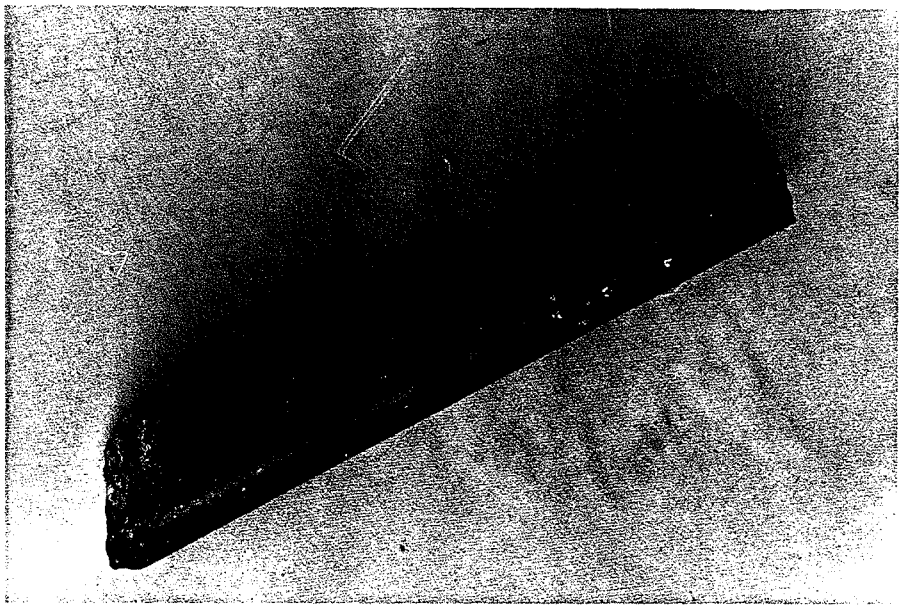

Plate 7 Core sample of mafic intrusive rock type (lamprophyre).

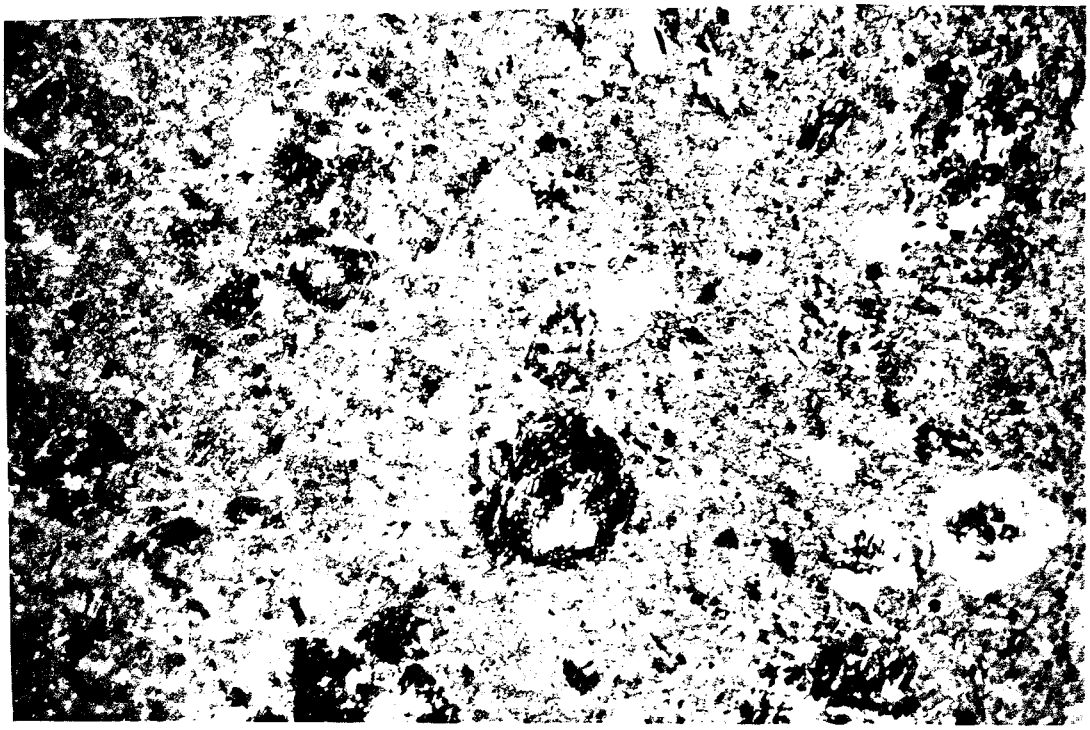

Plate 8 Thin section of mafic intrusive chilled margin showing a relatively fresh horndblende phenocryst (top right) and relict plagioclase phenocryst (upper left centre). Width of field of view is 8.0 mm.

be divided into two distinct types.

The first is a fine-to-medium grained, greenish gray, leucocratic to mesocratic rock exhibiting porphyritic to glomeroporphyritic textures (Plate 1). This rock type is characterized by abundant relict quartz and plagioclase (An_{0-15}) phenocrysts, and smaller proportions of relict hornblende and biotite phenocrysts, set in a quartzofeldspathic groundmass containing accessory apatite. Much of the present mineralogy and texture of this rock is due to extensive hydrothermal alteration: the feldspathic phases are abundantly sericitized (Plate 2); the quartz and feldspar phenocrysts are overgrown by later quartz (Plate 3); the groundmass contains abundant patches of granophyric quartz and K-feldspar (Plate 4); and the mafic minerals are largely pseudomorphosed by chlorite, calcite, sericite, rutile, and leucoxene (Plate 5). Other secondary mineral phases include sphene and epidote. Dykes of this type range from less than one metre up to 20 metres in width and make up the bulk of the intrusive rocks on the property.

The second felsic igneous rock type consists of an aphanitic to medium grained, leucocratic, green to yellowish-white, porphyry rock (Plate 6). It contains relict phenocrysts of quartz and plagioclase set in a pervasively sericitized quartzo-feldspathic groundmass which often exhibits a well developed serrate texture. This rock type is distinguished from the first type by the absence of mafic phases, a light greenish-yellow colour, and a conchoidal fracture. The alteration mineralogy is qualitatively the same as that mentioned above. This rock-type generally forms narrower dykes (up to 6-7 m in width), that may commonly show a banded texture along one or both dyke/wallrock contacts.

The mafic igneous rocks are narrow (less than 2 m wide) dykes that are generally subparallel to the felsic dykes. However, they commonly crosscut the latter at relatively high angles, and therefore represent a younger intrusive event. The mafic rock type is a fine-to-coarse grained, brown, melanocratic porphyritic variety (Plate 7) containing relict phenocrysts of plagioclase, green hornblende, and/or biotite, with smaller proportions of relict phenocrysts of diopsidic augite, and accessory apatite. In a significant proportion of the dykes, plagioclase occurs in the groundmass. Alteration is extensive, and consists primarily of abundant rounded calcite patches, as well as secondary biotite, chlorite, rutile, and minor sericite. In some cases, a chilled margin exists in which relatively fresh mafic phenocrysts are visible near the dyke/wallrock contact (Plate 8). These chilled margins make up only a small percentage of the dyke thickness and grade into pervasively altered rock within centimetres of the dyke/wallrock contact.

The dyke rocks on the Saint Robert property may be genetically related to a larger intrusive body at depth, the presence of which is suggested by a broad regional positive magnetic anomaly under the central part of the property (Fig. 2).

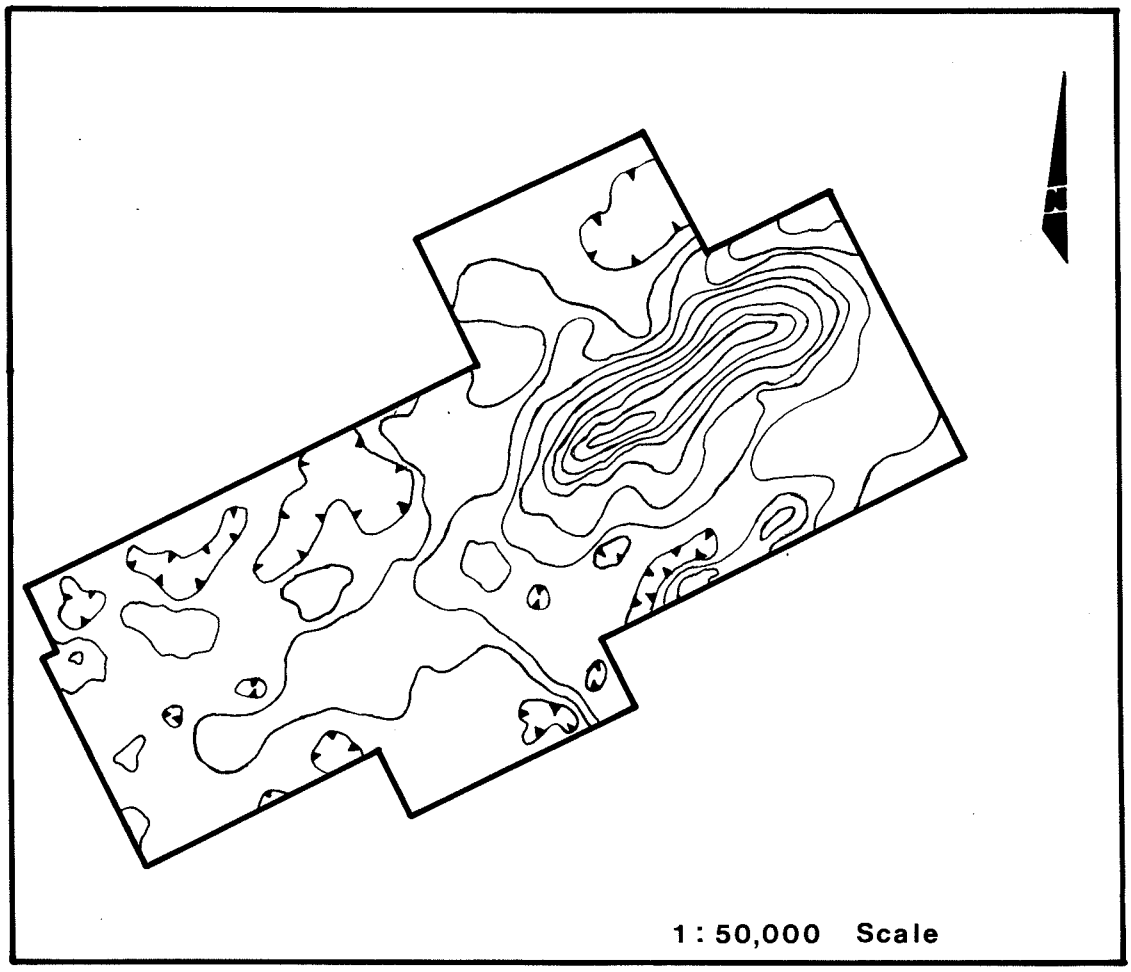

Figure 2. Regional magnetic anomaly map for the J.A.G. Mines, St. Robert property. Reproduced from Le Ministere d'Energie et des Ressources de Quebec.

1.21 Petrochemistry

A total of 46 rock samples, which includes 33 felsic igneous rocks of the first type, 3 felsic igneous rocks of the second type, and 10 mafic igneous rocks were analyzed by X-ray fluorescence. These samples vary greatly in their degree of alteration and were accordingly classified into least altered, moderately altered, and strongly altered (Appendix 1). Each sample was analyzed for the following elements: SiO_2, TiO_2, Al_2O_3, Fe_2O_3, MgO, MnO, CaO, Na_2O, K_2O, and P_2O_5, and the results used to compute normative compositions using a program written by Dr. Andrew Hynes of the department of Geological Sciences, McGill University. The results and corresponding norms are presented in Appendix 1 and 2 respectively.

The felsic rock types are classified using the scheme of Streckeisen (1976) (Fig. 3). The first felsic type ranges from granodiorite to quartz-rich granite, with the latter representing moderately and strongly altered samples. The second felsic rock type is restricted to granodiorite compositions. Based on its macroscopic appearance, as well as for reasons of clarity, the

second felsic rock type will be hereafter referred to as an intrusive dacite.

The mafic igneous rock type is classified using the classification scheme for lamprophyres of Streckeisen (1979). This particular classification scheme was selected on the basis of their textural, mineralogical, and chemical resemblance to the lamprophyre group of rocks. The mafic dykes are thus tentatively classified as spessartites and/or kersantites (Fig. 3).

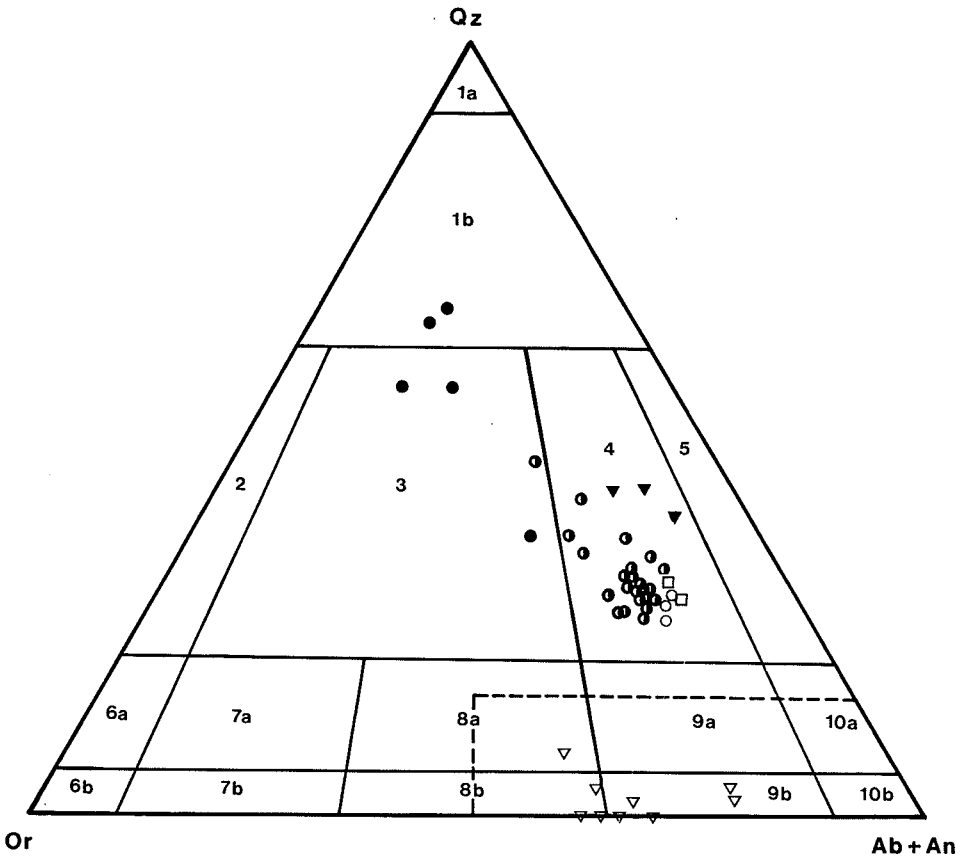

Figure 3. The pseudoternary Qz-Ab+An-Or diagram, after Streckeisen (1976). Open circles represent unaltered or weakly altered granodiorite porphyry, half-filled circles represent moderately altered granodiorite porphyry, solid circles represent strongly altered granodiorite porphyry, open squares represent granodiorite porphyry chilled margins, open triangles represent mafic dykes, filled triangles represent intrusive dacites. Fields marked 1a through 10b represent: 1a, quartzolite; 1b, quartz-rich granitoids; 2, alkali-feldspar granite; 3, granite; 4, granodiorite; 5, tonalite; 6a, quartz alkali-feldspar granite; 7a, quartz syenite; 8a, quartz monzonite; 9a, quartz-monzodiorite/quartz-monzogabbro; 10a, quartz diorite/quartz gabbro; 6b, alkali-feldspar syenite; 7b, syenite; 8b, monzonite; 9b,monzodiorite/monzogabbro; 10b, diorite/gabbro/anorthosite. Dashed lines outline the fields of spessartites and kersantites, after Streckeisen (1979).

1.24 Structure

The sedimentary strata on the property dip steeply to the north and south, forming a number of tight, upright isoclinal folds that trend east-northeast. A subvertical cleavage (F1) defines the principal foliation, and is generally indistinguishable from bedding. In addition, there is a weaker, subparallel cleavage (F2), which shows a maximum departure of 10° to 15° from F1. This results in a strong crenulation cleavage that is evident in the shaly units. A third, minor phase of deformation is represented by gentle, open folds, with axial planes lie nearly normal to F1 and F2. This event caused the F1 and F2 fold axes to dip locally at shallow angles either east-northeast or west-southwest.

Both the granodiorite porphyry dykes and the dacite dykes have intruded along F1, and therefore are sill-like in the fold limbs. Some dacite dykes have intruded along the cores of the granodiorite porphyry dykes, ie. they were subjected to the same structural controls as the porphyry dykes.

A major system of vertical faults, referred to as the Main Fault system, with a strike length of at least 2.5 km, cuts through the centre of the property, parallel to F1 (Fig. 4). Displacement appears to be dominantly dip-slip in character, with the downthrow to the north. Because vertical faults cut near-vertically dipping strata it is impossible to estimate the amount of displacement. Less numerous, apparently subvertical, late minor faults occur nearly normal to the Main Fault system in the western and central parts of the property.

1.25 Metamorphism

Regional metamorphism in the area is restricted to lower greenschist to greenschist facies. A local thermal metamorphic overprint is evident as a zone of brownish biotite hornfels. This zone is roughly oval in shape, and has its long axis coincident with the Main Fault system described above (Fig. 4). It measures at least 2.5 km in length and varies from about 400 to 500 metres in width. The hornfelsing coincides spatially with the zone of major igneous activity, as well as the magnetic anomaly mapped in the area, and is therefore interpreted to represent thermal metamorphism induced by an intrusive stock at depth. This thermal metamorphic effect is consistently overprinted by the hydrothermal alteration described below (Plate 9), and is therefore inferred to have preceded the hydrothermal event.

1.26 Alteration

The various lithotypes described above have undergone moderate to intense hydrothermal alteration in a zone which is roughly coincident with the biotite hornfels zone (Fig. 4).

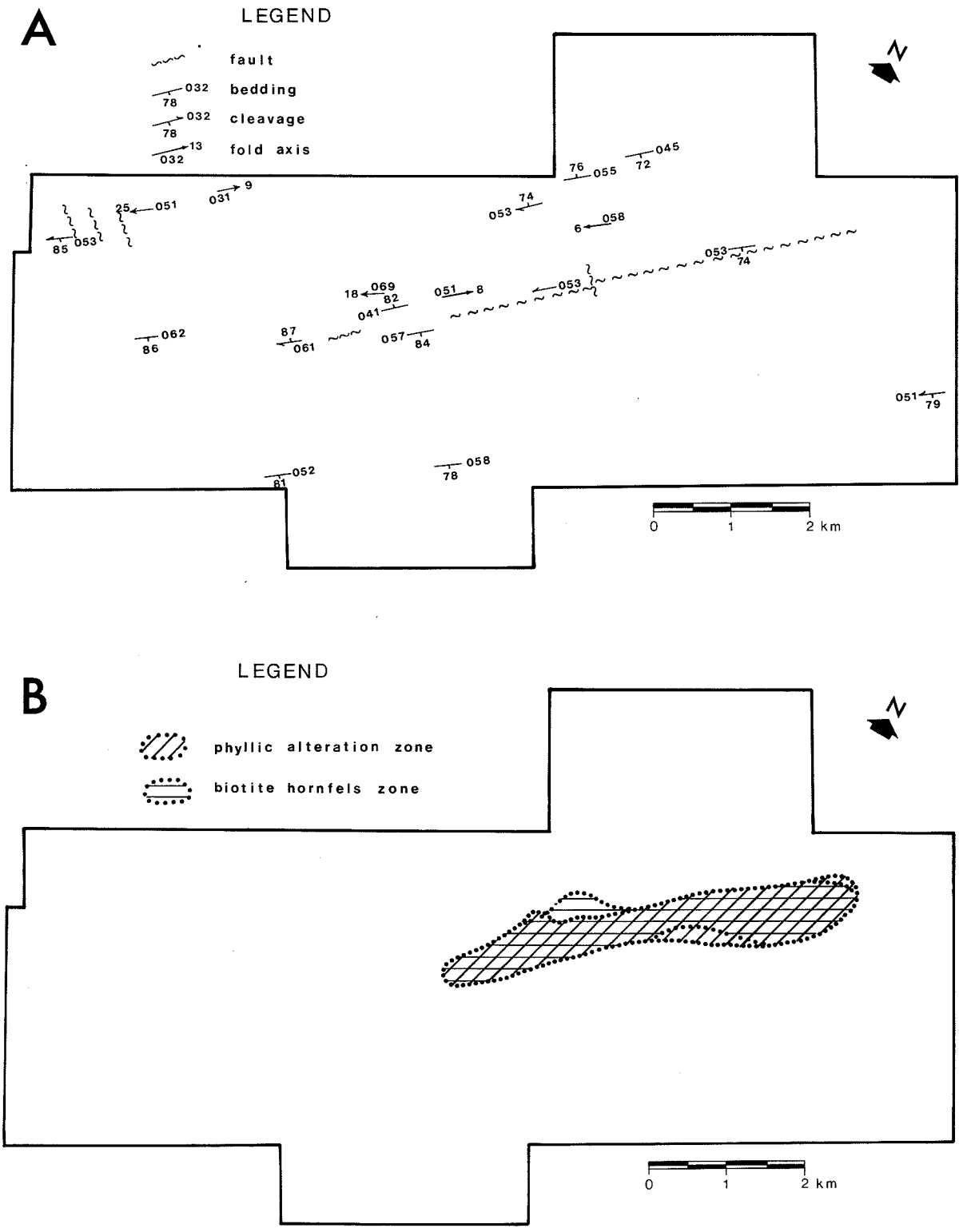

Figure 4. Simplified geological map of the St. Robert property: A) Location of the structural elements; B) location of the hydrothermal alteration and thermal metamorphic zones.

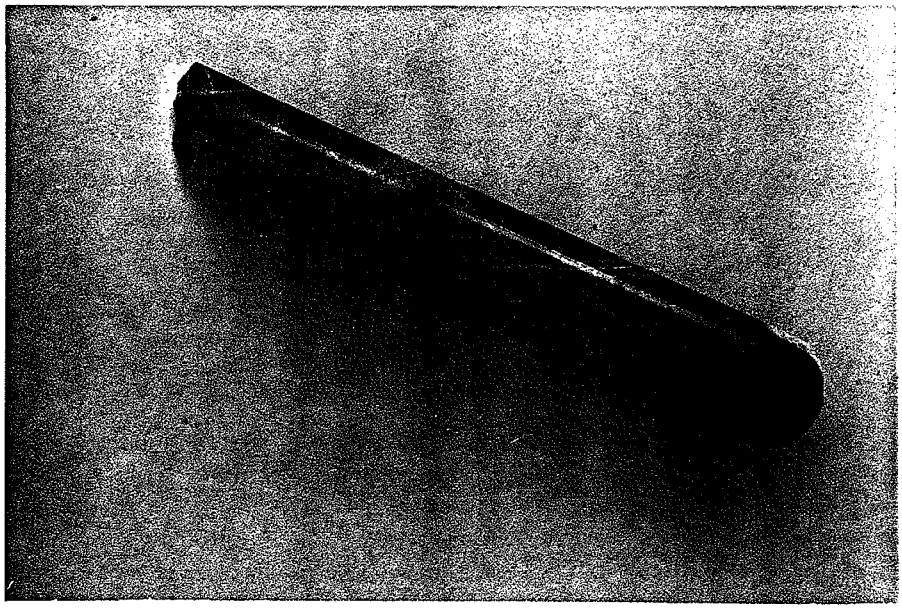

Plate 9 Core sample of biotite hornfels cut by several quartz-carbonate veinlets showing well developed phyllic alteration halo.

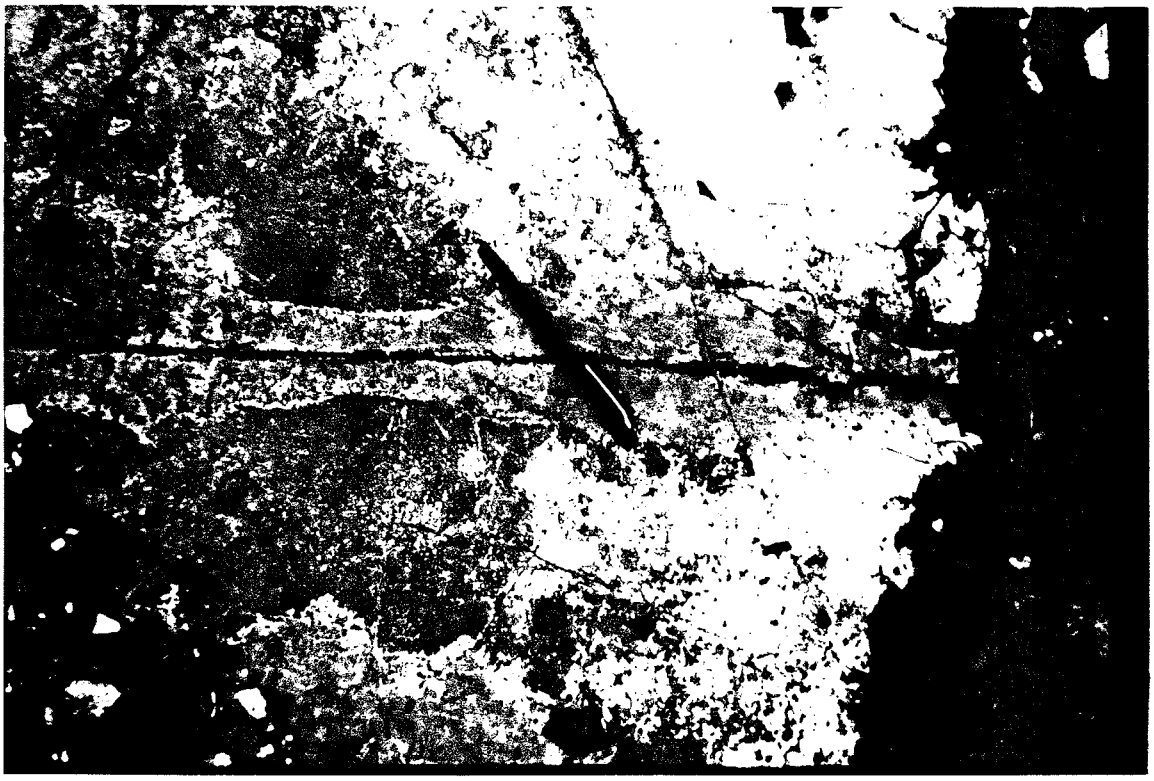

Plate 10 Phyllic alteration halo developed around a small fracture.

Alteration is generally phyllic in character (Plate 10), resulting in pale greyish-green rocks that consist mainly of quartz, sericite, illite, calcite, pyrite, and rutile. The degree of alteration and quartz veining increase visibly with proximity to the Main Fault system.

Adjacent to, and within faults of the Main Fault system however, the rocks are white, extremely friable and soft. X-ray diffraction analysis reveals that these rocks are composed mainly of kaolinite. The overall pattern of alteration is clearly fault-controlled and consists of narrow proximal argillic facies within a broad halo of distal phyllic facies.

A second smaller zone of phyllic alteration occurs to the northwest of the Main Fault system, in the North Zone of the property. Unfortunately, the smaller number of drillholes and scarcity of outcrops in the area make it difficult to delineate accurately the extent of this zone.

2- MINERALIZATION

The bulk of the mineralization on the property is contained within massive quartz veins which range from 10 cm up to almost 1 m in width, and up to about 150 m in length (Plate 11). These veins contain various Pb, Zn, Ag, Bi, Cu sulphides, as well as variable scheelite. The mineralized quartz veins at Saint Robert are of two main types: vertical or subvertical and subhorizontal. Aside from the South Zone, where a few porphyry dykes are seen cutting veins (Fig. 5), vein formation postdates emplacement of all major geologic units in the St. Robert area.

2.1 Vertical/Subvertical Veins

The vertical/subvertical veins can be subdivided into three sets on the basis of their location: North Zone, South Zone, and Central Zone vein sets (Fig. 5). These veins appear early in the paragenesis of the deposit and make up the bulk of the veins at Saint Robert. The North Zone and Central Zone vein sets occupy tensional fractures concordant to cleavage, striking approximately 060° and dipping subvertically. Evidence for a tensional environment during vein emplacement includes branching of the veins, variation in strike along individual veins, and the common occurence of vugs. The South Zone veins strike almost normal to foliation and dip 40-55° northeast. They have a tendency to pinch out both along strike and down dip and are, in a few cases, clearly crosscut by granodiorite porphyry dykes. The South Zone veins are thus pre- or syn-felsic dyking. Such a cross-cutting relationship is not seen in the Centre and North veins due to parallelism with the dyke rocks, and it therefore cannot be established whether or not the Central and North Zone vein sets are temporally equivalent to the South Zone vein set.

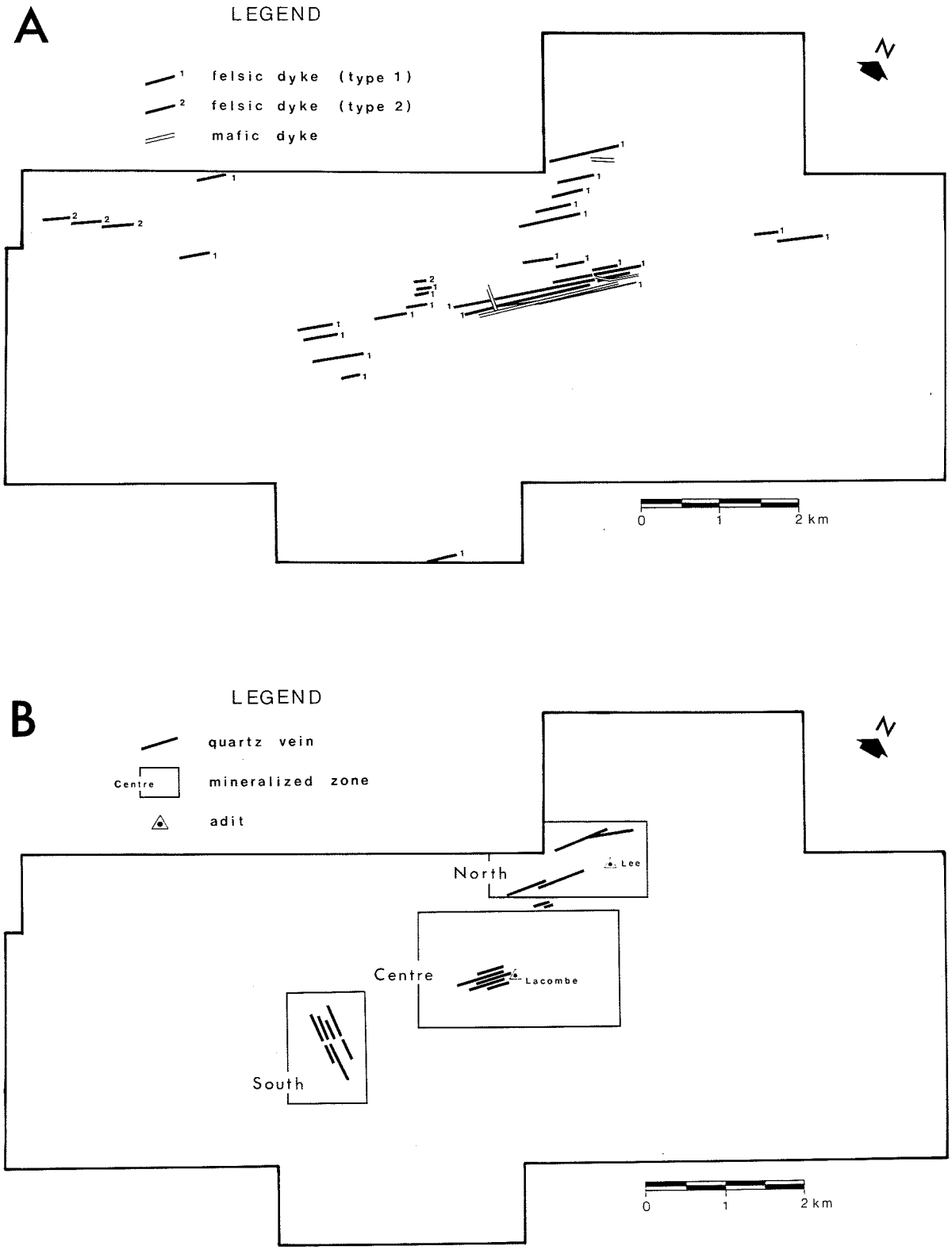

Figure 5 Simplified geolgical map of the St. Robert property: A) location of the intrusive dykes; B) delineation of the mineralized zones, veins and adits.

Plate 11 A large vertical quartz vein at the opening of the Lacombe adit, Centre zone.

Plate 12 A subhorizontal quartz vein cutting two subvertical veins in the Lacombe adit, Centre zone.

2.2 Subhorizontal Veins

The subhorizontal veins dip at angles commonly less than 20° and strike nearly normal to schistosity (Plate 12). They are considerably narrower (1 to 10 cm in width) and much less numerous than the vertical/subvertical veins. Subhorizontal veins occur throughout the North and Central Zones and always cross-cut the vertical/subvertical veins, indicating that they are younger than the latter.

2.3 Gangue Minerals

Gangue minerals present in the hydrothermal veins at St. Robert listed in order of decreasing abundance are as follows: quartz, calcite, sericite and kaolinite. The overwhelming bulk of each of the veins is composed of massive, milky white quartz, which may show abundant vug formation. These vugs are usually lined with clear to cloudy euhedral quartz crystals. The quartz veins commonly show evidence of repeated fracturing and resealing events, indicated by cross-cutting trains of secondary fluid inclusions. In fact, the bulk of the quartz contains a high density of small fluid inclusions, thereby giving it a milky white appearance.

Calcite is a common gangue mineral in the quartz veins, and, everywhere, has postdated the main stage of quartz precipitation. The mode of occurrence of calcite in these veins is generally that of a fracture-filling mineral in quartz and some sulphides and oxide ore minerals (eg. pyrite, scheelite). Calcite-filled secondary fractures may or may not be accompanied by additional quartz and/or sericite. In thin section, calcite is commonly the principal mineral in a fracture, in many cases completely enclosing the sulphide and oxide ore minerals with which it appears to have co-precipitated. Distinct growth zones, as delineated by primary fluid inclusions, can be seen to have formed in some calcite crystals within these secondary fractures (Plate 13). This strengthens the conclusion previously drawn that the environment of vein formation was predominantly tensional.

A third common gangue mineral is sericite or fine grained muscovite. This mineral is most often seen as a late stage mineral, filling fractures in the quartz veins in a fashion analogous to that of calcite. It occurs with or without calcite and/or late-stage quartz and commonly encloses or is intergrown with late-stage pyrite (Plate 14). In South zone veins, fine grained muscovite appears as a late stage gangue mineral lining the walls of the numerous vugs and cavities, where it is present with pyrite, sphalerite, and galena. By contrast, in the North zone veins, fine grained muscovite occurs most commonly as a relatively early mineral concentrated near the vein margins as coarse patches at the apices of cosalite fans (Plate 15).

Plate 13 Calcite-filled secondary fracture with distinct growth zones outlined by primary fluid inclusions in calcite crystals surrounding a cavity. Width of field of view is 2.1 mm.

Plate 14 Intergrowth of pyrite and muscovite. Width of field of view is 2.1 mm.

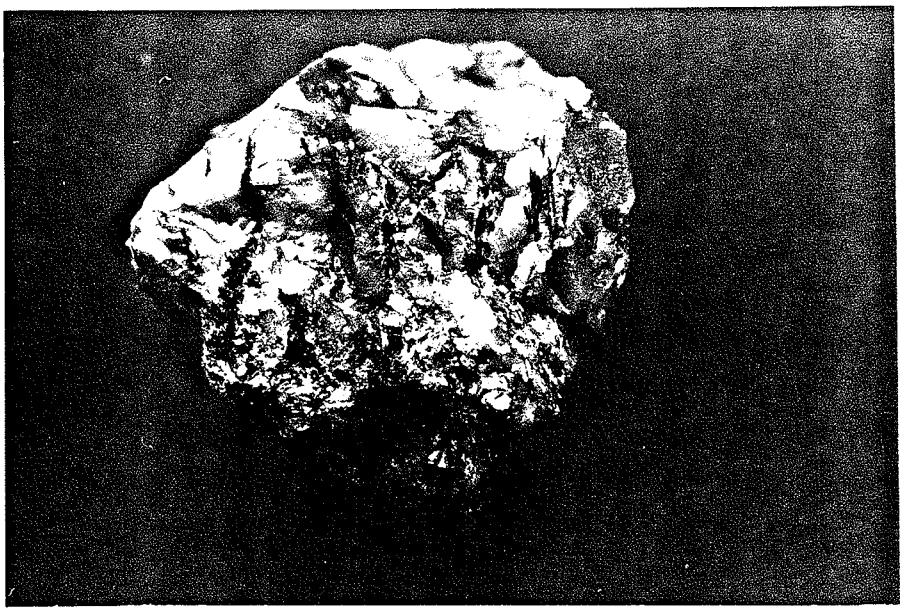

Plate 15 Sample of North zone quartz vein showing coarse patches of fine grained muscovite at the apices of cosalite bundles.

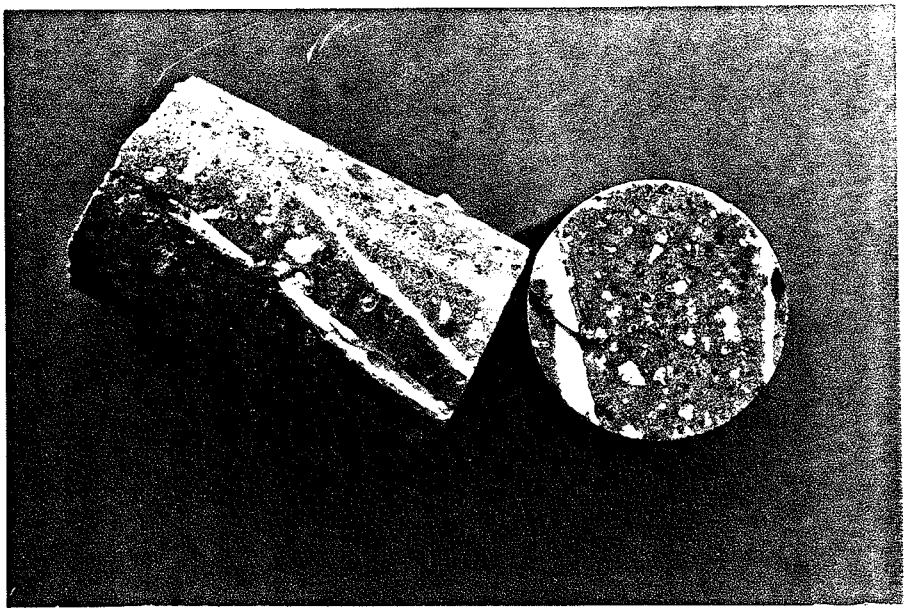

Plate 16 Core sample of granodiorite porphyry from the Main Fault zone showing kaolinite-filled fractures.

Kaolinite is the least abundant of the gangue minerals present in the quartz veins. It occurs exclusively as a secondary alteration mineral in veins in the Centre zone which are within or immediately adjacent to the Main Fault system. Kaolinite appears as a fracture-filling mineral, filling stress-related fractures and gashes in both the quartz veins and enclosing wallrocks (Plate 16).

2.4 Sulphide and Oxide Ore Minerals

The sulphide and oxide ore minerals present at St. Robert occur within the various hydrothermal quartz veins described earlier. In order of decreasing abundance, these minerals are pyrite, sphalerite, galena, scheelite, cosalite, and minor chalcopyrite, pyrrhotite and limonite. The main ore minerals are scheelite, cosalite and argentiferous galena.

Scheelite ($CaWO_3$) occurs in important amounts at St. Robert where it was mined for its tungsten content for several years. Scheelite mineralization is most abundant in subhorizontal and Centre zone veins, where it occurs as distinct euhedral crystals several millimetres in diameter, adjacent to vein/wallrock contacts (Plate 17). In some cases though, scheelite can be seen to occur both near the edge of the vein as well as along its core, thus indicating at least two distinct episodes of scheelitization. Later generations of scheelite, which may or may not be replaced by later sulphide minerals (Plate 18), occur as small, anhedral crystals within late veinlets that commonly contain calcite in the groundmass.

Cosalite ($Pb_2Bi_2S_5$) is the main sulphide mineral in North zone veins, and is a minor mineral in Centre zone veins. In the North zone, cosalite occurs as long (up to 10 cm), acicular needles, which, in places, radiate in from the vein/wallrock contact in a fan-like fashion (Plate 19). Cosalite also occurs with other sulphide minerals in stringers that cut the veins. In the Centre zone, cosalite occurs exclusively as acicular inclusions entirely within crystals of galena (Plate 20). A possible interpretation of this texture is that the two minerals were co-precipitated and that the cosalite used the galena as a source of lead, and hence, a surface on which to nucleate. The differences in the modes of occurence of cosalite in the North zone and Centre zone veins is difficult to explain, but may be related to the relative concentration levels of Pb and Bi, as well as to differences in the physico-chemical parameters of the fluids that mineralized the two vein sets.

Galena generally occurs in calcite-filled veinlets cutting early quartz. It is typically present as small euhedral cubes easily identifiable by their characteristic triangular pits. Galena also occurs as large crystals lining the walls of late-stage vugs and cavities in quartz veins of the South zone (Plate 21). Galena clearly replaces earlier pyrite (Plate 22). The galena at St. Robert is argentiferous and represented an

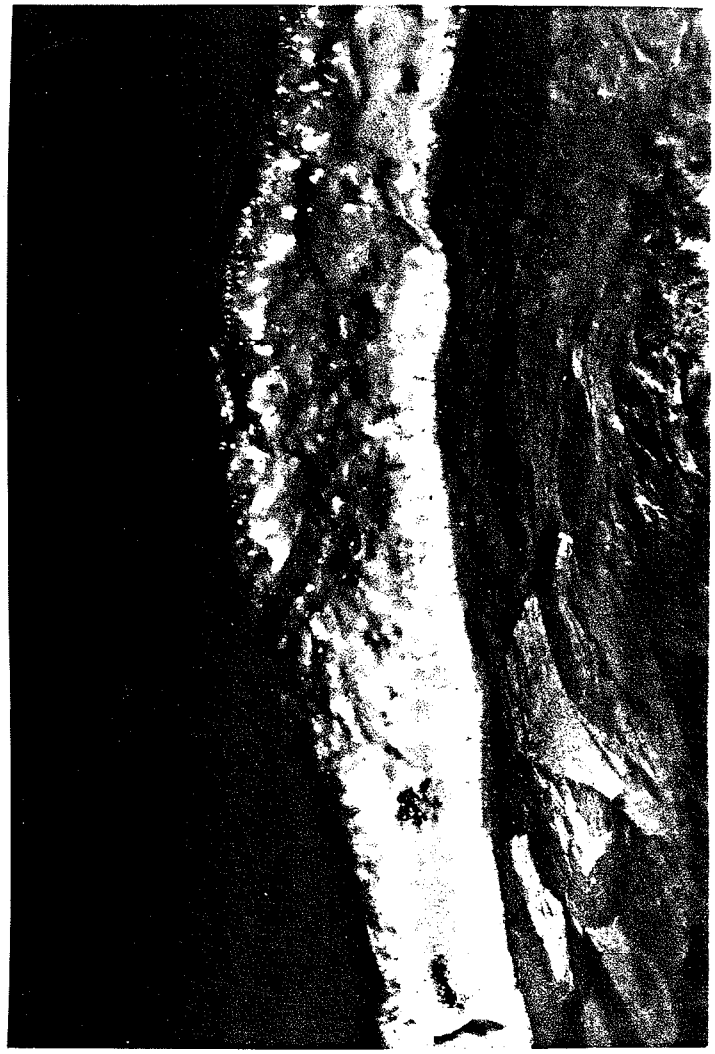

Plate 17 A large (~0.3 m wide) vertical quartz vein in the Lacombe adit. Photo was taken under ultraviolet light and shows scheelite mineralization restricted to edges of the vein.

Plate 18 Scheelite replacement by pyrite. Width of field of view is 2.1 mm.

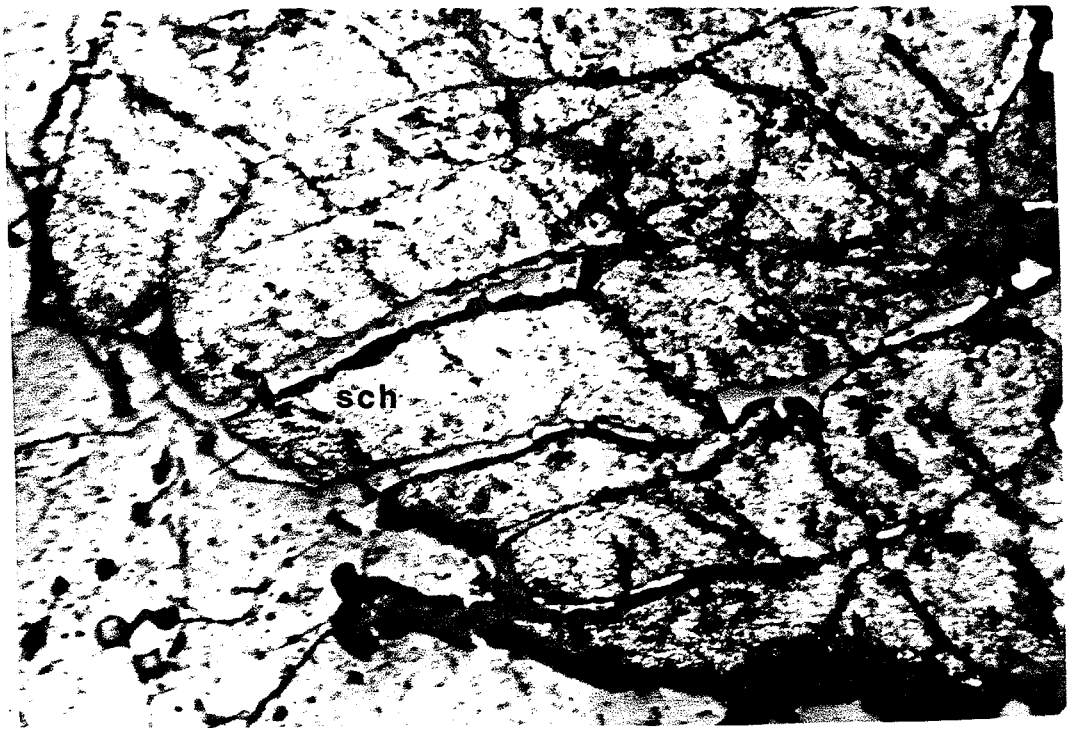

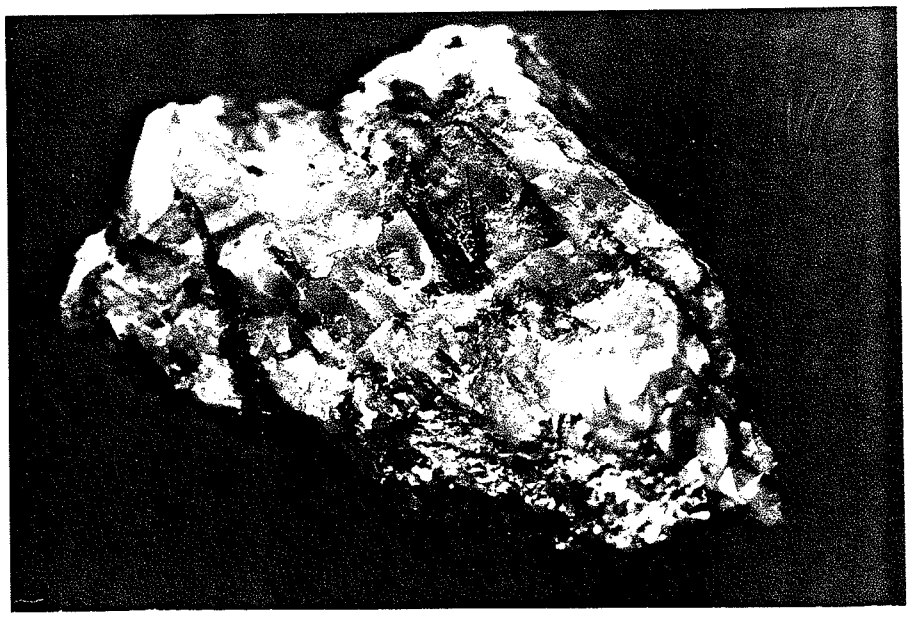

Plate 19 Sample of North zone quartz vein showing bundles of radiating cosalite needles.

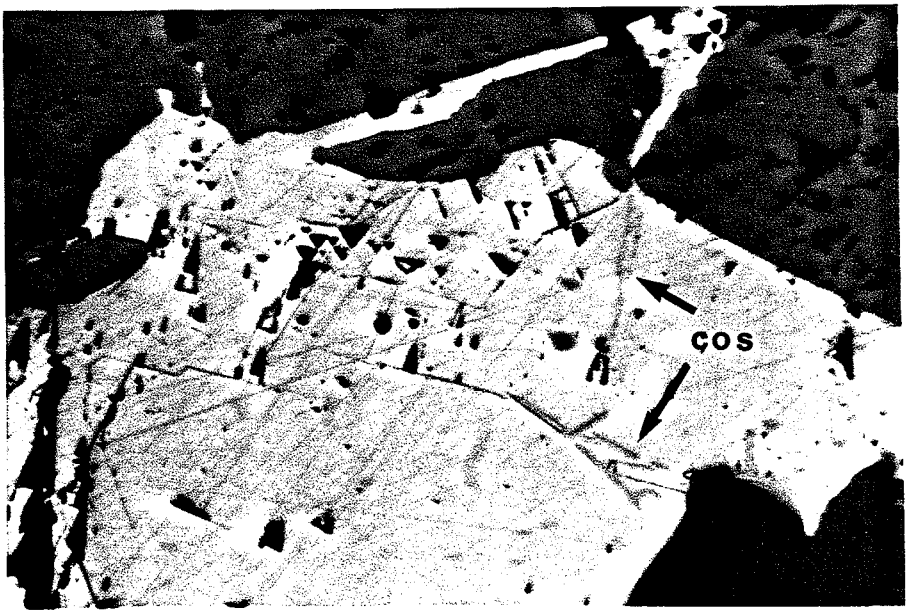

Plate 20 Polished section showing fine cosalite needles within a crystal of galena. Width of field of view is 2.1 mm.

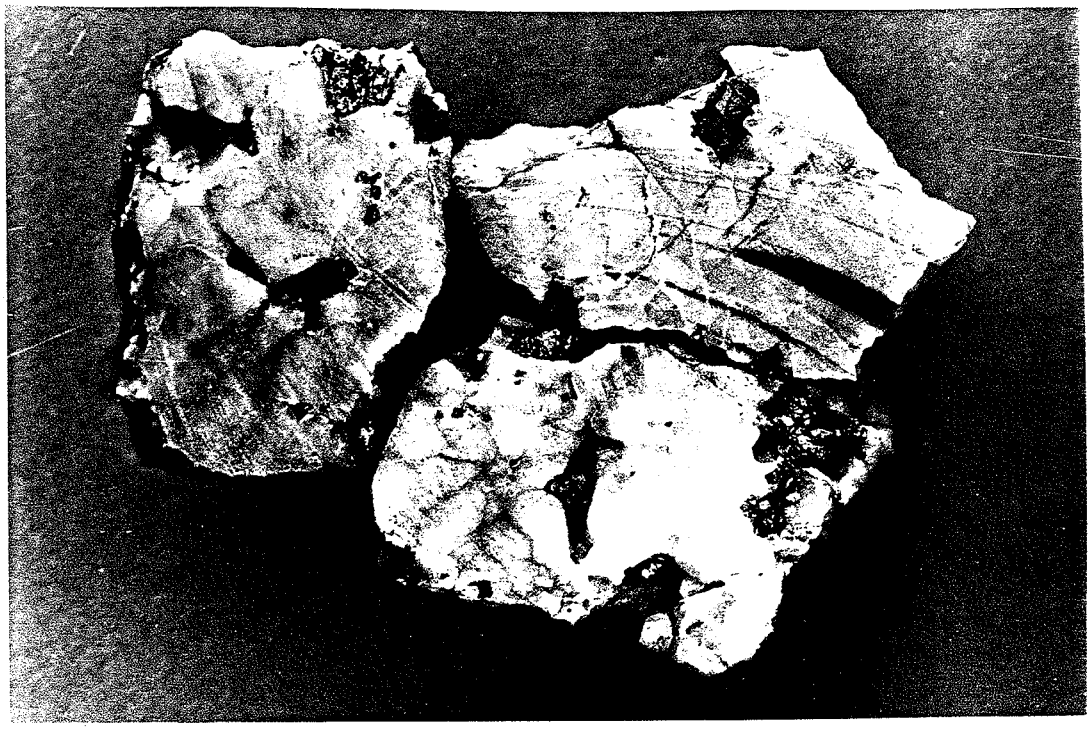

Plate 21 Samples of South zone quartz veins showing the development of vugs and cavitities enclosing pyrite, galena and sphalerite.

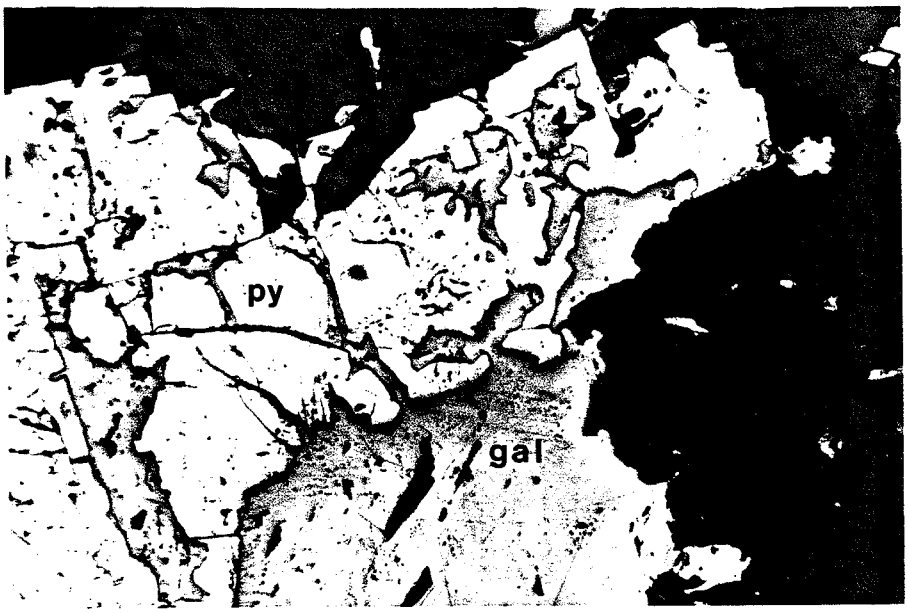

Plate 22 Polished section showing pervasive replacement of pyrite by galena. Width of field of view is 2.1 mm.

important source of silver during the period of mine production. There is, however, no evidence for the presence of a separate Ag-bearing mineral phase.

Sphalerite occurs largely as dark brown, anhedral crystals and more rarely as honey coloured crystals in calcite filled micro-veinlets that cut the main quartz veins. It commonly displays a texture with chalcopyrite which until recently has been interpreted to represent exsolution (Plate 23). The high proportion of chalcopyrite in some St. Robert sphalerite crystals is consistent with the proposal of Wiggins and Craig (1980) that "chalcopyrite disease" represents the replacement of sphalerite by chalcopyrite. Some sphalerite, particularly in late-stage vugs and cavities in South zone veins, occurs as large, euhedral crystals. Textural evidence clearly indicates that sphalerite postdated the precipitation of scheelite and appears to have either co-precipitated or immediately preceded precipitation of galena. It displays close spatial association with galena and rarely are textures observed that could be interpreted as replacement of one of these minerals by the other.

Pyrite is almost ubiquitously present as cubic crystals within secondary fractures in the quartz veins and shows varying degrees of replacement by later minerals (eg. galena, Plate 22). In a few cases, pyrite displays colloform textures possibly indicating its precipitation from a gel or colloid (Plate 24). In general, it is possible to distinguish at least three distinct generations of pyrite: an early generation which fills, along with some additional quartz, secondary fractures in the main North zone quartz veins; a later generation occurring within micro-veinlets filled largely by calcite that cross-cut the main quartz veins and the secondary fractures within them; and a presumably late generation which occurs within the vugs of the South zone (Plate 21).

Chalcopyrite and pyrrhotite are present in minor amounts as anhedral blebs or inclusions within sphalerite and/or pyrite crystals. Pyrrhotite is also sometimes seen as pseudomorphs of authigenic pyrite cubes in sedimentary rocks which have been affected by the biotite hornfelsing event (Plate 25). These occurences of pyrrhotite are interpreted to represent desulphurization of pyrite during thermal metamorphism (py --> po + 1/2 S_2).

Limonite occurs in minor amounts as late-stage encrustations forming network-like structures enclosing earlier sulphide and oxide ore minerals (Plate 26).

2.5 Mineral Distribution and Paragenesis

The distribution of sulphide and oxide minerals in vertical veins varies according to whether the veins occur in the North, South or Central zones. North zone veins are mineralized mainly in cosalite (up to 10% by mode), and pyrite (up to 5%), as well

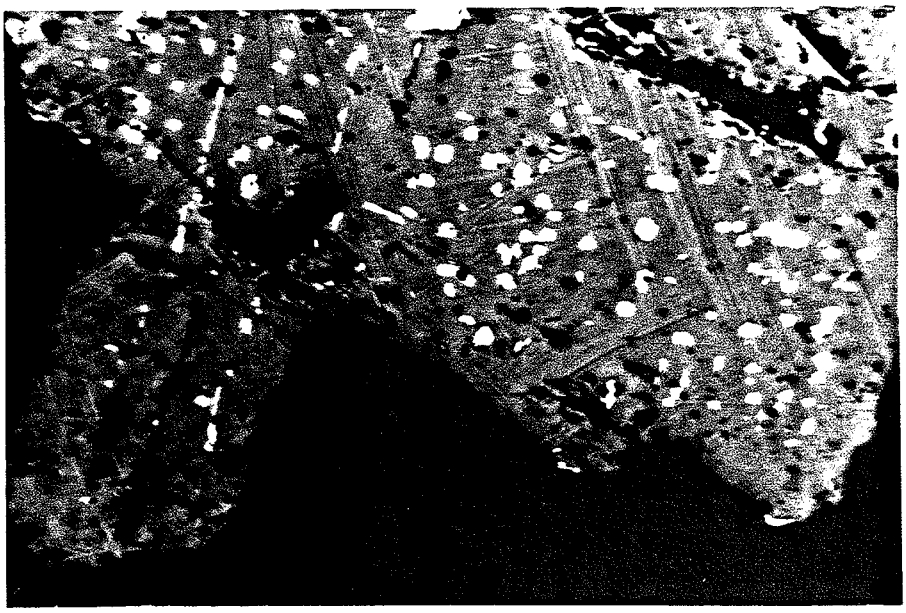

Plate 23 Polished section showing replacement of sphalerite by chalcopyrite. Width of field of view is 2.1 mm.

Plate 24 Polished section showing the development of colloform pyrite. Width of field of view is 2.1 mm.

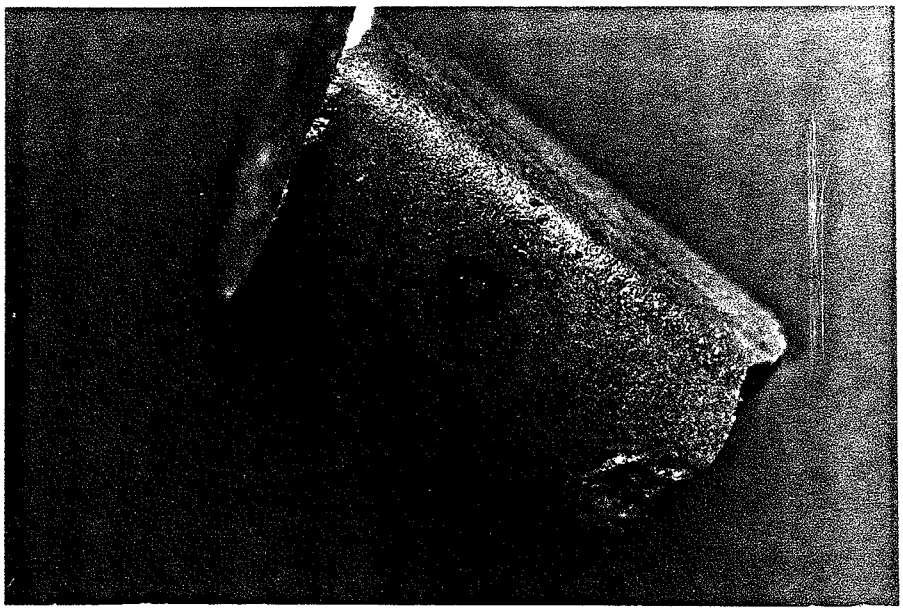

Plate 25 Core sample of thermally metamorphosed sediment showing the replacement of authigenic pyrite by pyrrhotite.

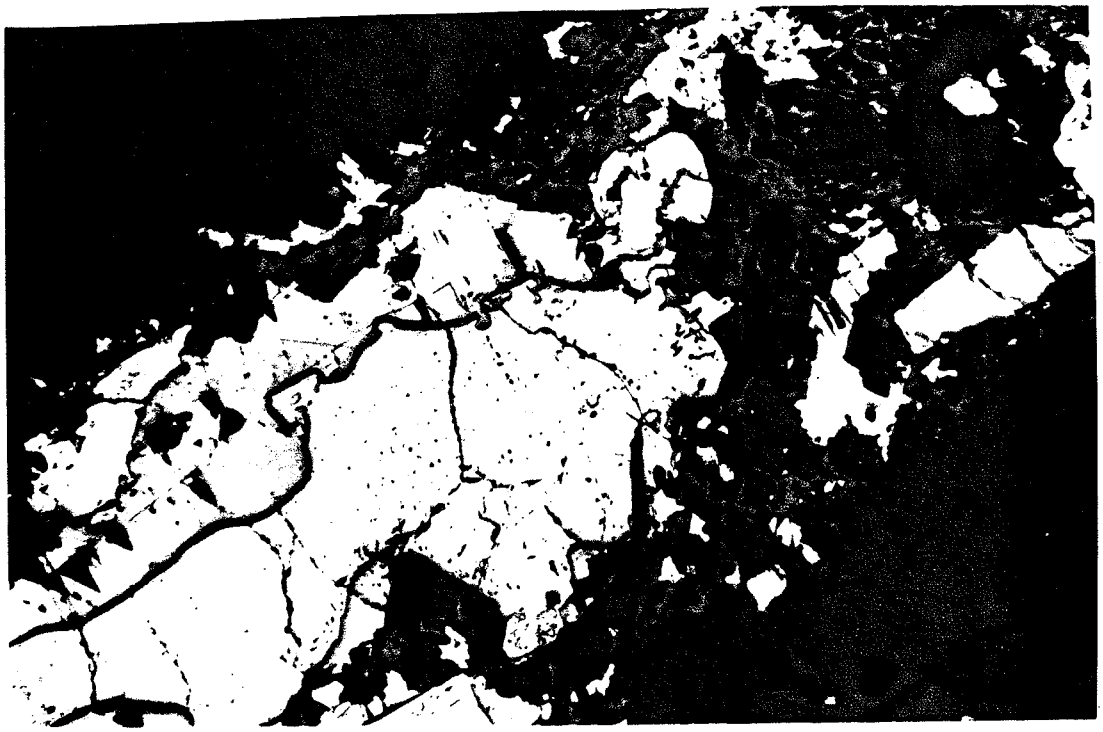

Plate 26 Polished section showing the late development of finely meshed limonite encrustations. Width of field of view is 2.1 mm.

as in minor amounts of argentiferous galena (<1%), sphalerite (<1%), and scheelite (<1%). Centre zone veins contain mostly scheelite (up to 10%), with lesser pyrite (5-10%), sphalerite (<5%), argentiferous galena (<5%), and minor cosalite (<1%). South zone veins contain abundant argentiferous galena (5-10%), sphalerite (5-10%), and pyrite (up to 10%), as well as minor scheelite (<1%). Subhorizontal veins occur in the Centre and North zones and are comparatively more mineralized than all other vein sets. In particular, they contain the highest scheelite concentrations found anywhere on the property, up to 25-30% of the veins by mode. Other minerals present in subhorizontal veins include pyrite (<5%), sphalerite (<5%), and argentiferous galena (<5%).

The deposit may thus be described as consisting of subvertical vein sets forming a southern, silver-rich zone, a central, tungsten-rich zone, and a northern, bismuth-rich zone. Subhorizontal vein sets served to enrich the Centre and North zones in tungsten.

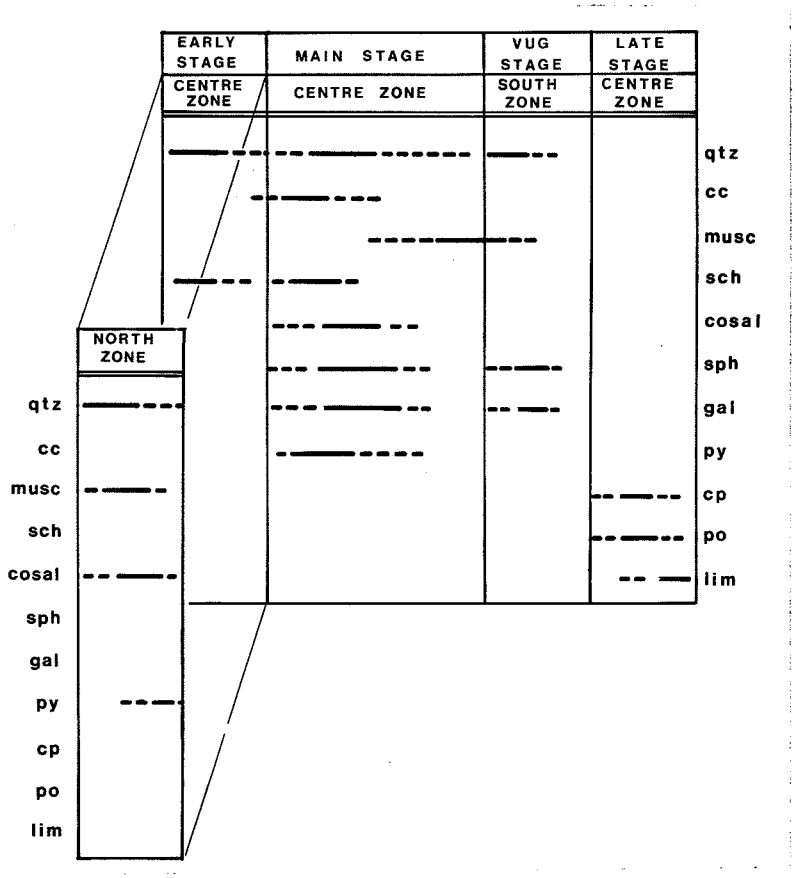

Figure 6 Paragenetic diagram for the sulphide, oxide and gangue mineralogy in the hydrothermal quartz veins. Early stage mineralization in the Centre and North zones are shown here as offsets in order to indicate that they formed simultaneously. Note: main stage and late stage mineralization is largely restricted to the Centre zone veins whereas vug stage mineralization is restricted to South zone veins.

The order of appearance, or paragenetic sequence of the minerals found within the various quartz veins on the property, can be deduced from the petrographic observations described earlier. The sequence of mineral precipitation at St. Robert can be generalized as follows: an early quartz stage which served to form the bulk of the veins and which contained scheelite in the Centre zone and cosalite, pyrite and muscovite in the North zone; tungsten enrichment (secondary scheelite) and introduction of base metal mineralization (galena, sphalerite, pyrite and cosalite as inclusions in galena) contained within late fractures and stringers related to cross-cutting subhorizontal veining inthe Centre and North zones; late-stage vug formation dominated by galena, sphalerite and pyrite mineralization with quartz and fine-grained muscovite appearing as gangue; late-stage replacement of pyrite and sphalerite by minor chalcopyrite and/or pyrrhotite and late encrustations by limonite. Figure 6 represents a generalized paragenetic sequence for the various stages of mineralization observed at St. Robert.

3- FLUID INCLUSION STUDY

3.1 Sample Preparation

A total of 44 doubly polished thin sections and 14 single quartz crystals were prepared for microthermometric analysis. Owing to the opaque nature of the quartz, a total of only 27 doubly polished sections and single crystals of quartz from various scheelite and sulphide-bearing quartz veins could be used for this study. The samples represent all four vein sets on the St. Robert property. A total of 517 fluid inclusions were investigated microthermometrically. Of these, 26 were scheelite-hosted and 8 were sphalerite-hosted inclusions. 77 of the quartz-hosted inclusions were also analyzed using a laser Raman microprobe.

3.2 Fluid Inclusion Petrography

After careful inspection of each sample, it was found that individual inclusions could generally be classified as carbonic or aqueous. Both inclusion types occur in all four vein sets. The ratio of carbonic to aqueous inclusions is about 5:1, and this ratio is generally constant in all four vein sets. This ratio appears to be maintained in scheelite and sphalerite, although no aqueous inclusions were analyzed from these minerals. Inclusions were classified as either primary, pseudosecondary, or secondary in origin, using the criteria for origin given in Roedder (1981). Although none of the inclusions characterized as primary occured along growth planes, many of them were large, isolated, and randomly distributed within the host mineral. Many of the inclusions analyzed had negative crystal morphology. Although this has often been presented as proof of primary origin, it may in many cases represent a negative criterion for primary origin (Roedder, 1981). The observation of such inclusion morphology was therefore not used as a criterion for origin.

3.21 Carbonic Inclusions

Carbonic inclusions contain 1 to 3 phases (liquid H_2O, and/or carbonic liquid, and/or carbonic vapour, Plates 27 to 29). They show highly variable carbonic fluid/H_2O volume ratios (estimated visually at a constant temperature of 40°C) ranging from nearly pure H_2O to pure carbonic fluid (liquid or vapour). Such variability can commonly be seen within 100 to 200 μm^2 areas of thin sections (Plate 30). Carbonic inclusions vary from a few micrometres to almost 100 micrometres in diameter. Their morphology is, in many cases, that of equant to slightly elongated negative crystals and they occur largely as isolated primary to pseudosecondary varieties. In a small number of cases, carbonic fluid inclusions occur in trains, and probably are of secondary origin (Plate 31).

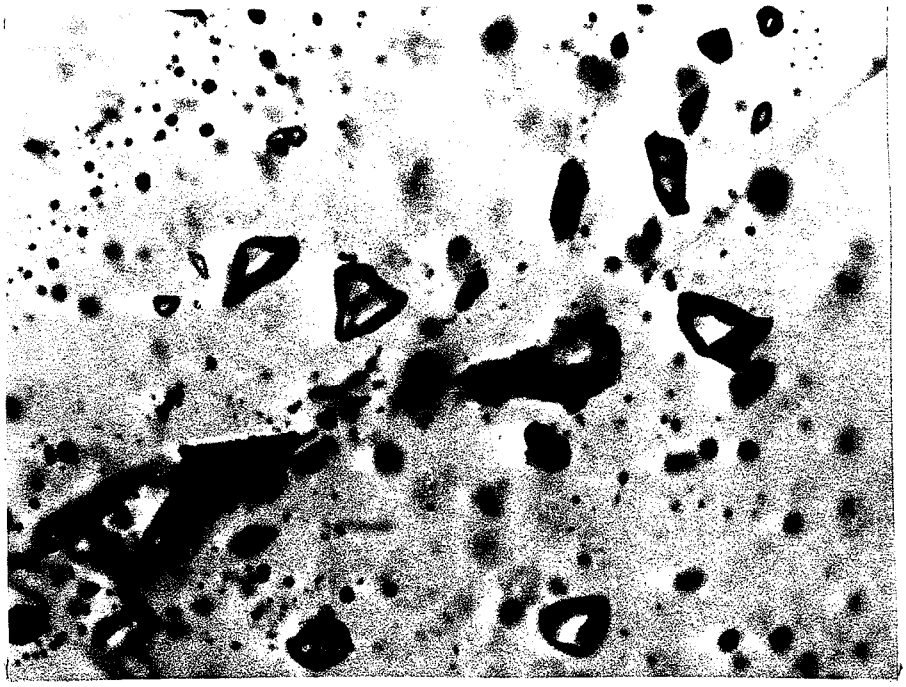

Plate 27 Single-phase vapour carbonic inclusions. Width of field of view is 0.21 mm.

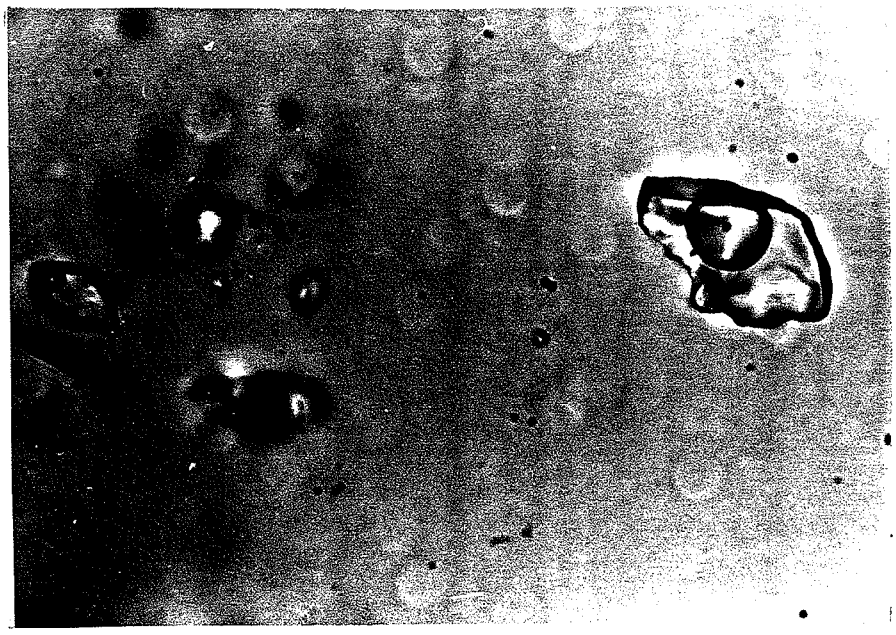

Plate 28 Two phase (H_2O liquid, carbonic vapour) carbonic inclusions. Width of field of view is 0.53 mm.

Plate 29 Three phase (H_2O liquid, carbonic liquid outer bubble, carbonic vapour inner bubble) carbonic inclusions. Width of field of view is 0.1 mm.

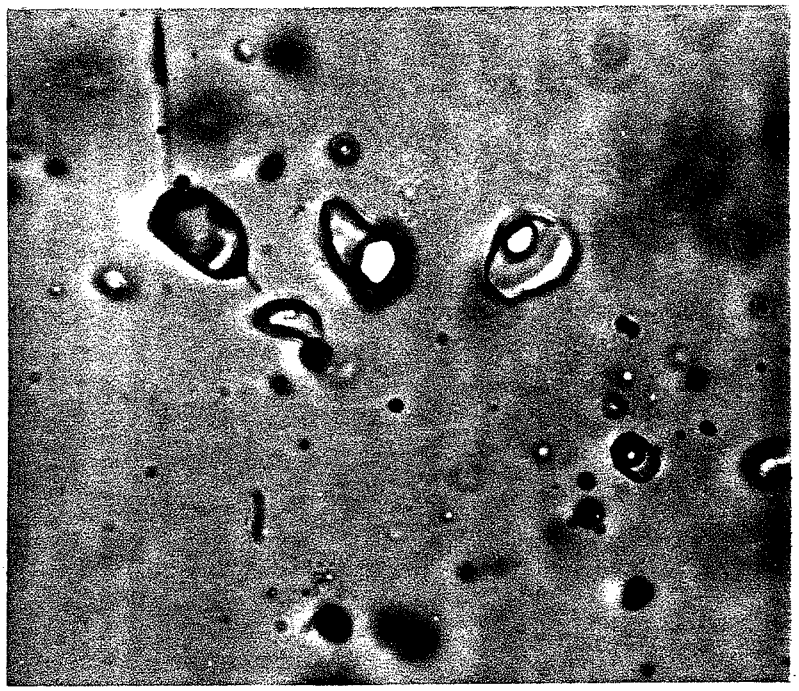

Plate 30 Group of carbonic inclusions showing highly variable phase relations. Width of field of view is 0.1 mm.

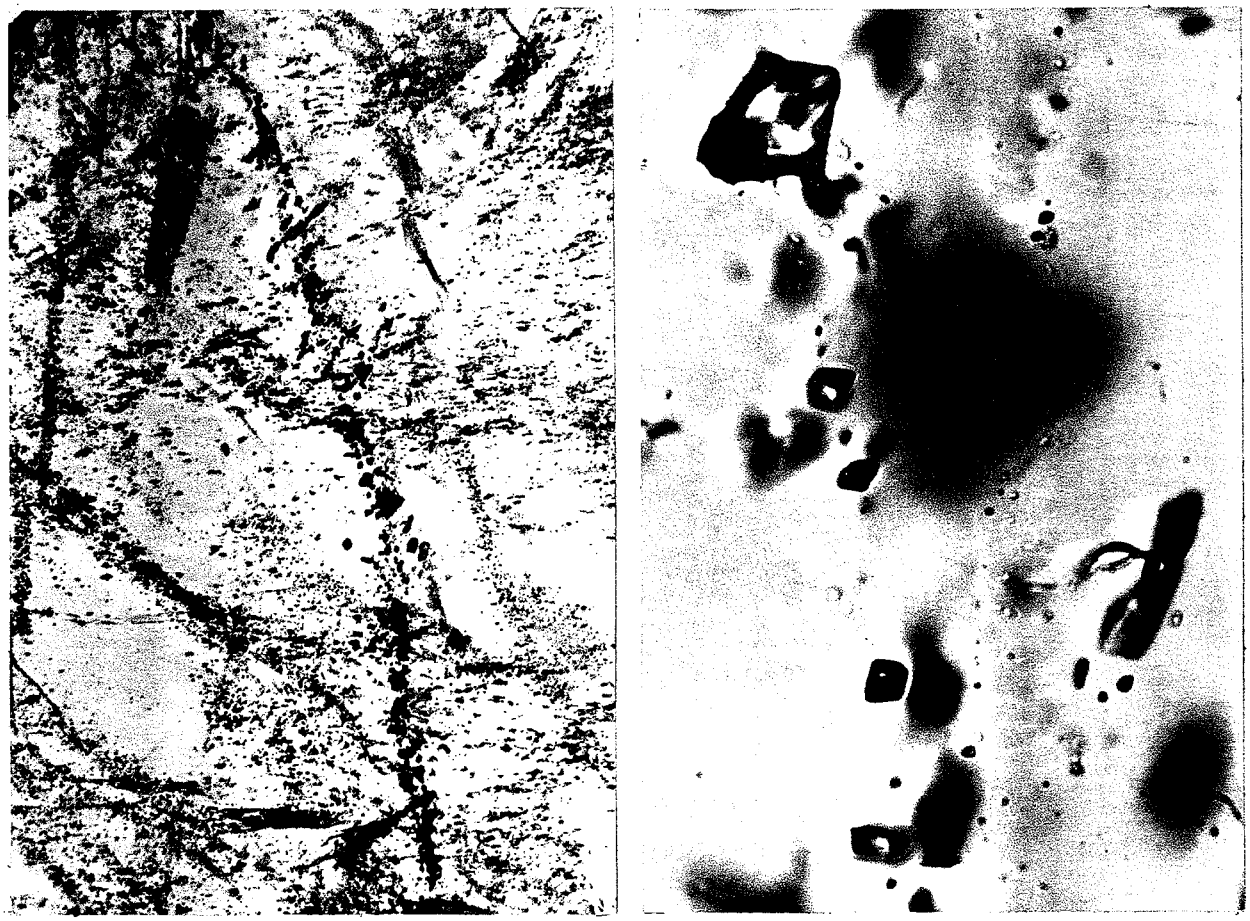

Plate 31 Healed fracture filled by single-phase vapour carbonic inclusions. Width of field of view is 8.0 mm (left) and 0.21 mm (right).

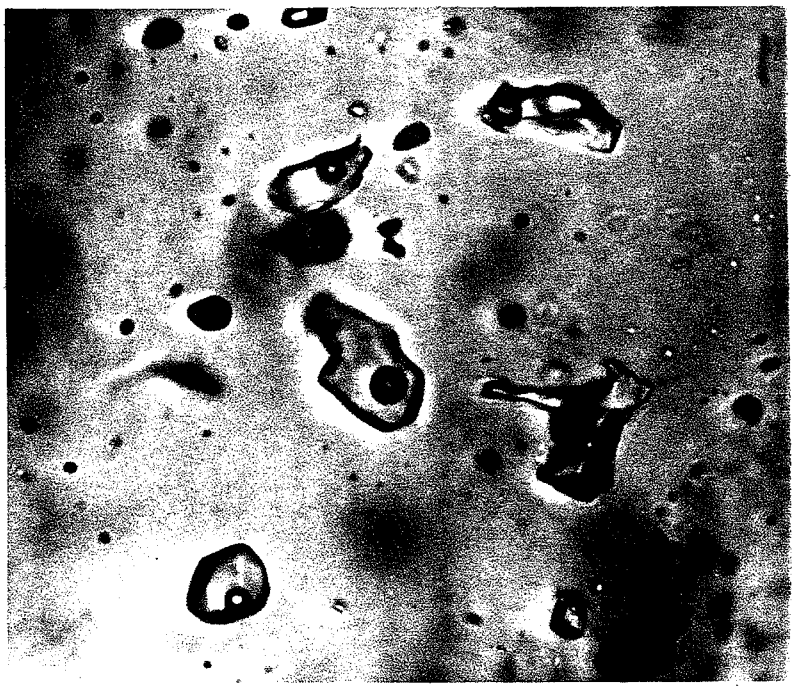

Plate 32 Group of aqueous inclusions. Width of field of view is 0.21 mm.

3.22 Aqueous Inclusions

Aqueous inclusions are two-phase (liquid, vapour) with high liquid/vapour ratios from 9:1 to 99:1 (Plate 32). They range from a few micrometres to well over 100 micrometres in diameter. They are commonly irregular in shape, and generally occur along healed fractures of clearly secondary origin. They are rarely isolated.

3.3 Microthermometric Analysis

3.31 Equipment and Methodology

Microthermometric analysis of the fluid inclusions was performed using an S.G.E., Model III heating-freezing stage based on a U.S.G.S. design. A technical description of this type of stage was first given in Werre et al. (1979), and is reviewed in Hollister et al. (1981). Temperatures of the various phase changes observed were measured using a chrome-alumel thermocouple, and were recorded on a digital trendicator. Gas flow was controlled by a valve which allowed the heating rate to be maintained below 1°C per minute, thus minimizing the chance of metastable phase changes.

The first step in the microthermometric analysis of a sample involved cooling it down to $< -135°C$ with a flow of N_2 gas that had been passed through a copper coil immersed in liquid nitrogen. The sample was then slowly warmed, first by reducing or stopping the flow of N_2 gas, and subsequently by heating the N_2 gas by passing it through a heating coil connected to a rheostat.

The following phase changes were measured for each inclusion: melting temperature of the carbonic phase, initial melting temperature of the H_2O ice (eutectic temperature), final melting temperature of the H_2O ice, final melting temperature of the clathrate, homogenization temperatures of carbonic phases, homogenization and decrepitation temperatures of the inclusion. Other fluid inclusion data collected included size, occurrence, and vapour to liquid ratio (at a constant temperature of 40°C).

3.4 Homogenization Data

3.41 Aqueous Inclusions

The homogenization and decrepitation data for the aqueous inclusions are displayed in a composite frequency histogram (Fig. 7), combining the results of the four vein sets described above. The four vein sets were treated collectively for the following reasons: little or no difference in data distribution was discernible between one vein set and another; aqueous inclusions are largely secondary in origin and probably post-date mineralization. Most of the aqueous inclusions homogenized

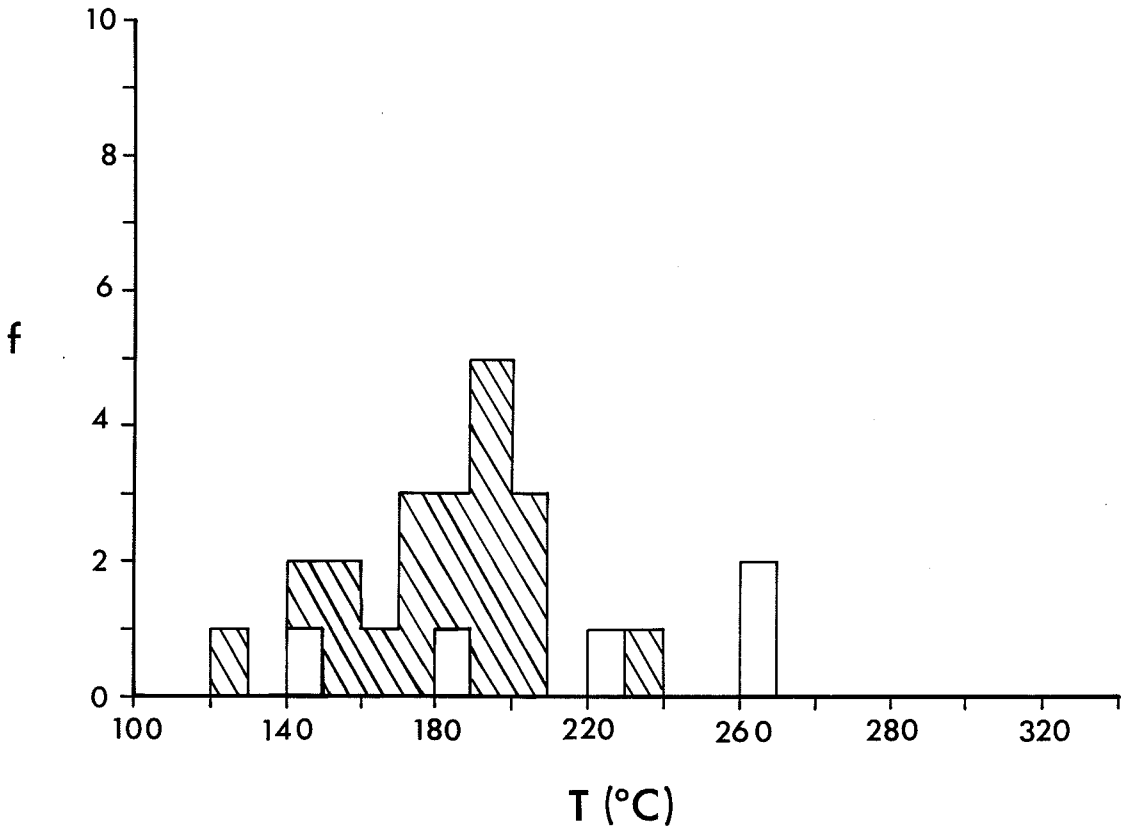

Figure 7 Composite homogenization/decrepitation temperature histogram for aqueous inclusions.

completely prior to decrepitating making the acquired data a reliable estimate of the minimum temperature of trapping. Aqueous inclusions show homogenization/decrepitation temperatures ranging from 120° to 270°C, with a peak between 170° and 210°C.

3.42 Carbonic Inclusions

An attempt to homogenize carbonic inclusions resulted in a high proportion of these inclusions decrepitating prior to complete homogenization. This observation is predictable from the fact that due to the high coefficient of thermal expansion of carbonic fluids, a small increase in temperature produces a large increase in internal pressure (Burruss, 1981). Thus, heating of inclusions to temperatures just slightly above those of entrapment will tend to produce internal pressures which exceed the strength of the quartz. For this reason, decrepitation and homogenization data for each vein set were plotted collectively. Frequency versus homogenization/ decrepitation temperature histograms similar to that for aqueous inclusions are presented for carbonic inclusions representing each of the four vein sets (Fig. 8 a-d). Homogenization/ decrepitation data for carbonic inclusions in scheelite are indicated separately on Fig. 8. Similar data for sphalerite were not gathered.

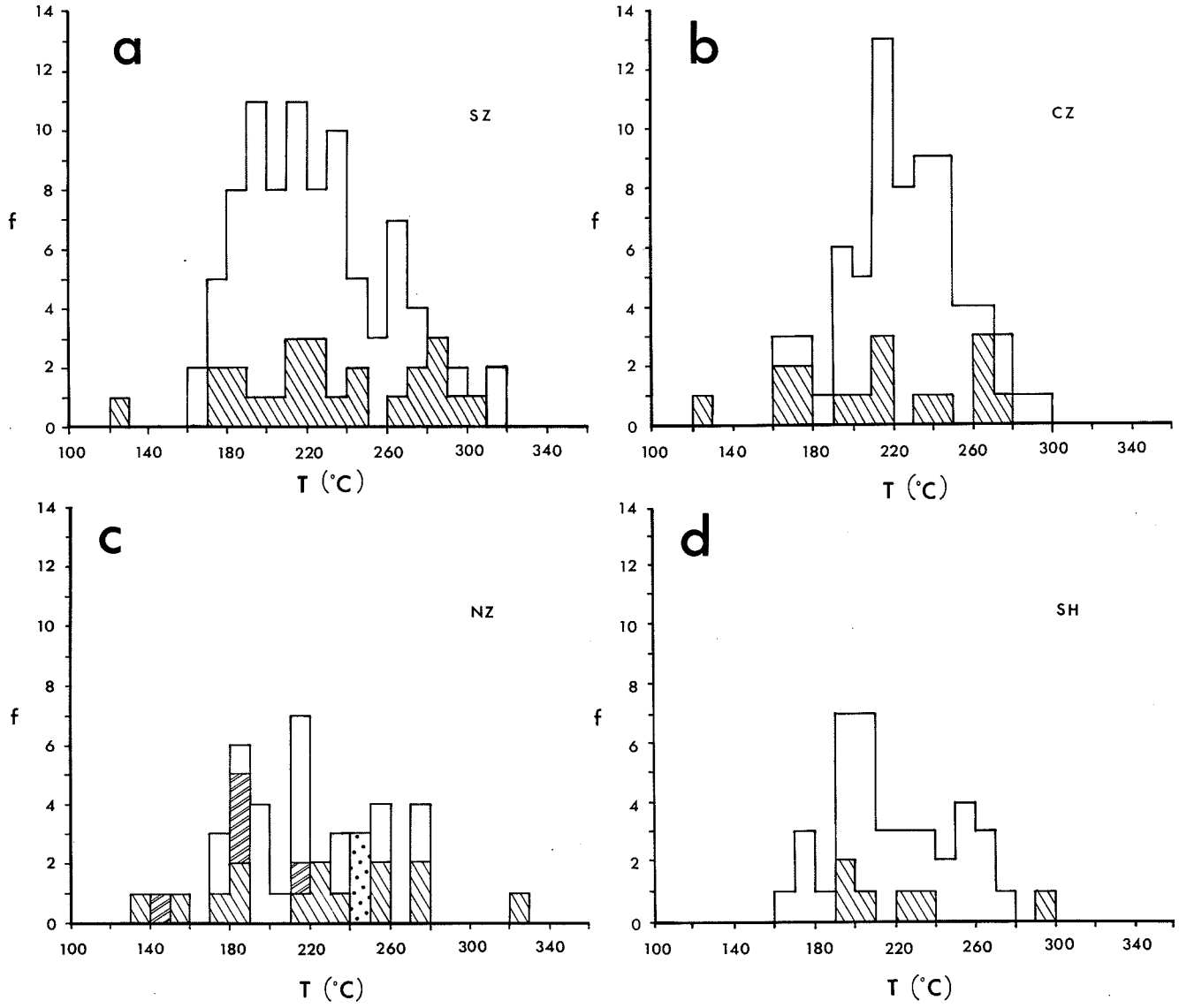

Figure 8 Composite homogenization/decrepitation temperature histograms for carbonic inclusions from the four vein sets. Open fields represent decrepitation of quartz-hosted inclusions, single-dashed fields represent homogenization of quartz-hosted inclusions, double-dashed fields represent decrepitation of scheelite-hosted inclusions, dotted fields represent homogenization of scheelite-hosted inclusions.

Although a large majority of carbonic inclusions decrepitated prior to homogenizing, those that homogenized, did so at temperatures higher than the homogenization temperatures for aqueous inclusions. The South zone vein set shows a range in homogenization/decrepitation temperatures from 120° to 300°C with a broad primary peak between 180° and 240°C, and a possible secondary peak at about 260° to 270°C. The Centre zone veins display a range in homogenization/decrepitation temperatures from 120° to 300°C, with a sharp, narrow peak between 210° and 250° C. The range in temperature for the North zone vein set is from 130° to 330°C, with a broad peak between 170° to 280°C. Subhorizontal veins show homogenization/decrepitation temperatures ranging from 160° to 300°C, with a possible bimodal distribution in which the main peak occurs between 190° and 210°C and the secondary peak is from 250° to 270°C. Homogenization and decrepitation temperatures from scheelite-hosted inclusions range from 240° to 250°C and 140° to 220°C respectively, i.e. they fall within the corresponding range for carbonic inclusions in quartz.

3.5 Melting Data

3.51 Aqueous Inclusions

Melting data measured for aqueous inclusions include the temperature of first melting of the H_2O ice (eutectic temperature) and the final melting of the H_2O ice. Accurate eutectic temperatures are generally difficult to establish. For this reason, eutectic data gathered for this study represent the average of several individual readings. The eutectic temperatures for aqueous inclusions are presented on Fig. 9, and range from -35° to -16.5°C with a well developed peak between -30° and -22.5°C.

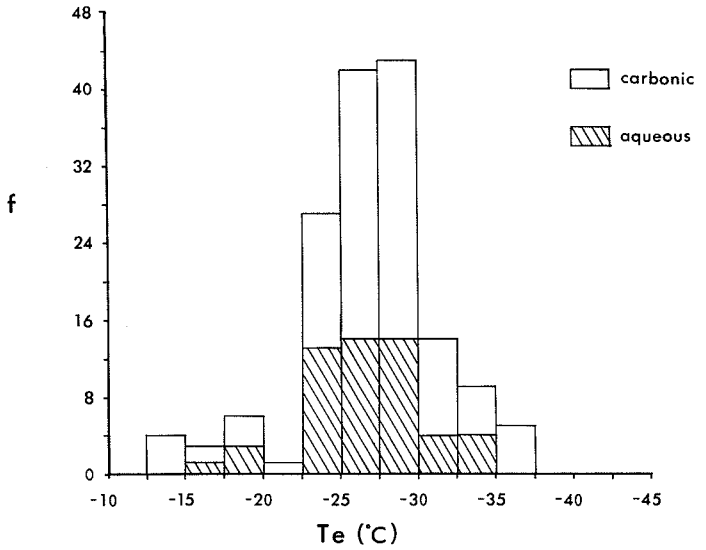

Figure 9 Composite eutectic temperature diagram for carbonic (open fields) and aqueous (dashed fields) inclusions.

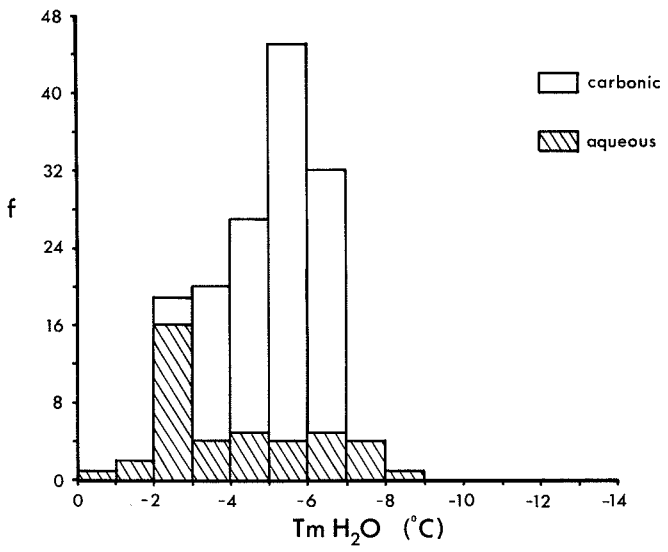

Figure 10 Composite histogram plotting final melting temperature of H_2O for carbonic (open fields) and aqueous (dashed fields) inclusions.

Final melting temperatures of H_2O ice for aqueous inclusions are plotted against frequency on Fig. 10. The observed range in temperature is from -6.8° to -0.3°C, with a mean of -3.7°C. The significance of the melting data for aqueous inclusions will be discussed in later sections.

3.52 Carbonic Inclusions

Melting data measured for carbonic inclusions include the final melting temperature of carbonic ice, the initial melting temperature of H_2O ice (eutectic temperature), the final melting temperature of H_2O ice, and the final melting temperature of clathrate. These data are summarized for each vein set in Table 1. Histograms of frequency versus the initial melting temperature of H_2O ice (eutectic temperature) and final melting temperature of H_2O ice are presented in Fig. 9 and Fig. 10, respectively. An X-Y plot of the final melting temperature of carbonic ice versus the final melting temperature of clathrate is presented in Fig. 13. The significance of the melting data presented in these figures is discussed in detail in later sections.

3.6 Salinity Data

3.61 Aqueous Inclusions

Final melting point temperatures of H_2O ice (Tm_{ice}) were used to determine salinities for aqueous inclusions using the equation developed by Potter et al. (1978), in which the concentration of dissolved salts is given as weight percent NaCl equivalent:

	Te (°C)		Tm H_2O ice (°C)	
Veins	Range	Mean	Range	Mean
South	-33.4 to -22.0	-29.4	-7.8 to -2.1	-4.8
Centre	-37.0 to -14.0	-26.9	-7.0 to -3.6	-5.5
North	-40.0 to -24.0	-31.8	-6.5 to -3.9	-5.2
Subh.	-31.0 to -24.0	-27.9	-8.0 to -3.9	-5.5
	Tm carbonic ice (°C)		Tm clathrate (°C)	
Veins	Range	Mean	Range	Mean
South	-62.7 to -55.0	-57.6	4.9 to 11.5	7.6
Centre	-64.2 to -57.1	-58.7	4.9 to 16.1	8.0
North	-60.0 to -55.8	-57.4	6.8 to 10.0	7.1
Subh.	-75.5 to -56.7	-61.7	4.9 to 17.0	9.0
sph.(Cz)	-62.6 to -57.1	-58.9	10.3 to 16.1	3.2
sch.(Nz)	-59.8 to -55.8	-57.5	7.6 to 10.1	9.2
sch.(Cz)	-59.8 to -58.0	-58.8	no data	

Table 1 Eutetic temperature, final melting of H_2O ice, final melting of carbonic ice and clathrate melting temperatures for carbonic inclusions in quartz, sphalerite and scheelite in the four vein sets.

$$\text{Salinity} = 1.76958\ Tm_{ice} - 3.2384\times10^{-2}\ Tm_{ice}^{2} + 5.2778\times10^{-4}\ Tm_{ice}^{3} \pm 0.028$$

The range of salinity for aqueous inclusions is from 0.52 to 16.82 equivalent Wt% NaCl, with a mean salinity of 8.13 equivalent Wt% NaCl. Salinities for aqueous inclusions are plotted against homogenization or decrepitation temperatures in Fig. 11. This figure shows a single distribution of data ranging from approximately 4 Wt% NaCl equivalent to 15 Wt% NaCl equivalent. There is no obvious correlation of salinity with temperature.

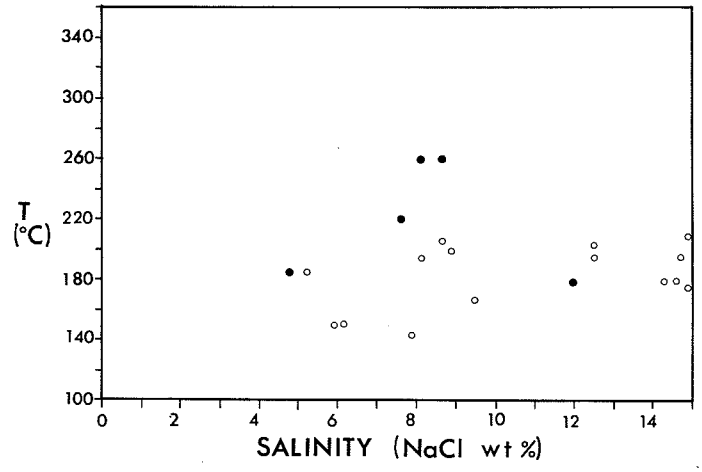

Figure 11 Composite homogenization/decrepitation temperature versus salinity diagram for aqueous inclusions. Open circles represent homogenization, closed circles represent decrepitation.

3.62 Carbonic Inclusions

Salinities for carbonic inclusions were calculated using the method outlined by Bozzo et al. (1973), in which the clathrate melting temperature is related to the salt content of the fluid by the following equation:

$$\text{Wt\% NaCl equiv.} = 0.05286\ (10 - Tm_{clath}) \times (Tm_{clath} + 29.361)$$

The salinities of the carbonic inclusions in the four vein sets are summarized in Table 2 presented below.

	Salinity (Wt % NaCl)	
Veins	Range	Mean
South	0 to 9.24	4.75
Centre	0 to 7.97	4.08
North	0 to 7.48	4.60
Subh.	0 to 9.24	3.21
sch.(NZ)	0 to 4.69	1.51

Table 2 Salinities of carbonic inclusions in quartz and scheelite from the four vein sets.

Salinities of carbonic inclusions are plotted against homogenization or decrepitation temperature in Fig. 12. South zone and Centre zone inclusions (Fig. 12 a and 12 b) show a unimodal distribution ranging from 0 to about 9 Wt% NaCl equivalent over a temperature range from 160° to 300°C. By contrast, North zone inclusions (Fig. 12 c) clearly show a bimodal distribution with a cluster of points in the salinity range from 1 to 3 Wt% NaCl equivalent, and a second cluster ranging from 5 to 8 Wt% NaCl equivalent. The range in temperature is similar to that seen in Fig. 12 a and 12 b. There is some indication that the subhorizontal vein inclusions also have a bimodal salinity distribution, with a series of data points tightly clustered around 2 to 3 Wt% NaCl equivalent, and a few scattered points ranging from about 5 to 9 Wt% NaCl equivalent. Equivalent data from scheelite-hosted inclusions was gathered only from samples originating from North zone veins. Salinity for these inclusions ranges from 0 to 4.69 Wt% NaCl equivalent, with a mean of 1.51 Wt% NaCl equivalent. These data do not appear on Figure 12 because corresponding homogenization/ decrepitation temperatures for these inclusions were not recorded.

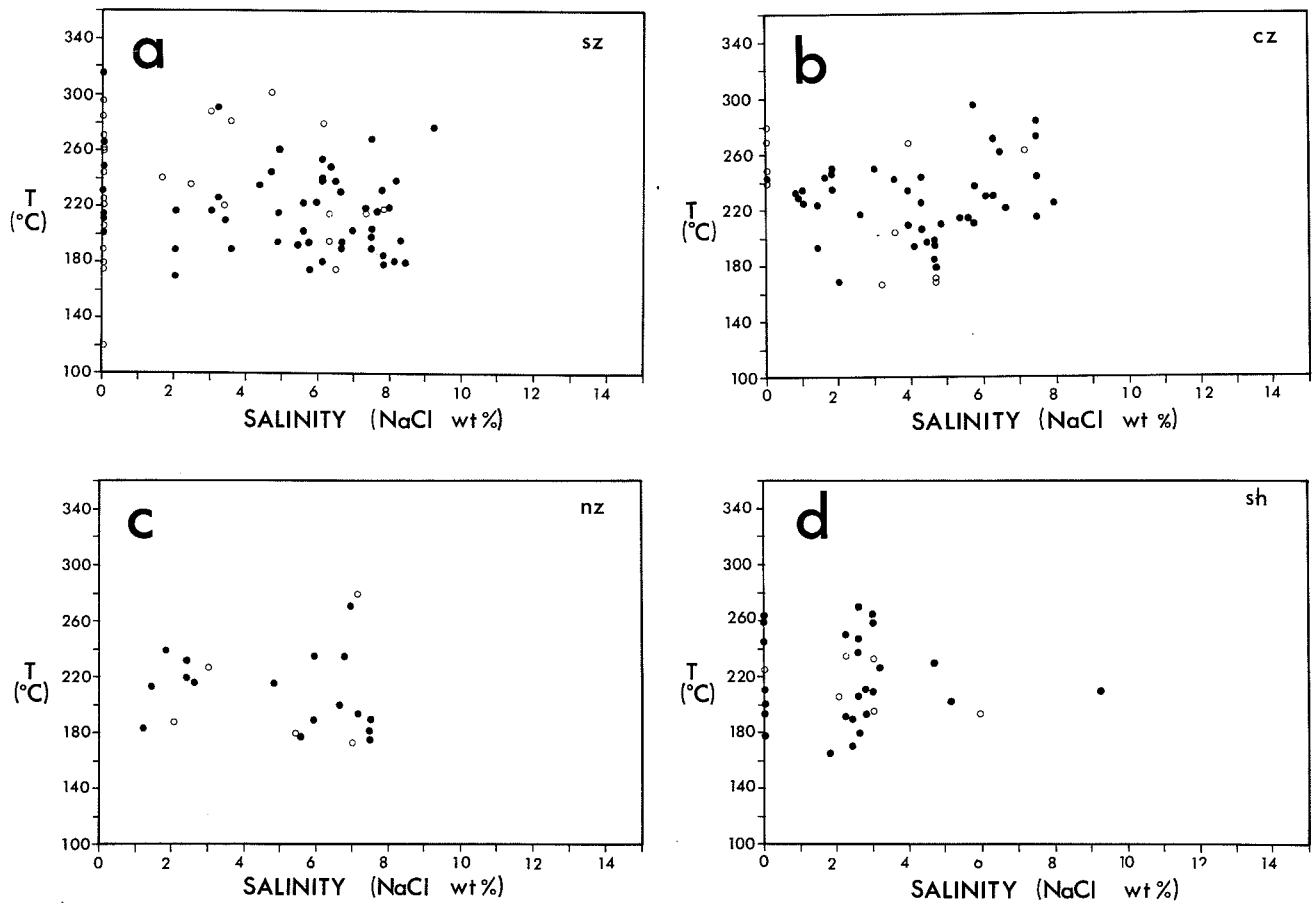

Figure 12 Composite homogenization/decrepitation temperature versus salinity diagrams for carbonic inclusions in the four vein sets. Open circles represent homogenization, closed circles represent decrepitation.

3.7 Nature of Dissolved Species

3.71 Aqueous Inclusions

The eutectic temperatures of liquid H_2O for aqueous inclusions, as discussed earlier, show a very well defined peak within the range -23° to -30°C. This range in eutectic temperatures falls well below the stable eutectic point (-20.8°C) for a pure H_2O-NaCl solution, and therefore suggests the presence of additional dissolved species in the H_2O liquid fraction of the aqueous inclusions. Candidates for these additional species include $MgCl_2$ and $CaCl_2$ (Crawford, 1981). It is suggested that the most likely species is $CaCl_2$ for the following reasons: the calcareous sediments serve as hosts to the quartz veins; and there is a predominance of carbonic inclusions which probably reflect the dissolution of calcareous rocks.

3.72 Carbonic Inclusions

3.721 Aqueous Phase

The range in the eutectic temperatures of liquid H_2O in carbonic inclusions is similar to that of the aqueous inclusions. This suggests that the aqueous phase of the carbonic inclusions also contains significant $CaCl_2$. It is, however, possible that CO_2 dissolved in the aqueous phase may be partly responsible for the low eutectic temperature measured in the carbonic inclusions (Higgins, 1985).

3.722 Carbonic Phase

A qualitative estimate of the composition of the carbonic phase in carbonic fluid inclusions can be made using the final melting temperature of the carbonic phase and the final clathrate melting temperature (Burruss, 1981). A final melting temperature below that of the liquid-solid-vapour invariant point (-56.6°C) for the pure CO_2 system, indicates an additional component dissolved in the carbonic fluid fraction. Additional dissolved components in the carbonic phase are also indicated by final clathrate melting temperatures above 10°C (Burruss, 1981).

Fig. 13 a-d plots the final melting temperature of carbonic ice versus the final clathrate melting temperature for carbonic inclusions in the South zone, Centre zone, North zone, and subhorizontal vein sets respectively. It is clear from Fig. 13 that inclusions in each vein set show a wide range of ice and clathrate melting temperatures and that the lowest final melting temperature corresponds to the highest final clathrate melting temperature, ie. that additional dissolved species are present in the carbonic phase in inclusions from all four vein sets. The data also suggest that this/these dissolved species is/are relatively more abundant in inclusions from the subhorizontal and Centre zone vein sets, and least abundant in inclusions from North zone veins. The most likely candidate for such a species is CH_4 (Swanenberg, 1979). Data from scheelite or sphalerite-hosted inclusions are few (Fig. 13). It is therefore difficult to draw any conclusions based on these data alone.

A more quantitative approximation of the composition of the carbonic phase can be made using the method outlined in Burruss (1981). This method provides estimates of the mole fraction of CH_4 and the molar volume of a carbonic inclusion based on the fact that all two-phase tie lines for a specific system must pass through the position of that system on a V-X (molar volume-mole fraction) diagram. Two such tie lines can be accurately drawn for each inclusion using the final melting temperature of the carbonic ice, and the final homogenization temperature of the carbonic phase. Their point of intersection defines the bulk composition and the molar volume of the corresponding system.

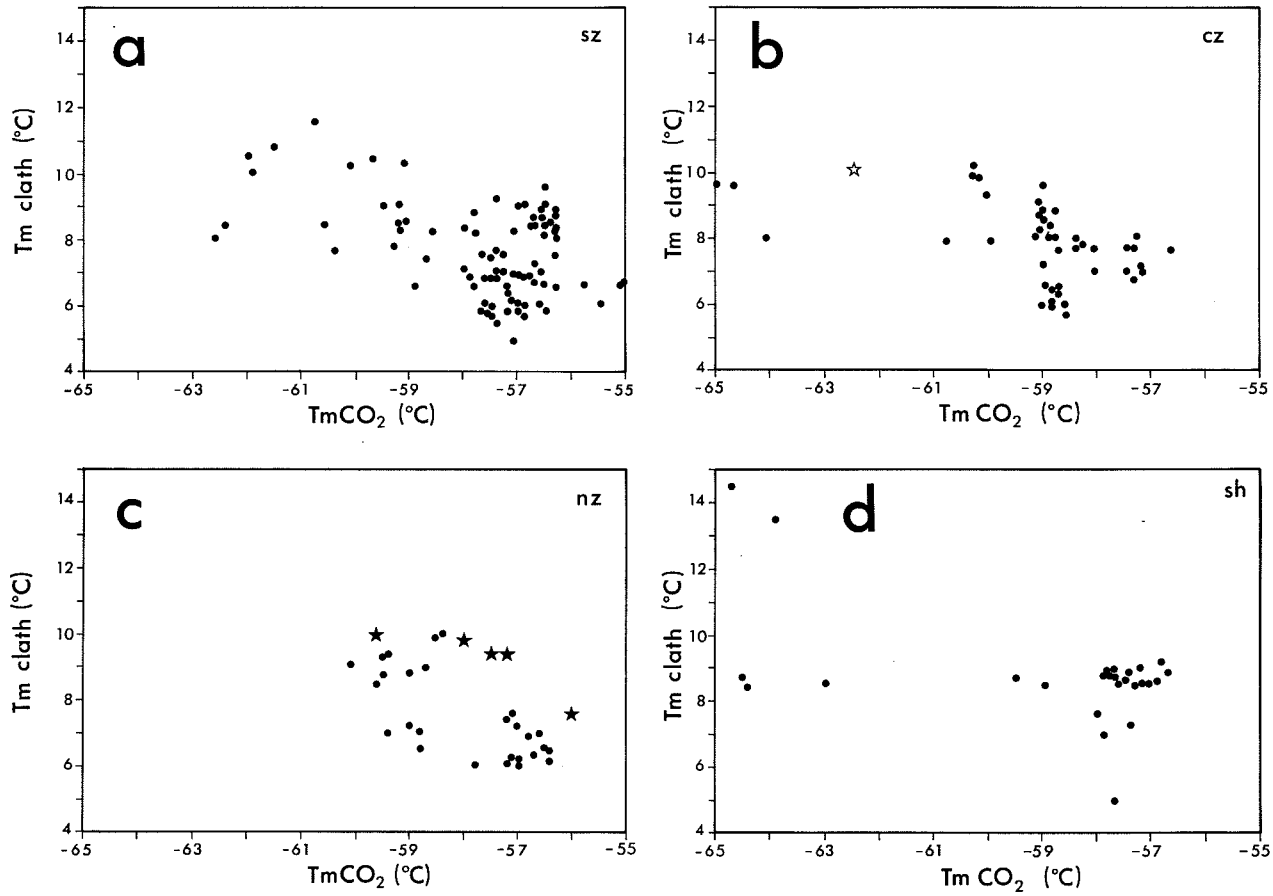

Figure 13 Diagrams plotting final clathrate melting temperature versus final melting temperature of carbonic ice for carbonic inclusions from the four vein sets. Circles represent quartz-hosted inclusions, open stars represent sphalerite-hosted inclusions, closed stars represent scheelite-hosted inclusions.

It should be noted that quantitative V-T-X data are available only for the pure CO_2-CH_4 system, and that any effect attributable to additional volatile species cannot be acounted for by this method. Nitrogen is the most important of these additional species and partitions largely into the vapour phase along with methane. The mole fraction CH_4 measured by this method is thus more accurately referred to as the equivalent mole fraction CH_4.

Fig. 14 shows the final melting temperature of carbonic ice versus the temperature of homogenization of the carbonic phase for inclusions in the South zone, Centre zone, North zone, and subhorizontal vein sets respectively. Figures 14 a - 14 c all contain relatively uniform, single distributions of points. The South zone vein inclusions show final melting temperatures of carbonic ice which range from about -63° to -55°C and a homogenization temperature for the carbonic phase which ranges from

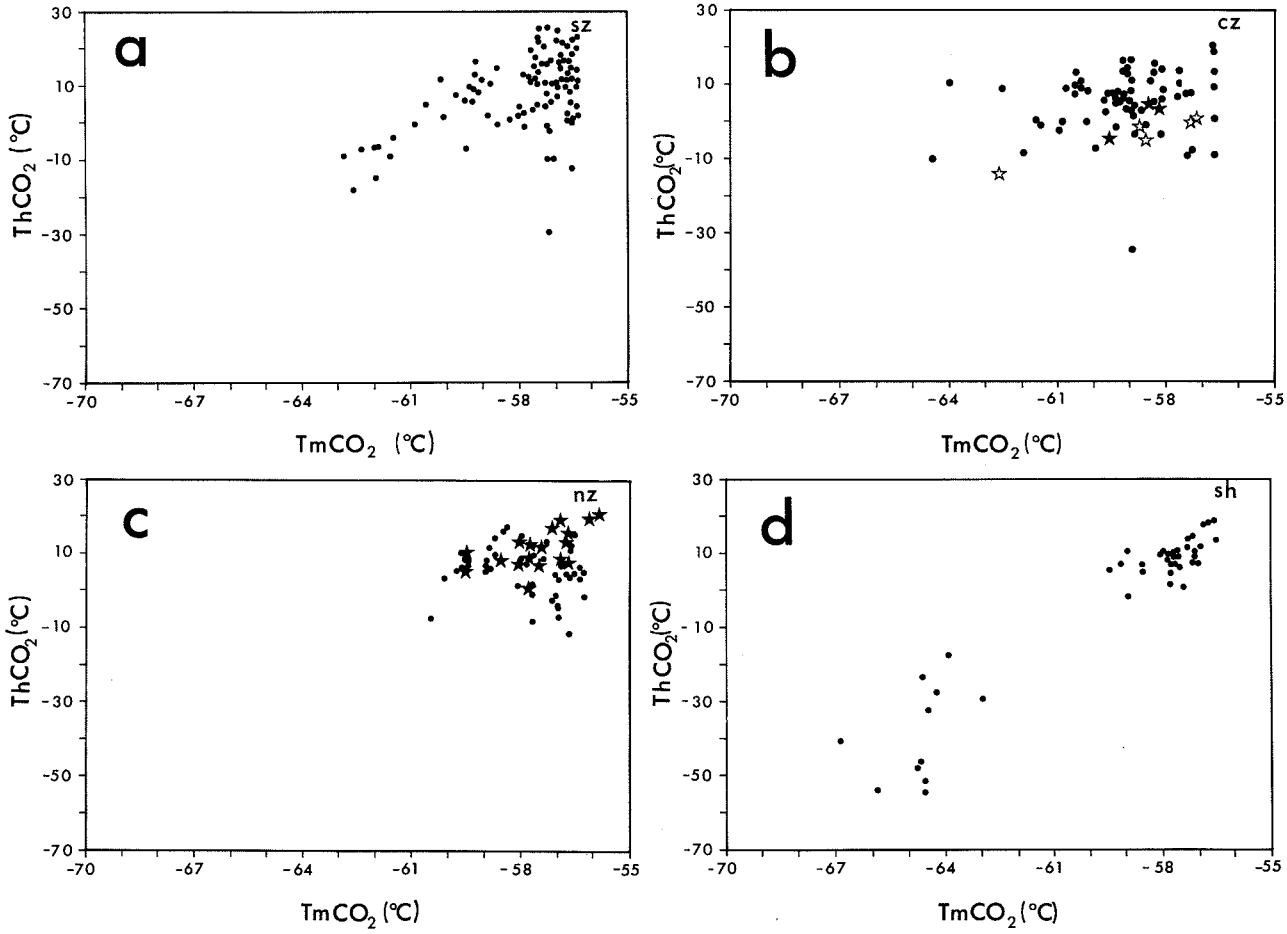

Figure 14 Diagrams plotting carbonic phase homogenization temperature versus final melting temperature of carbonic ice for carbonic inclusions from the four vein sets. Circles represent quartz-hosted inclusions, open stars represent sphalerite-hosted inclusions, closed stars represent scheelite-hosted inclusions.

about -20° to about 30°C. Centre zone vein inclusions show final melting temperatures ranging from about -64° to about -56°C and homogenization temperatures which range from about -30° to 25°C. North zone vein inclusions show a more restricted distribution in which the final melting temperature ranges from about -60° to -56°C and homogenization temperature ranges from about -15° to 20°C. By contrast, subhorizontal vein inclusions (Fig. 14d), show a clearly bimodal distribution of data in which the final melting temperature of carbonic ice ranges from -67° to -63°C and from -60° to almost -56°C. The corresponding temperatures of homogenization of the carbonic phase range from -55° to -15°C and from -5° to 20°C.

Data from scheelite and sphalerite range as follows: Centre zone scheelite-hosted inclusions show final CO_2 melting temperatures ranging from -59.8° to -58.0°C, and CO_2 homogenization temperatures from -7.0° to +4.8°C; final melting temperatures from North zone scheelite-hosted inclusions range from -59.6° to -55.8°C with homogenization temperatures ranging from -0.4° to +19.9°C; Centre zone sphalerite-hosted inclusions show final melting temperatures ranging from -62.6° to -57.1°C with homogenization temperatures ranging from -14.0° to -0.5°C. The distribution of data from scheelite and sphalerite-hosted inclusions is indistinguishable from that of inclusions in quartz.

In all cases, homogenization of the carbonic phase was to the vapour phase, reflecting the relatively low density of the additional components involved. Moreover, the lowest homogenization temperatures correspond to the lowest final melting temperatures, and an increase in one corresponds to an increase in the other. This confirms the conclusions drawn earlier that the carbonic phase contains varying amounts of an additional species and that this species is of relatively low density.

The equivalent mole fraction CH_4 and the molar volume of the carbonic phase, estimated using the method outlined above can, in turn, be used, along with several equations from Ramboz et al. (1985), reproduced in Appendix 3, to determine XH_2O and XCO_2. Fig. 15 plots the mole fraction H_2O of the inclusions versus the equivalent mole fraction methane of the carbonic phase for the four vein sets. In addition to CO_2 and CH_4, the carbonic phase is assumed to contain N_2, evidence for which will be presented later in the section on Raman analysis. The South and Centre zones are characterized by inclusions which have either low or high XH_2O. By contrast, North zone and Subhorizontal veins show a nearly complete range of XH_2O from 0 to 1, although inclusions with intermediate XH_2O are less common. Fig. 15 clearly indicates that in all four vein sets the highest methane and nitrogen contents occur in inclusions with high XH_2O or low XH_2O values. At high XH_2O values, $CH_4 + N_2$ contents range as follows: 0 to 0.4 for the South zone veins; 0 to 0.3 for the Centre zone, North zone and subhorizontal veins. At low XH_2O values, $CH_4 + N_2$ contents range in the following manner: 0 to 0.4 for the South

zone veins; 0 to 0.3 for the North zone veins. The values for the Centre zone and subhorizontal veins are bimodally distributed where low XH_2O values range as follows: 0 to 0.4 and 0.7 to 0.9 for Centre zone veins; 0 to 0.2 and 0.4 to 0.55 for subhorizontal veins. At intermediate XH_2O values $CH_4 + N_2$ contents are consistently below 0.1.

The significance of Fig. 15 is that it allows us to clearly classify the specific fluid types present. Generally, we see three specific carbonic fluid types, these being: a largely

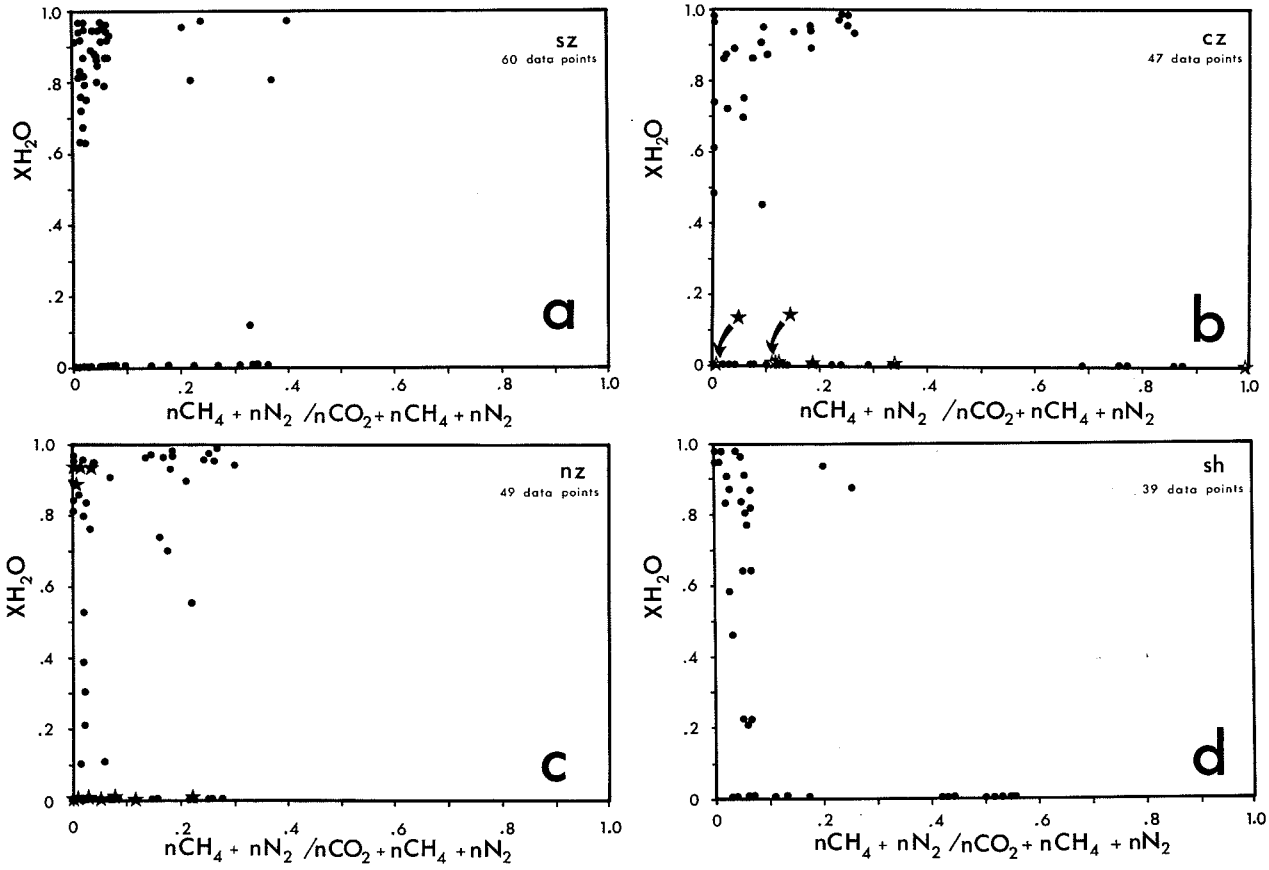

Figure 15 Diagrams plotting mole fraction H_2O versus the CH_4+N_2 content of the carbonic phase for carbonic inclusions from the four vein sets. Circles represent quartz-hosted inclusions, open stars represent sphalerite-hosted inclusions, closed stars represent scheelite-hosted inclusions.

aqueous, carbonic-poor fluid, in which the carbonic phase consists largely of CO_2, with appreciable to negligible amounts of CH_4 and N_2; a predominantly carbonic-rich fluid, with little or no H_2O, in which the carbonic phase is largely CO_2-bearing ($XCO_2 > 0.6$); and a predominantly carbonic-rich fluid, with negligible H_2O, in which the carbonic phase contains > 0.6 $XCH_4 + N_2$. The first and second fluid types are present in all four vein sets whilst the third fluid type is restricted to Centre Zone and subhorizontal veins. The highest XCH_4+N_2 contents of inclusions representing this third fluid type are found in Centre Zone veins.

Figure 16 plots the homogenization or decrepitation temperature versus the mole fraction CO_2 of the carbonic inclusions (see Appendix 3 for calculations involved). The data distribution for the Centre zone and subhorizontal vein sets (Figures 16 b and 16 d) indicate a complete range in XCO_2, whereas for the South and North zone vein sets (Figures 16 a and 16 c), a bimodal distribution is evident through XCO_2 gaps from 0.35 to 0.65 and 0.25 to 0.60 respectively. There is no obvious correlation between XCO_2 and temperature. The significance of Figure 16 is discussed in the section on entrapment conditions.

3.8 Conditions of Entrapment

Fig. 16 indicates that XCO_2 of carbonic inclusions in the four vein sets varies widely from 0 to almost 1.0 for a relatively constant homogenization/decrepitation temperature interval. Such a wide variation in XCO_2 can also be seen within a very restricted area in a single crystal of quartz. This kind of distribution points to entrapment of a fluid in which the H_2O and CO_2 existed as separate immiscible phases (Ramboz et al., 1982).

Fluid inclusions formed by the entrapment of a hypersolvus and homogeneous aqueous-carbonic fluid at constant P and T will homogenize at a single point on the solvus defined for the specific composition of the original fluid at the pressure of trapping (Pichavant et al., 1982). If, however, an initially homogeneous fluid is at subsolvus conditions during fluid inclusion formation, it will be present as separate immiscible aqueous-rich and carbonic-rich fluids. The homogeneous entrapment of such fluids (i.e., of single phases) will produce a bimodal distribution of XCO_2 corresponding to the intersections of the appropriate solvus with the temperature of trapping.

The distribution of data obtained in Fig. 16 clearly shows that this was not the case at St. Robert. By contrast, heterogeneous or mixed entrapment of subsolvus fluids (entrapment of both fluids in the same inclusion) at constant P and T, will result in the distribution of data over a wide range in compositions, i.e. the same as that observed in this study. Inclusions with end-member compositions (pure H_2O and pure CO_2) will homogenize on the solvus, at temperatures more or less

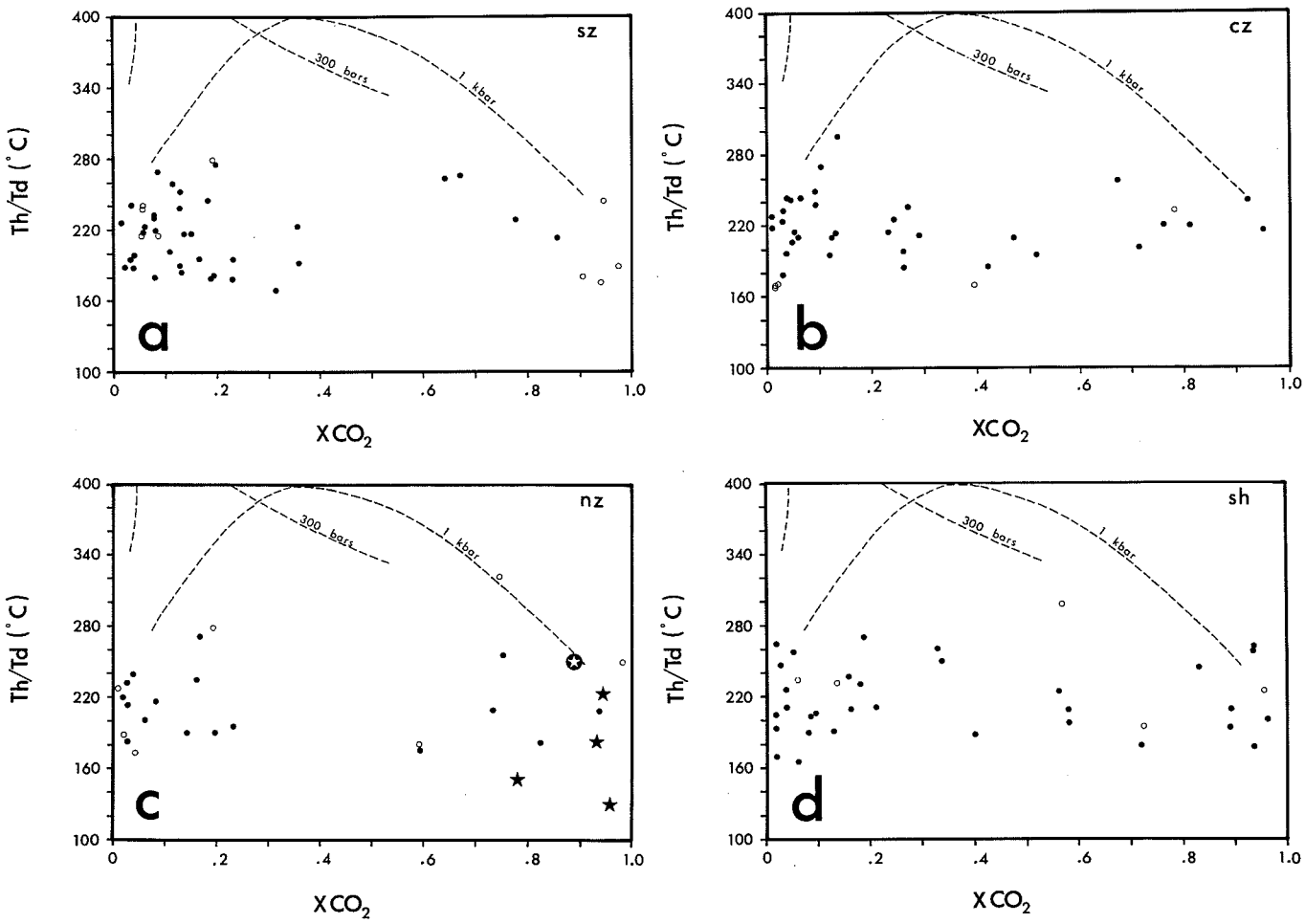

Figure 16 Composite homogenization/decrepitation temperature versus mole fraction CO_2 diagrams for carbonic inclusions from the four vein sets. Open and closed circles represent homogenization and decrepitation of quartz-hosted inclusions respectively. Circled and closed stars represent analogous data for scheelite-hosted inclusions respectively. The 300 bar and 1 kbar solvi for the system CO_2-H_2O-6 Wt % NaCl equiv. shown by the dashed lines are taken from Takenouchi and Kennedy (1965) and Gehrig et al. (1979) respectively.

equivalent to the trapping temperature. Inclusions of intermediate compositions should likewise homogenize on the solvus, and therefore at much higher temperatures than those of entrapment. For reasons outlined earlier (see section 3.42), these inclusions will tend to decrepitate at temperatures just above their entrapment temperatures and will therefore not define their corresponding solvus crest.

Inspection of Figures 8 and 16 indicates that most inclusions homogenize/decrepitate at temperatures between 160° and 300°C with a mean of 222.6° ± 36.7°C. It is suggested, for the reasons discussed earlier, that this is probably a reasonable reflection of the temperatures of entrapment of the carbonic inclusions.

Pressures of entrapment for carbonic inclusions cannot be reliably estimated from the data, but considering the abundant evidence of vein emplacement into wide open tension fractures, it is likely that entrapment pressures were relatively low and largely hydrostatic.

The entrapment temperatures for aqueous inclusions have not been estimated but, depending on the density, would have been within about 15°C of the homogenization temperatures for pressures up to 500 bars (Roedder and Bodnar, 1980). This suggests that aqueous inclusions were trapped at temperatures in the range 140° to 210°C (Fig. 7).

3.9 Raman Spectroscopy

As is evident from the above discussion, conventional fluid inclusion microthermometric analysis provides, at best, only semi-quantitative estimates of the compositions of carbonic inclusions. Furthermore, microthermometry may, in many cases, result in the destruction of the fluid inclusion itself. By contrast, laser-excited Raman spectroscopy provides a non-destructive and accurate means of obtaining the molecular compositions of individual carbonic inclusions (Rosasco, 1980; Dhamelincourt et al., 1979).

3.91 Equipment and Methodology

A total of 77 fluid inclusions were analyzed using an Yvon-Jobin Raman spectrometer, equipped with a Spectra Physics 164 ionized 6 watt argon laser source. The exciting frequency used in this study was 514.5 nm at a laser beam power of 300 to 500 mW. The sample material in all cases was quartz. Analyses were restricted to the carbonic phase of carbonic inclusions originating from all four vein sets. All inclusions were analyzed for the following species: CO_2, CH_4, N_2, NH_3, NO, H_2S, and SO_2. Only CO_2, CH_4, and N_2 were detected. Although peak intensities cannot be converted directly into concentrations, the relative proportions of the latter species were determined by measuring the areas under their principal peaks. The calculations required to obtain compositional data were performed using a program specifically designed for this purpose, which is part of the software package supplied by the manufacturer.

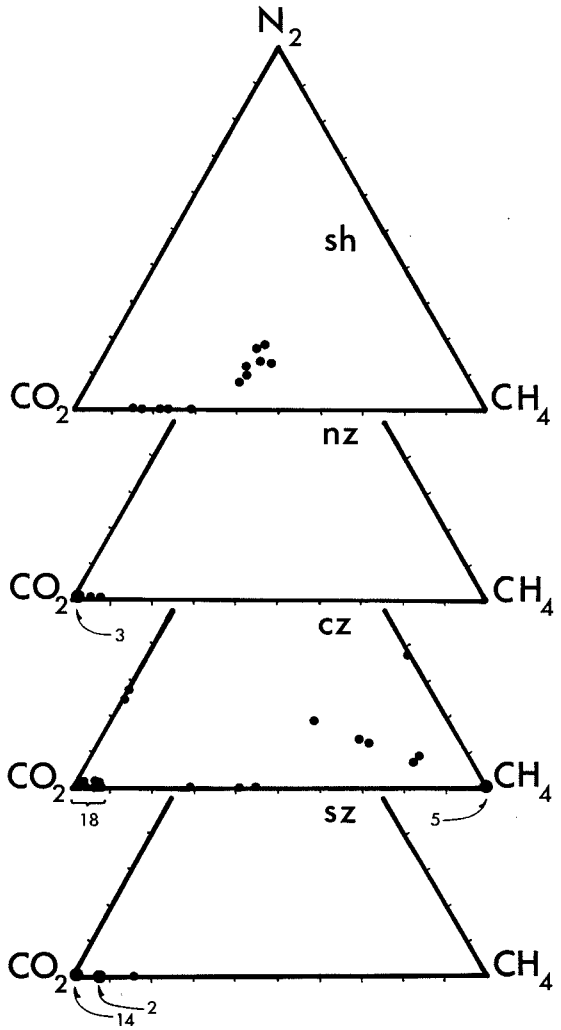

Figure 17 CO_2-CH_4-N_2 ternary diagrams plotting the composition of carbonic inclusions from the four vein sets.

3.92 Results

Figure 17 presents the results of the Raman analyses as a ternary plot of XCO_2, XCH_4, and XN_2 of the carbonic fluid fraction of the carbonic inclusions in the four vein sets. The most common component in the carbonic phase in inclusions from all samples is CO_2, followed by CH_4 and N_2 in that order. South zone and North zone veins contain only CO_2 and minor CH_4. The range in XCO_2 in these vein sets is from 0.84 to 1.0 and 0.92 to 1.0 respectively. By contrast, inclusions from the Centre zone and subhorizontal veins have appreciable concentrations of N_2 present. The range in composition of the carbonic phase in inclusions from these vein sets is as follows: Centre zone, XCO_2 = 0 to 1.0, XCH_4 = 0 to 1.0, XN_2 = 0 to 0.37; and subhorizontal veins, XCO_2 = 0.45 to 0.87, XCH_4 = 0.13 to 0.41, XN_2 = 0 to 0.18. Two important observations can be drawn from Figure 17: inclusions from subhorizontal veins show a clear bimodal distribution of data where a number of points are tightly clustered at intermediate XCH_4 values with significant proportions of N_2, and others are clustered along the CO_2-CH_4 line at XCH_4 from 0.15 to 0.29; a compositional trend may exist in data from Centre zone veins, extending from the CH_4 apex to about the XCO2 = 0.7 point on the diagram. This apparent trend suggests the dilution of a CO_2-N_2-bearing fluid by a separate, CH_4-rich fluid.

24- STABLE ISOTOPE STUDY

4.1 Equipment and Methodology

The sulphur isotopic compositions of pyrite, sphalerite and galena, and the oxygen isotopic compositions of quartz and scheelite were analysed for this study. Isotopic analyses of sulphur and oxygen were performed at McMaster University by Dr. C. C. McMullen and Dr. H. P. Schwarcz, respectively, using a non-commercial, 6", 90° magnetic sector mass spectrometer, equipped with a double ion collector system. The analysis and data acquisition were computer controlled. Estimated analytical precision for sulphur and oxygen isotopes were 0.4 °/₀₀ and 0.1 °/₀₀ respectively.

Standard stable isotope notation is used in this study. All isotope values are reported as a permil difference in the ratio R, between the sample (A) and the appropriate standard:

$$I_A = ((R_A - R_{std})/R_{std}) \times 1000$$

where R = ($^{18}O/^{16}O$) or ($^{34}S/^{32}S$), I = ^{18}O or ^{34}S, and R_{std} is the reference ratio from the Canon Diablo troilite for sulphur (Thode et al., 1961), and SMOW (Standard Mean Ocean Water) for oxygen (Craig, 1957, 1961).

4.2 Oxygen Isotopes

4.21 Sample Preparation

Quartz and scheelite samples were carefully examined for purity, and, if acceptable, were crushed to approximatly sand size using an agate mortar and pestle for later isotopic analysis. The aggregates were bathed in a concentrated HCl solution for 24 hours to remove any carbonates that might have been present and then washed several times in doubly distilled water. They were thereafter dried in an oven set at 100°C for a period of 24 hours.

4.22 Results

The $\delta^{18}O$ values for 22 samples of vein quartz from the four mineralized vein sets as well as 4 samples of scheelite from the Centre zone and subhorizontal vein sets are presented in Table 3. Duplicate analyses were performed on 10 % of the quartz samples to check reproducibility. The average variation of the duplicate analyses is about 0.3 permil. The $\delta^{18}O$ values range from +8.06 to +12.41 permil, with an average of +9.57 permil for quartz, and from +10.04 to +11.91 permil, with an average of +10.97 permil for scheelite. There is little variation in $\delta^{18}O$ from one mineralized vein set to another for either quartz or scheelite.

4.23 Source of Hydrothermal Fluids

The $\delta^{18}O$ results were used to calculate the isotopic composition of the water which would have been in equilibrium with the analyzed quartz and scheelite samples, with the objective of trying to establish a plausible source for the water. Calculations were performed at a temperature of 250°C

Sample	Analyses		Qtz-H_2O		Sch-H_2O	Qtz - Sch	
S. Zone	Quartz	Scheelite	250 °C[1]	250°C[2]	250 °C[3]	Temp.[1]	Temp.[2]
SC-37b	10.66		-0.5	1.1			
SC-50	9.44		-1.8	-0.2			
SC-51	10.69		-0.5	1.1			
SC-52	8.73		-2.5	-0.9			
SC-54	10.70		-0.5	1.1			
J-11-82-4	8.74		-2.5	-0.9			
J-84-3-2	9.84		-1.4	0.2			
C. Zone							
J-83-13-1	10.35		-0.9	0.8			
J-83-08-9	9.44		-1.8	-0.2			
SC-53	9.46		-1.7	-0.1			
LAC-NE	10.17	-0.30	-1.0	0.6	-0.10	285	235
LAC-EXIT	8.57		-2.6	-1.0			
LAC-NW	9.27		-1.9	-0.3			
LAC-SW	9.00		-2.2	-0.6			
J-2-82-2	11.58		0.4	2.0			
J-1-82-9	10.58	0.54	-0.6	1.0	0.74	298	242
N. Zone							
SC-84-49	8.06		-3.1	-1.5			
SC-84-44	12.32		1.1	2.7			
Subhoriz.							
LAC-SW Fl.	12.41	0.96	1.2	2.8	1.16	250	208
SC-84-23	9.14		-2.1	-0.5			
NZ. Horiz.	11.31	-0.60	0.1	1.7	-0.40	241	195

Table 3 Oxygen isotope analytical results for quartz and scheelite, calculated isotopic composition of waters in equilibrium with quartz and scheelite and calculated temperatures of formation from quartz and scheelite pairs. Superscripts represent fractionation factors used: 1- Blattner (1975); 2- Clayton et al. (1972); 3- Wesolowski and Ohmoto (1986).

(from fluid inclusion microthermometry) using the oxygen isotope fractionation equations for the quartz-water system from Blattner (1975), and Clayton et al. (1972), and the scheelite-water system from Wesolowski and Ohmoto (1986). Table 3 presents the resultant $\delta^{18}O$ H_2O values which range as follows: -3.14 to +1.21 with a mean of -1.24, using the equation of Blattner (1975); and -1.54 to +2.81 with a mean of +0.32, using the equation of Clayton et al. (1972). Corresponding values calculated from scheelite range from -0.40 to +1.16 with a mean of +0.35. $\delta^{18}O$ values for water calculated from oxygen isotopic values of quartz and scheelite are indistinguishable with a mean of very similar, ie. mean of 0 °/₀₀ ± 1.5 °/₀₀. This suggests that precipitation of quartz and scheelite occurred under conditions in which the two minerals were in isotopic equilibrium.

The $\delta^{18}O$ values determined for the water present during ore deposition at St. Robert are clearly too low to represent typical magmatic or metamorphic waters (Fig. 18). Oceanic water is also rejected on the grounds that it could not have been involved in the formation of the St. Robert deposit. It has already been established that vein emplacement occurred after deformation and uplift, and hence that the deposit formed following the middle Devonian Acadian orogeny, ie. in a cratonic environment. Finally, because of the generally low salinity of the water trapped as primary fluid inclusions, connate or formation brines are also ruled out as possible candidates for the origin of the water at St. Robert. It is therefore concluded that the primary source of hydrothermal water at the St. Robert deposit was meteoric.

Generally, high $\delta^{18}O$ values point to an evolved fluid and/or alternatively to low latitudes. The latter is entirely consistent with available paleogeographic data which suggests that during and shortly following the Acadian orogeny, the Appalachian belt was situated well within equatorial latitudes (Briden and Irving, 1964; Ma, 1958; Opdyke, 1962).

4.24 Geothermometry

Since it is clear that scheelite and quartz were in isotopic equilibrium, their temperature of crystallization can be calculated using known fractionation factors for scheelite-water (Wesolowski and Ohmoto, 1986), and quartz-water (Blattner, 1975; Clayton et al., 1972). Table 3 presents the results of these calculations, based on the difference between measured $\delta^{18}O$ values for quartz and scheelite, which are as follows: 241° to 298°C, with a mean of 268.5°C, using the quartz-water equation from Blattner (1975); and 195° to 245°C, with a mean of 220°C, using the equation from Clayton et al. (1972).

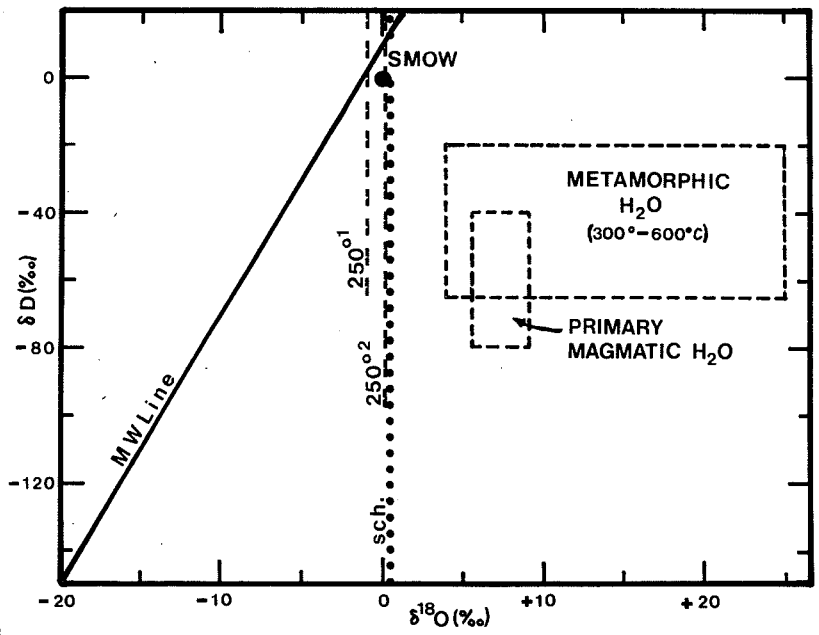

Figure 18 δD versus $\delta^{18}O$ diagram showing the mean water composition for the St. Robert hydrothermal system calculated from quartz and scheelite $\delta^{18}O$ values. The two dashed lines represent the mean water values obtained from quartz using fractionation factors published by: 1- Blattner (1975); 2- Clayton et al., (1972). The dotted line is the mean water value obtained from scheelite using the fractionation factor of Wesolowski and Ohmoto (1986). The fields of metamorphic and primary magmatic waters and the meteoric water line are also shown.

These temperatures agree well with estimates of entrapment temperatures based on fluid inclusion microthermometry, and make legitimite the estimate of 250°C used for calculating the isotopic composition of the water. Furthermore, although the data are few, there is an indication of a bimodal temperature distribution. Temperatures calculated for vertical veins (samples J-1-82-9 and Lac-NE, with mean temperatures of 291.5° and 238.5°C using Blattner (1975) and Clayton et al. (1972) respectively) are clearly higher than those for subhorizontal veins (samples N.Z. Horiz. and Lac-SW Flat, with mean temperatures of 245.5° and 201.5°C using Blattner (1975) and Clayton et al. (1972) respectively). This is consistent with cross-cutting relationships observed in the field in which subhorizontal veins consistently postdate vertical veins.

4.3 Sulphur Isotopes

4.31 Sample Preparation

Numerous sulphide-bearing samples were examined in polished thin section to select a subset for isotopic analysis, using the criteria of crystal homogeneity and apparent textural equilibrium between different sulphide phases. The selected samples were crushed to a size sufficient to liberate individual mineral grains which were sorted by hand with the aid of a binocular stereoscopic microscope. A total of 15 pyrite samples, 7 sphalerite samples, and 14 galena samples were analyzed from 19 sample localities. Only 4 samples, 3 from the South zone and 1 from the Centre zone, contained all three minerals.

4.32 Results

The sulphur isotopic data are presented in Table 4 and are grouped by mineral and fractionation factors. Duplicate analyses were performed on ten percent of the samples. The reproducibility of duplicate analyses for a mineral sample is 0.15 permil. The $\delta^{34}S$ values for all the sulphide minerals range from +3.7 to +8.3 permil. Three of the four samples in which all three sulphide minerals were analyzed displayed the following order of enrichment of $\delta^{34}S$: sphalerite > pyrite > galena. Since a pyrite-sphalerite-galena triplet deposited in isotopic equilibrium must have δpy > δsph > δgn (Grootenboer and Schwarcz, 1969), it follows that sulphur isotopic equilibrium was generally not established between pyrite and the other two minerals. This implies that pyrite was deposited separately and under different conditions to sphalerite and galena. This conclusion is consistent with textural evidence in which pyrite is clearly replaced by galena (Plate 22), and in places by sphalerite.

The $\delta^{34}S$ values for pyrite, sphalerite, and galena in the South zone vein set average +5.94, +6.23, and +4.41 permil, respectively. The corresponding values for the Centre zone vein set are +6.15, +6.25, and +3.95 permil, respectively. Two sulphur isotope analyses were performed on minerals from the subhorizontal vein set with the following isotopic compositions: +7.2 permil for pyrite; +4.5 permil for galena. No sulphide samples were analyzed from the North zone vein set. The above data indicate that there was little variation in $\delta^{34}S$ between one mineralized vein set and another. The average $\delta^{34}S$ for all samples is +6.24 permil for sphalerite, +6.12 permil for pyrite, and +4.18 permil for galena.

Sample	Analyses ($\delta^{34}S$)			Temperature (°C)				
S. Zone	py	sp	gn	py-gn[1]	py-gn[2]	sp-gn[1]	sp-gn[2]	sp-gn[3]
SC-37b	5.6		4.8	856.2	649.0			
SC-51	5.6		4.5	690.0	535.6			
J-84-1	6.1	5.9	3.9	407.9	322.1	328.0	287.6	318.6
SC-77-1	6.1		4.2	459.7	363.2			
J-11-82-2	5.8		4.1	501.6	395.9			
SZ Vein 4	6.1	6.3	4.5	525.5	414.2	360.6	316.4	350.6
J-84-3-2	6.2	6.5	4.9	612.8	479.8	399.0	350.1	388.4
SC-80	5.7							
C. Zone								
J-83-13-1	6.4		3.8	353.4	278.0			
J-84-10-1			3.7					
J-84-10-2	5.0	5.1	3.7	612.8	479.8	445.4	390.3	434.1
J-83-08-9	6.3		4.0	398.0	310.1			
SC-81	6.7							
LAC-SE	5.8		4.8	737.0	568.6			
LAC-NE	6.7							
J-84-13-21		5.8	3.7			313.6	274.7	304.4
SC-82		5.8						
J-84-11		8.3						
Subhoriz.								
NZ Horiz.	7.2		4.5	341.7	268.4			

Table 4 Sulphur isotope analytical results for pyrite, sphalerite and galena and calculated temperatures of formation using two different mineral pairs. Superscripts represent fractionation factors used: 1- Ohmoto and Rye (1979); 2- Grootenboer and Schwarcz (1969); 3- Czamanske and Rye (1974).

4.33 Geothermometry

Temperatures of formation of the various sphalerite-galena mineral pairs were determined using the measured ^{34}S values of the two sulphide minerals and several published isotopic fractionation factors. The fractionation factors used were determined by Grootenboer and Schwarcz (1969), Czamanske and Rye (1974), and Ohmoto and Rye (1979). Calculated temperatures based on these factors are presented in Table 4 above.

The sulphur isotope temperatures calculated from sphalerite-galena pairs range as follows: 390.3° to 274.7°C with a mean of 323.8°C using the fractionation factor of Grootenboer and Schwarcz (1969); 434.1° to 304.4°C with a mean of 359.2°C using the fractionation factor of Czemanske and Rye (1974); and 445.4° to 313.6°C with a mean of 369.3°C using the fractionation factor of Ohmoto and Rye (1979). The analytical uncertainty for the sulphur isotopic values, a sum of the inherent analytical precision and the reproducibility, is 0.55 permil. Depending on

the fractionation factor used, this corresponds to a temperature uncertainty of 65° to 80°C. It should be noted that the uncertainty varies with temperature and that an increase in the temperature leads to an increase in the uncertainty.

The average temperature obtained from sphalerite-galena mineral pairs is 323.8° to 369.3°C. This is significantly higher (approximately 100°C) than that predicted by fluid inclusion microthermometry and oxygen isotope thermometry. The good agreement between fluid inclusion and oxygen isotopic thermometry and the fairly wide scatter in the above temperatures suggest that sphalerite and galena may not have completely equilibrated. It is however possible, though unlikely, that the discrepancy simply reflects analytical uncertainty (65-80°C).

4.34 Conditions of Ore Deposition

The $\delta^{34}S$ of sulphides precipitating from a solution depends upon several variables, the most important of which are the $\delta^{34}S$ of total sulphur in solution, pH, fO_2, and temperature (Ohmoto, 1972). Estimates from fluid inclusion microthermometry and oxygen isotope thermometry indicate that the temperature of vein formation was approximately 220° and 245°C respectively.

An estimate of the maximum and minimum solution K^+/H^+ can be made from the observation that the pervasive alteration mineral is muscovite and that K^+/H^+ of the solution must therefore have been lower than and greater than those represented by the equilibrium constants for the reactions:

$$3KalSi_3O_8 + 2H^+ \text{ --> } KAl_3Si_3O_{10}(OH)_2 + 6SiO_2 + 2K^+$$

$$2KAl_3Si_3O_{10}(OH)_2 + H_2O + 2H^+ \text{ --> } 3Al_2Si_2O_5(OH)_4 + 2K^+$$

The log k for these reactions, calculated using free energy data from Helgeson et al. (1978), for a temperature of 250°C, are 7.98 and 3.96 respectively. These values can, in turn, be used to determine the minimum and maximum pH if the activity of K^+ is known. The latter was estimated from the salinity data presented earlier and an assumption, based on other studies of tungsten-bearing systems, that K^+/Na^+ was 0.3 (Weisbrod, 1981; Kelly and Turneaure, 1970). The activity coefficient of K^+ was calculated from the Debye Huckel expression using values for the a and b parameters from Helgeson et al. (1981) and the closest approach parameter from Truesdell and Jones (1974).

The minimum and maximum pH values calculated by the above method for the aqueous fluids from the mixed aqueous-carbonic stage are as follows: 2.98 to 4.99 for South Zone veins; 3.04 to 5.05 for Centre Zone veins; 3.00 to 5.01 for North Zone veins; and 3.15 to 5.16 for subhorizontal veins. These values and the data on which they are based are presented in Table 5. It may thus be assumed that the pH of the mineralizing fluid was generally > 3 and < 5.

Veins	Salinity (NaCl wt.% eq.)	Molality K^+	Act. Coeff K^+	pH 250 °C	
				K-spar-musc	musc-kaol
South	4.75	0.2595	0.3822	4.99	2.98
Centre	4.08	0.2220	0.3936	5.05	3.04
North	4.60	0.2505	0.3847	5.01	3.00
Subh.	3.21	0.1703	0.3925	5.16	3.15

Table 5 Calculated molalities and activity coefficients of K^+ and solution pH based on average measured salinities for the four vein sets. Solution pH was calculated for both the K-feldspar-muscovite and muscovite-kaolinite breakdown reactions and represent maximum and minimum estimates respectively.

4.35 Source of Sulphur

If pH and temperature are known, it is possible to calculate $\Sigma\delta^{34}S$ from the sulphur isotopic data of the related sulphide minerals. The $\Sigma\delta^{34}S$ so calculated can, in turn, be used to determine the source of the sulphur in the hydrothermal fluids, and provide an estimate of the fO_2 conditions. In order to define the range of possible total $\delta\Sigma^{34}S$ in solution, the pH conditions calculated above and the average sulphur isotopic values of sulphide minerals presented earlier are plotted on a log fO_2-pH diagram. Figure 19 shows contours of isotopic compositions of sphalerite for various log fO_2-pH conditions at 250°C relative to $\delta\Sigma^{34}S$ = 0 permil. The stability fields for various iron sulphide mineral phases are also indicated.

The observation that muscovite is the stable phase in the alteration reaction restricts pH conditions to have been below about 5.0 and above 3.0 at 250°C. Furthermore, because pyrite is the stable iron phase, fO_2 conditions are restricted to have been within the pyrite stability field, at least for the period involving sulfide mineral deposition. The range of ^{34}S values of sphalerite provides a means for making maximum and minimum estimates of $\Sigma\delta^{34}S$.

The $\Sigma\delta^{34}S$ in solution calculated using average sulphur isotopic values of sphalerite within the calculated range of pH, at a temperature of 250°C and for ΣS = 0.001 moles/kg H_2O (this represents the low end of the range of ΣS likely to occur in nature (Ohmoto, 1972)) ranges from about 7.3 to 22.6. Equivalent calculations using pyrite and galena yield values of 6.3 to 21.6 and 8.6 to 23.6 respectively. At higher ΣS values, the pyrite stability field expands thereby increasing the maximum predicted $\Sigma\delta^{34}S$ values. It is thus reasonable to conlude that $\delta\Sigma^{34}S$ was strongly positive, suggesting that the source of sulphur was from sedimentary rocks of marine origin, ie. that it was ultimately derived from seawater which has $\delta\Sigma^{34}S \approx 20‰$.

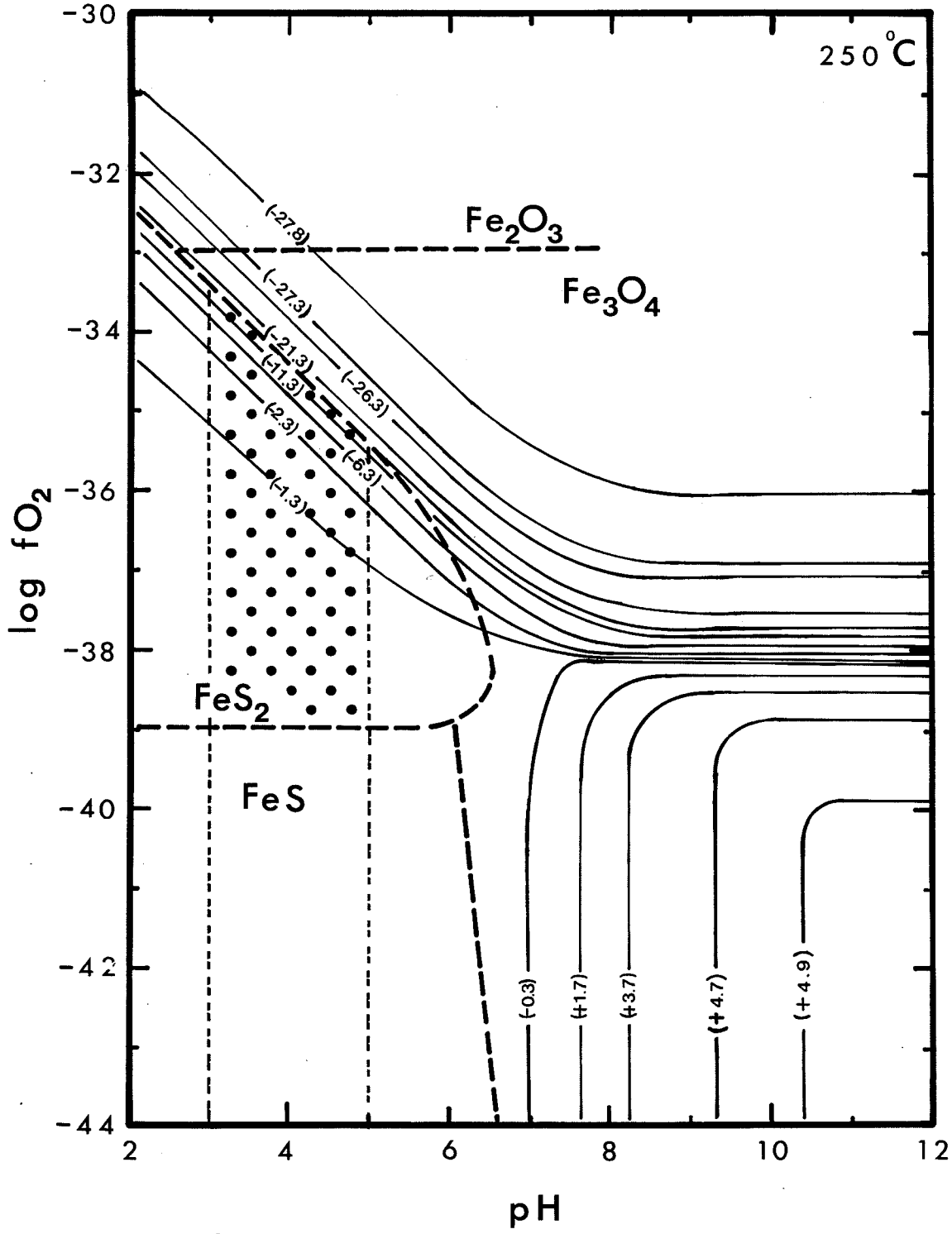

Figure 19 Log fO_2 versus pH diagram showing $\delta^{34}S$ contours for sphalerite, for $\delta\Sigma^{34}S$ of °/₀₀, ΣS = 0.001 moles/ kg H_2O and T = 250°C. Diagram modified after Ohmoto (1972).

25- CONCLUSION

5.1 Discussion

The mineralization at St. Robert occurs in thick, sheeted, massive quartz veins that were emplaced into an Ordovician sequence of turbiditic sediments. These veins, for the most part, tend to branch and vary in direction along strike, suggesting a relatively shallow level of emplacement. This is supported by the fact that fluid inclusions within these veins point to pressure conditions that were too low to provide for significant miscibility of CO_2 and H_2O (discussed later in this section).

Associated with these veins are numerous felsic and mafic porphyry dykes. Both the dykes and veins are concentrated in the central part of the property where a well defined proximal argillic and distal phyllic alteration halo overprints a thermal metamorphic biotite hornfels zone and is coincident with a clearly defined positive magnetic anomaly. Both the alteration and hornfels zones are concentric about a well developed shear zone which extends for some 2.5 kilometres. This suggests that the deposit is genetically related to an unexposed pluton at depth, for which the porphyry dykes represent the only surface expression. It also suggests that the pluton provided the heat engine necessary to drive a hydrothermal system which resulted in quartz vein emplacement and associated alteration.

The nature of this hydrothermal system can be deduced from various sources of evidence, including fluid inclusions and stable oxygen isotopes. The temperature of the fluid varied about a mean of 220.6°C from fluid inclusion microthermometry, and 220° to 268.5°C from oxygen isotope geothermometry, depending on the fractionation factor used. The fluid was carbonic in character, with a salinity ranging between 0 and 8 Wt% NaCl equivalent. Furthermore, the nature of the alteration (phyllic and argillic) suggests that it was mildly to strongly acidic. Thermodynamic calculations based on alteration mineral assemblages indicate a pH for the hydrothermal solution that was restricted between about 3.0 and 5.0. Oxygen isotope data from vein quartz and scheelite indicate that $\delta^{18}O$ values for the water averaged ≈ 0 °/₀₀. These data are consistent with a meteoric origin for the hydrothermal fluid (a seawater origin can be ruled out because of the low salinity of the fluids and the cratonic setting of the deposit).

The St. Robert deposit exhibits a clear spatial zonation: bismuth mineralization is predominant in the North zone; tungsten mineralization is richest in the Centre zone, particularily in the subhorizontal veins present in the Centre and North zones; and the highest concentrations of silver-bearing galena occur in the South zone. Lead and zinc mineralization on the other hand, are found in roughly equal proportions throughout the property. The nature of this metal distribution is not easily explained. Factors which might be responsible include temperature, pressure,

fO_2, pH, fluid composition and/or source rock variability. There is no evidence to indicate that temperature and pressure changed from one vein set to another. On the other hand, fluid composition, and hence fO_2, varied markedly between vein sets.

Inclusions from the Centre zone and subhorizontal veins contain considerable CH_4 and N_2 relative to inclusions from the South and North zones. In addition, CH_4+N_2-bearing inclusions from the subhorizontal veins are tightly clustered around intermediate CO_2-CH_4 contents, whereas corresponding inclusions from the Centre zone define a clear trend from CH_4-rich compositions to one corresponding to a CO_2:N_2 ratio of approximately 2:1. This trend may be interpreted as representing the dilution of a CO_2+N_2-bearing fluid by a separate, CH_4-rich fluid. It is tentatively proposed that this CO_2+N_2 fluid represents the result of a process in which organic-rich, N_2-bearing source beds underwent oxidation by circulating, meteoric groundwaters. It is uncertain as to how the nitrogen was fixed within the organic beds, but it is likely that it occurred as NH_2 groups in chitinous material (Manskaya and Drozdova, 1968). It is perhaps surprising that no ammonia or ammonium ion were detected by Raman spectroscopy.

The wide range of XCH_4 in the carbonic inclusions, particularily in the Centre zone and subhorizontal veins, suggests that oxygen fugacity may have varied considerably. The positive correlation between the ocurrence of high nitrogen-bearing inclusions and the tungsten content of the veins, and the abundance in these veins of methane-rich inclusions suggests that the tungsten may have been derived from organic-rich, CH_4+N_2-bearing source beds (organic radicals including NH_2 groups are well known for their ability to chelate metals). If this is so, then the steep dips of the various units likely served to enhance the observed heterogeneity in metal distribution.

An alternative explanation for the apparent association of tungsten with nitrogen-rich fluids is that of tungsten transport by nitrogen complexes. Although such complexes have been shown to exist (Allen, 1974; Chatt et al., 1974) there is, however, no evidence that they are stable at the conditions in question. Other possible modes of tungsten transport are as tungstenates (HWO_4^{-1} or WO_4^{-2}) or as oxyhalide, chloride, cyano, or bicarbonate complexes. Of these, transport as tungstenate or bicarbonate complexes seem the most likely. Data of Halley (1982) and Wesolowski et al. (1982) indicate that the dominant form of tungsten below 400°C is as a tungstenate. On the other hand, the association of tungsten mineralization with carbonic-rich fluid inclusions suggests that it may have been transported as a bicarbonate complex. A similar suggestion was made by Higgins (1985) for the Gray River deposit. The CO_2 could have been generated by the interaction of meteoric waters with organic-rich beds by the following reaction:

$$RNH_2 + CH_4 + O_2 \rightarrow N_2 + CO_2 + H_2O$$

or where they interacted mainly with calcareous sediments, CO_2 would have been generated by the dissolution of those beds. The latter is supported by the fact that the low eutectic temperature estimates from the majority of fluid inclusions studied (-22° to -40°C) are consistent with the presence of significant Ca in solution. These calcareous units may represent the source beds for the Ag, Bi and base metals at St. Robert. Although sulphur isotope data clearly indicate a marine origin for the sulphur in solution, it is not possible to specify which sediment-type (organic-rich, calcareous, or both) the sulphur originated from.

The nature of the XCO_2-temperature distribution of the early fluids suggests that there was subsolvus heterogeneous entrapment of immiscible carbonic and H_2O-bearing fluids at the level of mineralization. This could indicate the unmixing of a formerly miscible H_2O-carbonic fluid as it moved up to higher level, lower pressure regimes. The resulting effervescence of the carbonic fluid fraction would have increased the solution pH, which, in turn, would have effectively promoted the precipitation of W as scheelite, Ag, Bi and other metals as sulphides, and excess Ca^{2+} as calcite. Moreover, if the upward migration of the fluid due to unmixing and effervescence was into tension fractures, as appears to have been the case at St. Robert, it would have resulted in a significant drop in pressure. This pressure drop would have been particularly sharp as it would have been accompanied by a change from near-lithostatic to largely hydrostatic conditions. The multiple mineral zonation as evidenced by the Centre zone subvertical veins suggests episodic fracturing and resealing of these veins. This would have resulted in local pressure fluctuations which could have led to alternating periods of volatile loss and volatile enrichment, with concomitant periods of precipitation and leaching, respectively.

5.2 Genetic Model

Any model for the genesis of the St. Robert deposit should reconcile the following: that inclusions heterogeneously trapped immiscible H_2O and CO_2 fluids during effervescence of the ore-forming hydrothermal fluid; and that samples with CH_4+N_2-bearing inclusions are from zones with high tungsten concentrations.

A possible model for the deposit is one in which convection of oxidizing, meteoric groundwater was initiated by the cooling of a granitic pluton at depth. This fluid percolated through the existing bedrock and, in doing so, gained CO_2, CH_4, N_2, sulphur of marine origin and metals, in proportions that varied with the nature of the sedimentary successions traversed. That is, where organic-rich beds were more abundant, the fluid gained CO_2 (through oxidation of the organics), CH_4 $\pm N_2$ and tungsten (transported as either a tungstenate or bicarbonate complex) and where the rocks were predominantly calcareous, the fluid gained only CO_2, Ag, Bi and other metals. Subsequently, these hydrothermal fluids deposited their metals through a process of

CO_2-dominant carbonic fluid phase effervescence and wall-rock alteration as they moved into overlying tension fractures. The associated pressure release and resultant volatile loss, along with the wall-rock alteration, would have resulted in a pH increase, a drop in temperature, and in fO_2 fluctuations. The mineral zonation seen at St. Robert was likely controlled by the local stratigraphy, the orientation of which enhanced its definition.

Thus, in summary, the evidence of this study suggests that St. Robert is an example of a high level, hydrothermal vein-type polymetallic deposit, genetically related to a relatively deep-seated granitic pluton. Metal leaching and transport is believed to have occurred via a meteoric water-dominated convection system initiated by the cooling of this pluton. Furthermore, it is suggested that metal deposition occurred through a process in which tensional wall-rock fracturing resulted in a concomitant pressure release, CO_2 effervescence, and fO_2 fluctuations, where tungsten concentrations can be related specifically to a fluid in which CH_4 and N_2 were the important species in solution.

REFERENCES

Allen, A.D.
1974: Dinitrogen complexes of the transition metals; in: Proceedings of the 1st International Symposium on Nitrogen Fixation, vol. 1, Newton, W.E. and Nyman, C.J. (eds.), Washington State Univ. Press, p. 1-16.

Blattner, P.
1975: Oxygen isotopic composition of fissure-grown quartz, adularia, and calcite from Broadlands geothermal field, New Zealand, with an appendix on quartz - K-feldspar - calcite - muscovite oxygen isotope geothermometers; American Journal of Science, v.275, p. 785-800.

Bozzo, A.T., Chen, J.R., and Borduhn, A.J.
1973: The properties of the hydrates of chlorine and carbon dioxide; in: 4th International Symposium on Fresh Water from the Sea, eds. A. Delyannis and E. Delyannis; v. 3, p. 437-451.

Briden, J.C. and Irving, E.
1964: Paleolatitude spectra of sedimentary paleoclimatic indicators; in: Problems in Paleoclimatology, ed. A.E.M. Nairn, p. 199-224.

Burruss, R.C.
1981: Analysis of phase equilibria in C-O-H-S fluid inclusions; in: Short Course in Fluid Inclusions: Applications to Petrology, eds. L.S. Hollister and M.L. Crawford; Mineralogical Association of Canada, p. 39-69.

Chatt, J., Diamantis, A.A., Heath, G.A., Leigh, G.J. and Richards, R.L.
1974: Some reactions of ligating dinitrogen in stable mononuclear complexes: in: Proceedings of the 1st International Symposium on Nitrogen Fixation, vol. 1, Newton, W.E. and Nyman, C.J. (eds.), Washington State Univ. Press, p. 17-26.

Clayton, R.N., O'Neil, J.R., and Mayeda, T.
1972: Oxygen isotope exchange between quartz and water; Journal of Geophysical Research, v. 77, p. 3057-3067.

Craig, H.
1957: Isotopic standards for carbon and oxygen, and correction factors for mass-spectrometric analysis of carbon dioxide; Geochimica Cosmochimica Acta, v. 12, p. 133-149.

1961: Standards for reporting concentrations of deuterium and oxygen-18 in natural waters; Science, v. 133, p. 1833-1834.

Crawford, M.L.
1981: Phase equilibria in aqueous fluid inclusions; in Short Course in Fluid Inclusions: Applications to Petrology, eds. L.S. Hollister and M.L. Crawford; Mineralogical Association of Canada, p. 75-100.

Czamanske, G. and Rye, R.O.
1974: Experimentally determined sulfur isotope fractionation between sphalerite and galena in the temperature range 600 to 275 xC; Economic Geology, v. 69, p. 17-25.

Dhamelincourt, P., Beny, J-M., Dubessy, J. and Poty, B.
1979: Analyse d'inclusions fluides @2 la microsonde MOLE @2 effet Raman; Bull. Min{2ral., v. 102, p. 600-610.

Eadington, P.J.
1983: A fluid inclusion investigation of ore formation in a tin-mineralized granite, New England, New South Wales; Econ. Geol., v. 78, p. 1204-1221.

Gehrig, M., Lentz, H., and Franck, E.U.
1979: Thermodynamic properties of water-carbon dioxide-sodium chloride mixtures at high temperatures and pressures; in: High-Pressure Science and Technology, eds. K.D. Timmerhaus and M.S. Barber, 1, Physical Properties and Material Synthesis, Plenum Press, p. 539-542.

Grootenboer, J. and Schwarcz, H.P.
1969: Experimentally determined sulfur isotope fractionations between sulfide minerals; Earth and Planetary Science Letters, v. 7, p. 162-166.

Halley, S.
1982: Solubility of the tungstate minerals; unpub. B.Sc. Honours Rept., Univ. Tasmania, 91 pp.

Harron, G.A.
1976: Metallogeny of sulphide deposits in the Eastern Townships; Minist}2re des Richesses Naturelles, Qu{2bec, Paper ES-27, 42 pp.

Helgeson, H.C., Delany, J.M., Nesbitt, H.W., and Bird, D.K.
1978: Summary and critique of the thermodynamic properties of rock forming minerals; American Journal of Science, v. 278-A, p. 1-229.

Helgeson, H.C., Kirkham, D.H., and Flowers, G.C.
1981: Theoretical prediction of the behaviour of aqueous electrolytes at high pressures and temperatures: Calculation of activity coefficients, osmotic coefficients, and apparent molal and standard and relative partial molal properties to 600 xC and 5 kb; American Journal of Science, v. 281, p. 1249-1516.

Higgins, N.C.
1985: Wolframite deposition in a hydrothermal vein system: The Grey River tungsten prospect, Newfoundland, Canada; Economic Geology, v. 80, p. 1297-1327.

Hollister, L.S., Crawford, M.L., Roedder, E., Burruss, R.C., Spooner, E.T.C. and Touret, J.
1981: Practical aspects of microthermometry; in: Short Course in Fluid Inclusions: Applications to Petrology, eds. L.S. Hollister and M.L. Crawford; Mineralogical Association of Canada, p. 278-304.

Hosking, K.F.G.
1967: The relationship between primary tin deposits and granitic rocks; in: A Technical Conference on Tin; Internat. Tin Council, London, v. 1, p. 267-311.

Kelly, W.C. and Turneaure, F.S.
1970: Mineralogy, paragenesis, and geothermometry of the tin and tungsten deposits of the eastern Andes, Bolivia; Economic Geology, v. 65, p. 609-680.

Kelly, W.C. and Rye, R.O.
1979: Geologic, fluid inclusion and stable isotope studies of the tin-tungsten deposits of Panasqueira, Portugal; Economic Geology, v. 74, p. 1721-1822.

Landis, G.P. and Rye, R.O.
1974: Geology, fluid inclusion and stable isotope studies of the Pasto Bueno tungsten-base metal ore deposit, Northern Peru; Economic Geology, v. 69, p. 1025-1059.

Little, H.W.
1959: Tungsten deposits of Canada; Canada Geological Survey, Economic Geology Series, No.17, 251 pp.

Ma, Y.T.M.
1958: The shiftings in pole-positions with diastrophism since the end of the Cretaceous and the accompanying drift of continents; Research on Continental Drift, V., p. 1-176.

Manskaya, S.M. and Drozdova, T.V.
1968: Geochemistry of Organic Substances; International Series of Monographs in Earth Sciences, vol. 28, Pergamon Press, New York, 347 pp.

Mulligan, R.
1983: Geology of Canadian tungsten occurences; Geological Survey of Canada, Economic Geology report, No. 32, 121 pp.

Ohmoto, H.
1972: Systematics of sulfur and carbon isotopes in hydrothermal ore deposits; Economic Geology, v. 67, p. 551-578.

Ohmoto, H. and Rye, R.O.
1979: Isotopes of sulfur and carbon; in: Geochemistry of Hydrothermal Ore Deposits (second edition), ed. H.L. Barnes, p. 509-567.

Opdyke, N.D.
1962: Paleoclimatology; in: Continental Drift, ed. S.K. Runcorn, Academic Press, 338 pp.

Pichavant, M., Ramboz, C., and Weisbrod, A.
1982: Fluid immiscibility in natural processes: Use and misuse of fluid inclusion data; I. Phase equilibria analysis - a theoretical and geometrical approach; Chemical Geology, v. 37, p. 1-27.

Potter, R.W., II, Clynne, M.A., and Brown, D.L.
1978: Freezing point depression of aqueous sodium chloride solutions; Economic Geology, v. 73, p. 284-285.

Ramboz, C.
1980: Fluid phases associated with Sn-W deposits from South of Massif Central, France; 26th Int. Geol. Cong., Paris, Abstr., v. 1, p. 80.

Ramboz, C., Pichavant, M., and Weisbrod, A.
1982: Fluid immiscibility in natural processes: Use and misuse of fluid inclusion data; II. Interpretation of fluid inclusion data in terms of immiscibility; Chemical Geology, v. 37, p. 29-48.

Ramboz, C., Schnapper, D., and Debussy, J.
1985: The P-V-T-X-fO_2 evolution of H_2O-CO_2-CH_4-bearing fluid in a wolframite vein: Reconstruction from fluid inclusion studies; Geochimica Cosmochimica Acta, v.49, p. 205-219.

Roedder, E.
1981: Origin of fluid inclusions and changes that occur after trapping; in: Short Course in Fluid Inclusions: Applications to Petrology; eds. L.S. Hollister and M.L. Crawford; Mineralogical Association of Canada, p. 101-137.

Roedder, E. and Bodnar, R.J.
1980: Geological pressure determinations from fluid inclusion studies; Earth and Planetary Science Annual Reviews; v. 8, p. 263-301.

Roedder, E. and Skinner, B.J.
1968: Experimental evidence that fluid inclusions do not leak; Economic Geology, v. 63, p. 715-730.

Rosasco, G.J.
1980: Chapter 4; in: Advances in Infrared and Raman Spectroscopy, eds. R.J.H. Clark and R.E Hester, v. 7, p. 223-282.

Streckeisen, A.
1976: To each plutonic rock its proper name; Earth Science Reviews, v. 12, p. 1-33.

1979: Classification and nomenclature of volcanic rocks, lamprophyres, carbonatites, and melilitic rocks: Reccomendations and suggestions of the IUGS subcomission on the systematics of igneous rocks; Geology, v. 7, p. 331-335.

Swanenberg, H.E.C.
1979: Phase equilibria in carbonic systems, and their application to freezing studies of fluid inclusions; Contributions to Mineralogy and Petrology, v. 68, p. 303-306.

Takenouchi, S. and Kennedy, G.C.
1965: The solubility of carbon dioxide in NaCl solutions at high temperatures and pressures; American Journal of Science, v. 263, p. 445-454.

Thode, H.G., Monster, J., and Dunford, H.B.
1961: Sulphur isotope geochemistry; Geochimica Cosmochimica Acta, v. 25, p. 159-174.

Truesdell, A.H. and Jones, B.F.
1974: WATEQ, a computer program for calculating chemical equilibria of natural waters; Journal Research, U.S. Geological Survey, v. 2, p. 233-248.

Weisbrod, A.
1981: Fluid inclusions in shallow intrusives; in: Short Course in Fluid Inclusions: Applications to Petrology, eds. L.S. Hollister and M.L. Crawford, Mineralogical Association of Canada, p. 241-271.

Werre, R.W., Jr., Bodnar, R.J., Bethke, P.M. and Barton, P.B., Jr.
1979: A novel gas-flow fluid inclusion heating/freezing stage; Geological Society of America Abstr. with Prog., v. 11, p. 539.

Wesolowski, D., Drummond, S.E., Mesmer, R.E. and Ohmoto, H.
1982: Tungsten speciation in NaCl solutions to 300 xC; Geol. Soc. America Abstracts with Programs, v.14, p. 645.

Wesolowski, D. and Ohmoto, H.
1986: Calculated oxygen isotope fractionation factors between water and the minerals scheelite and powellite; Economic Geology, v. 81, p. 471-477.

Wiggins, L.B. and Craig, J.R.
1980: Reconnaisance of the Cu-Fe-Zn-S system: Sphalerite phase relationships; Economic Geology, v. 75, p. 742-752.

APPENDIX ONE

XRF Analyses (results reported as major oxide percentages)

Sample	Type	Alt.	SiO_2	TiO_2	Al_2O_3	Fe_2O_3	MgO	MnO
SC-DD	lamp		48.32	1.14	15.07	8.95	7.84	0.33
J83-9A	gran	M	67.49	0.48	17.05	3.66	1.57	0.06
J83-10A	lamp		51.28	1.04	15.17	8.64	7.33	0.30
J83-10E	gran	H	73.94	0.36	15.56	2.81	1.00	0.06
J83-10F	lamp		51.48	1.26	15.72	8.54	5.19	0.26
J83-10O	gran	M	67.81	0.46	15.70	3.27	1.13	0.06
J83-11A	gran	H	75.77	0.03	14.51	0.60	0.03	0.05
J83-11B	lamp		51.13	1.05	15.29	8.73	7.21	0.33
J83-11E	gran	H	68.40	0.55	18.22	3.78	1.42	0.07
J83-11H	gran	H	75.62	0.11	13.82	0.96	0.17	0.10
J83-11J	gran	L-M	68.54	0.47	16.05	3.38	1.21	0.06
J83-11K	gran	M	68.22	0.47	15.72	3.18	1.15	0.10
J83-11L	lamp		47.82	0.99	12.49	9.34	13.82	0.25
J83-13C	lamp		50.51	1.08	15.52	8.70	6.61	0.28
J83-13F	gran	M-H	70.77	0.44	15.57	3.16	1.22	0.09
J83-13G	gran	L	69.15	0.44	15.67	3.02	1.08	0.05
J83-14B	garn	H	76.26	0.03	14.44	0.74	0.03	0.03
J83-14C	gran	M	69.54	0.43	15.50	2.89	0.93	0.07
J83-14D	gran	L	68.32	0.47	15.99	3.33	1.24	0.06
J83-18A	gran	M	74.89	0.13	13.66	1.28	0.16	0.04
J83-19A	gran	M-H	67.81	0.46	15.83	3.29	1.19	0.05
J83-19B	gran	M	75.11	0.11	14.09	1.11	0.16	0.04
J83-19C	gran	H	67.68	0.49	15.36	3.76	1.29	0.07
J83-20A	gran	L-M	67.87	0.50	16.34	3.54	1.22	0.06
J83-20B	gran	M-H	69.18	0.45	15.54	3.27	1.16	0.06
J83-21C	gran	M	69.81	0.41	15.37	2.91	1.10	0.05
J83-22A	gran	L-M	68.65	0.43	15.82	3.10	1.17	0.06
SC84-13	gran	M-H	75.41	0.13	13.80	1.28	0.15	0.05
SC84-14	gran	H	68.56	0.41	15.50	3.07	1.04	0.07
SC84-20	gran	M-H	70.68	0.33	15.34	2.52	0.78	0.05
SC84-24	lamp		52.23	1.36	16.00	8.22	4.14	0.39
SC84-26	gran	M	68.24	0.39	15.17	2.92	0.97	0.06
SC84-27	gran	M	69.05	0.43	15.70	3.00	1.11	0.05
SC84-28	gran	M	70.26	0.50	14.93	2.44	1.25	0.05
SC84-29	lamp		51.55	1.27	15.86	8.55	5.28	0.19
SC84-30	gran	H	75.08	0.36	15.56	2.78	1.01	0.07
SC84-34	gran	M-H	69.46	0.44	15.71	2.91	0.98	0.14
SC84-35	gran	M	75.17	0.19	14.49	1.80	0.35	0.06
SC84-36	gran	M	75.27	0.20	14.30	1.68	0.43	0.06
SC84-39	gran	M	71.29	0.28	15.03	2.27	0.62	0.05
SC84-40	lamp		51.37	1.06	15.72	8.43	5.78	0.17
SC84-46	gran	L-M	71.37	0.35	14.84	2.58	0.85	0.05
SC84-47	gran	M	71.82	0.33	14.28	2.49	0.74	0.06
SC84-53	gran	M	69.99	0.39	15.41	2.81	1.04	0.05
SC84-54	gran	M-H	70.36	0.40	15.06	3.01	0.97	0.06

Sample	CaO	Na_2O	K_2O	P_2O_5
SC-DD	8.96	2.07	4.08	0.52
J83-9A	2.77	3.59	3.11	0.14
J83-10A	8.74	1.68	3.68	0.01
J83-10E	2.10	0.17	3.10	0.00
J83-10F	7.88	2.82	3.58	0.45
J83-10O	3.75	3.55	3.21	0.13
J83-11A	1.15	5.28	1.69	0.02
J83-11B	7.57	2.48	3.89	0.42
J83-11E	1.99	0.29	3.87	0.16
J83-11H	2.72	3.42	2.53	0.03
J83-11J	3.84	4.25	2.45	0.13
J83-11K	3.68	3.65	3.15	0.12
J83-11L	11.70	0.42	1.42	0.51
J83-13C	8.47	2.54	3.72	0.45
J83-13F	3.24	0.14	3.37	0.13
J83-13G	3.51	4.22	2.35	0.12
J83-14B	1.01	4.70	1.87	0.02
J83-14C	3.38	3.78	2.70	0.13
J83-14D	3.80	4.14	2.40	0.11
J83-18A	1.71	4.33	2.49	0.03
J83-19A	3.89	3.79	2.87	0.12
J83-19B	1.54	4.04	3.40	0.03
J83-19C	4.43	3.23	1.95	0.15
J83-20A	3.64	4.17	2.50	0.13
J83-20B	3.27	4.12	2.43	0.11
J83-21C	3.16	4.01	2.56	0.12
J83-22A	3.84	4.05	2.43	0.11
SC84-13	1.37	3.83	3.44	0.04
SC84-14	3.21	3.67	2.77	0.11
SC84-20	2.99	4.04	2.63	0.08
SC84-24	7.11	1.90	4.33	0.48
SC84-26	3.42	3.75	2.71	0.11
SC84-27	3.58	3.93	2.70	0.12
SC84-28	3.25	3.61	2.77	0.15
SC84-29	7.73	3.18	3.48	0.47
SC84-30	2.27	0.17	2.74	0.10
SC84-34	3.27	2.10	3.83	0.13
SC84-35	1.76	2.63	3.10	0.06
SC84-36	1.81	3.36	2.73	0.06
SC84-39	2.92	4.29	2.53	0.08
SC84-40	7.94	3.25	3.52	0.47
SC84-46	2.58	4.06	2.64	0.10
SC84-47	2.50	4.07	2.59	0.10
SC84-53	3.38	3.99	2.61	0.11
SC84-54	3.35	3.69	2.13	0.11

Note: The column headed "alteration" indicates a visual estimate of the degree of alteration using the following scheme: L = low degree of alteration; M = moderate degree of alteration; and H = high degree of alteration.

APPENDIX TWO

Normative calculations (calculated on a cation percent basis).

	SC-DD	J83-9A	J83-10F	J83-10O	J83-10E	J83-10A	J83-11L
qz	0.00	25.05	1.52	24.16	53.86	2.65	1.35
or	24.81	18.52	21.91	19.32	19.23	22.29	8.48
ab	19.13	32.49	26.24	32.48	1.60	15.46	3.81
an	20.36	12.93	20.38	17.76	10.25	23.57	28.32
ne	0.00	0.00	0.00	0.00	0.00	0.00	0.00
di	15.32	0.00	10.88	0.00	0.00	12.35	19.78
hy	0.00	4.37	9.41	3.18	2.90	14.57	28.70
ol	10.97	0.00	0.00	0.00	0.00	0.00	0.00
mt	0.00	0.00	0.00	0.00	0.00	0.00	0.00
il	0.53	0.09	0.42	0.10	0.10	0.48	0.40
ap	1.12	0.30	0.97	0.28	0.22	0.94	1.08
pl-an	0.52	0.28	0.44	0.35	0.86	0.60	0.88
di-en	7.66	0.00	5.44	0.00	0.00	6.18	9.89
hy-en	0.00	4.37	9.41	3.18	2.90	14.57	28.70
ol-fo	10.97	0.00	0.00	0.00	0.00	0.00	0.00

	J83-11A	J83-11B	J83-11E	J83-13G	J83-11K	J83-11J	J83-13C
qz	33.75	0.00	44.60	25.08	24.18	23.13	0.00
or	10.07	23.46	23.95	14.02	18.88	14.50	22.52
ab	47.48	22.73	2.73	38.26	33.24	38.22	23.37
an	5.62	19.50	9.25	16.80	17.46	17.51	20.45
ne	0.00	0.00	0.00	0.00	0.00	0.00	0.00
di	0.00	10.90	0.00	0.00	0.00	0.00	13.49
hy	0.08	12.71	4.11	3.01	3.22	3.35	7.77
ol	0.00	1.62	0.00	0.00	0.00	0.00	3.14
mt	0.06	0.00	0.00	0.00	0.00	0.00	0.00
il	0.04	0.53	0.12	0.08	0.16	0.09	0.45
ap	0.04	0.90	0.35	0.25	0.25	0.27	0.96
pl-an	0.11	0.46	0.77	0.31	0.34	0.31	0.47
di-en	0.00	5.45	0.00	0.00	0.00	0.00	6.75
hy-en	0.08	12.71	4.11	3.01	3.22	3.35	7.77
ol-fo	0.00	1.62	0.00	0.00	0.00	0.00	3.14

	J83-13F	SC84-13	J83-14B	J83-14C	J83-14D	SC84-14	J83-18A
qz	47.22	34.73	37.19	27.25	23.71	27.08	34.38
or	20.86	20.64	11.20	16.21	14.28	16.79	15.02
ab	1.32	34.92	42.77	34.49	37.45	33.81	39.69
an	15.95	6.64	4.95	16.18	18.09	15.60	8.46
ne	0.00	0.00	0.00	0.00	0.00	0.00	0.00
di	0.00	0.00	0.00	0.00	0.00	0.00	0.00
hy	3.53	0.42	0.08	2.61	3.45	2.95	0.45
ol	0.00	0.00	0.00	0.00	0.00	0.00	0.00
mt	0.00	0.00	0.01	0.00	0.00	0.00	0.00
il	0.15	0.08	0.04	0.11	0.09	0.11	0.06
ap	0.28	0.08	0.04	0.28	0.23	0.24	0.06
pl-an	0.92	0.16	0.10	0.32	0.33	0.32	0.18
di-en	0.00	0.00	0.00	0.00	0.00	0.00	0.00
hy-en	3.53	0.42	0.08	2.61	3.45	2.95	0.45
ol-fo	0.00	0.00	0.00	0.00	0.00	0.00	0.00

	83-19A	J83-19B	J83-19C	J83-20A	SC84-20	J83-20B	J83-21C
qz	23.68	32.92	29.10	23.11	27.94	25.75	26.84
or	17.21	20.31	11.89	14.86	15.74	14.52	15.31
ab	34.54	36.69	29.94	37.67	36.75	37.41	36.46
an	17.97	7.53	21.68	17.32	14.50	15.68	15.08
ne	0.00	0.00	0.00	0.00	0.00	0.00	0.00
di	0.00	0.00	0.00	0.00	0.00	0.00	0.00
hy	3.33	0.45	3.68	3.39	2.18	3.24	3.08
ol	0.00	0.00	0.00	0.00	0.00	0.00	0.00
mt	0.00	0.00	0.00	0.00	0.00	0.00	0.00
il	0.08	0.06	0.11	0.09	0.08	0.10	0.08
ap	0.25	0.06	0.32	0.27	0.17	0.23	0.25
pl-an	0.34	0.17	0.42	0.31	0.28	0.30	0.29
di-en	0.00	0.00	0.00	0.00	0.00	0.00	0.00
hy-en	3.33	0.45	3.68	3.39	2.18	3.24	3.08
ol-fo	0.00	0.00	0.00	0.00	0.00	0.00	0.00

	J83-22A	SC84-24	SC84-26	SC84-27	SC84-28	SC84-29	SC84-30
qz	24.55	6.54	26.38	25.15	28.51	0.19	55.42
or	14.50	27.07	16.53	16.12	16.65	21.15	16.84
ab	36.72	18.05	34.76	35.66	32.98	29.37	1.59
an	17.99	23.64	16.78	17.16	15.41	19.27	11.04
ne	0.00	0.00	0.00	0.00	0.00	0.00	0.00
di	0.00	5.58	0.00	0.00	0.00	10.60	0.00
hy	3.26	9.31	2.76	3.10	3.51	9.70	2.90
ol	0.00	0.00	0.00	0.00	0.00	0.00	0.00
mt	0.00	0.00	0.00	0.00	0.00	0.00	0.00
il	0.10	0.65	0.10	0.08	0.08	0.31	0.11
ap	0.23	1.06	0.24	0.25	0.32	1.01	0.22
pl-an	0.33	0.57	0.33	0.32	0.32	0.40	0.87
di-en	0.00	2.79	0.00	0.00	0.00	5.30	0.00
hy-en	3.26	9.31	2.76	3.10	3.51	9.70	2.90
ol-fo	0.00	0.00	0.00	0.00	0.00	0.00	0.00

	SC84-34	SC84-39	SC84-40	SC84-46	SC84-47	SC84-54	J83-11H
qz	32.96	27.85	0.00	29.25	30.28	30.68	37.84
or	23.34	15.13	21.28	15.82	15.60	12.85	15.25
ab	19.45	39.00	29.86	36.97	37.26	33.83	31.32
an	15.86	14.14	18.33	12.32	11.98	16.24	13.57
ne	0.00	0.00	0.00	0.00	0.00	0.00	0.00
di	0.00	0.00	12.60	0.00	0.00	0.00	0.00
hy	2.79	1.73	4.99	2.38	2.08	2.73	0.48
ol	0.00	0.00	3.78	0.00	0.00	0.00	0.00
mt	0.00	0.00	0.00	0.00	0.00	0.00	0.01
il	0.23	0.08	0.27	0.08	0.10	0.10	0.16
ap	0.28	0.17	1.01	0.21	0.21	0.23	0.06
pl-an	0.45	0.27	0.38	0.25	0.24	0.32	0.30
di-en	0.00	0.00	6.30	0.00	0.00	0.00	0.00
hy-en	2.79	1.73	4.99	2.38	2.08	2.73	0.48
ol-fo	0.00	0.00	3.78	0.00	0.00	0.00	0.00

	SC84-35	SC84-36	SC84-53
qz	41.95	38.53	26.48
or	18.80	16.39	15.57
ab	24.24	30.67	36.17
an	8.00	8.73	16.21
ne	0.00	0.00	0.00
di	0.00	0.00	0.00
hy	0.99	1.21	2.90
ol	0.00	0.00	0.00
mt	0.00	0.00	0.00
il	0.10	0.10	0.08
ap	0.13	0.13	0.23
pl-an	0.25	0.22	0.31
di-en	0.00	0.00	0.00
hy-en	0.99	1.21	2.90
ol-fo	0.00	0.00	0.00

APPENDIX THREE

Calculation of the bulk composition and bulk density of carbonic inclusions in the H_2O-CO_2-CH_4-N_2 system is possible provided that, at a given temperature, the degree of filling of the inclusion (Flw, volumetric fraction of the aqueous liquid in the inclusion), and the density of the aqueous part of the inclusion (dl) are known. Flw is estimated visually at a constant temperature of 40°C. Similarily, the density of the non-aqueous part of the inclusion (dv) and the mole fraction of the gas species in the non-aqueous part of the inclusion (ZCO_2, ZCH_4, ZN_2) must be known. The latter can be directly measured by Raman spectroscopy analysis, while the former can be estimated by interpretation of the microthermometric data Tm_{clath} and $TmCO_2$, as outlined in Burruss (1981). The following formulas, taken from Ramboz et al. (1985), outline the calculations involved:

$$nH_2O = Flw.dl/18$$

$$nCO_2 = [(1-Flw).dv.ZCO_2/44-28ZCH_4-16ZN_2] + Z`CO_2.nH_2O$$

$$nCH_4 = (1-Flw).dv.ZCH_4/44-28ZCH_4-16ZN_2$$

$$nN_2 = (1-Flw).dv.ZN_2/44-28ZCH_4-16ZN_2$$

$$X_i = n_i/nH_2O+nCO_2+nCH_4+nN_2$$

$$d = Flw.dl+(1-Flw).dv$$

Note: $Z`CO_2$ represents the mole fraction CO_2 dissolved into the aqueous part at $ThCO_2$ or Tm_{clath}, and is considered to be negligible at this temperature range.